The response of the cryoconite microbial community to cryospheric stresses

Eleanor Furness

Thesis submitted for the degree of Biological Sciences MPhil

Supervised by Dr Arwyn Edwards

and Prof Luis Mur

The Institute of Biological, Environmental and Rural Sciences

Aberystwyth University

September 2020

Declaration and Statements

Word Count of thesis: 30726 (excludes references and appendices)

DECLARATION

This work has not previously been accepted in substance for any degree and is not being concurrently submitted in candidature for any degree.

Candidate name: Eleanor Furness

Signature:

Date : 22/09/2020

STATEMENT 1

This thesis is the result of my own investigations, except where otherwise stated. Where *correction services have been used, the extent and nature of the correction is clearly marked in a footnote(s).

Other sources are acknowledged by footnotes giving explicit references. A bibliography is appended.

Signature:

Date : 22/09/2020

STATEMENT 2

I hereby give consent for my thesis, if accepted, to be available for photocopying and for inter-library loan, and for the title and summary to be made available to outside organisations.

Signature:

Date : 22/09/2020

Acknowledgements

First and foremost, thank you to my primary supervisor Arwyn Edwards. For mentoring, guiding, inspiring and encouraging me. For providing me with samples and sequence data. For demonstrating techniques such as DNA extraction and nanopore sequencing. For your patience. For writing me references with (very) minimal notice. Mostly though, thank you for giving me the freedom and trust to go my own way whilst supporting me to do so.

Many thanks to both the Higher Education Funding Council for Wales (HEFCW) and the James Pantyfedwen Foundation for their tuition fee grants which covered the costs of my MPhil tuition fees and made this possible.

Thanks also to the rest of the lab group, you were and are, helpful, supportive and great lab mates. Thanks to, and in no particular order…

Andre Soarés – bioinformatics guru, you taught me so much, most importantly how to teach myself via wonders such as GitHub. And for being so supportive and helpful. Thank you.

Alvaro Garcia – also bioinformatics marvel, nanopore demultiplexer and for showing me your gel electrophoresis techniques. And for being a super helpful lab mate. Thank you.

Aliyah Debbonaire – for teaching me some lab basics really early on and for demonstrating your colony PCR and multi-channel pipetting wonders. Also, for providing me with the A18.2 isolate that you had maintained from the lab's culture collection. Thank you.

Sara Rassner – for showing me how to use the meter and DO probe and for being full of tips and advice during lab meetings. Thank you.

Sarah Easter and Jenny McGowan – for being great friends and lab mates to be around, fun, helpful, supportive and curious. Thank you both.

Melanie Hay – for your awesome presentations and general helpful tips and advice. And especially for the use of the samples you collected. Thank you.

Pallavee Srivastava – for sharing nanopore channels with me and for your great advice during lab meetings. Thank you.

Luis Mur – for bouncing ideas around and being a great second supervisor. Thank you.

Thank you also to Joseph Cook for the use of samples you collected, Francesco Sauro for use of the metagenome you sequenced and Sophie Cook for use of the isolate A18.2 you originally isolated.

Thanks to Colin Sauze and Martin Swain for your bioinformatics lessons, help and support. Also, thanks to Hacky Hour and the Aber Bioinformatics Workshops.

Massive thanks also to my children, partner, family and friends who supported and encouraged me - you know who you are. Thanks all.

Table of contents

List of tables

Appendix tables

List of figures

Appendix Figures

List of Acronyms and Abbreviations

A18.2 – *Cryobacterium* isolate

AMWS - Artificial Melt Water Solution

ANI – Average Nucleotide Identity

ANOVA - Analysis of Variance

antiSMASH - secondary metabolite analysis (online tool)

AU – Absorbance Unit

BANDAGE – genome assembly graph visualization tool

BLASTn - The Basic Local Alignment Search Tool (nucleotide option)

CANU – genome assembly tool

CDS – Coding Sequence

CFU/ml $^{-1}$ – colony forming units per millilitre

DO – Dissolved Oxygen

EC – Enzyme Commission (number)

FASTA – text file for assembled nucleotide sequence

FASTQ – text file for raw nucleotide sequence

G17 – Greenland 2017 sample

G18 - Greenland 2018 sample

HGT – Horizontal Gene Transfer

IBERS – Institute of Biological, Environmental and Rural Sciences (Aberystwyth University)

ITS – Internal Transcribed Spacer

KAIJU - taxonomic classification (online tool)

KEGG - Kyoto Encyclopaedia of Genes and Genomes

KO - KEGG Orthology

LCA – Lowest Common Ancestor

MEP - the 2-C-methyl-D-erythritol 4-phosphate carotenoid biosynthesis pathway

MG RAST – Metagenome Rapid Subsystem Technology online tool for taxonomic classification and annotation

MinION – portable nanopore sequencing platform

MinIT – GPU for base-calling during Nanopore sequencing

MUSCLE - Multiple Sequence Comparison by Log-Expectation

MVA - the mevalonate carotenoid biosynthesis pathway

NanoPlot – sequencing and assembly tool for Nanopore reads

NCBI – National Center for Biotechnology Information

OD_{600} – Optical Density (600 nano metres)

OM – Organic Matter

ORFs – Open Reading Frames

PCR – Polymerase Chain Reaction

PhyML – maximum likelihood tree construction tool

PROKKA - rapid prokaryotic genome annotation tool

R2A – Reasoner's 2A agar

RA – Relative Abundance

RAST – Rapid Annotation Subsystem Technology (online annotation tool)

rRNA – ribosomal ribonucleic acid

S11 - Svalbard 2011 sample

S16 - Svalbard 2016 sample

S19 - Svalbard 2019 sample

SEED viewer – annotation and comparative genomics tool

TreeDyn - tree visualization and annotation tool

UV – Ultraviolet light

wks – weeks

wtdbg2 – genome assembly tool

Abstract

The cryosphere covers a substantial proportion of our planet and although a harsh environment, is home to various, relatively understudied, microbial ecosystems. Cryoconite holes are one such ecosystem and form when a mixture of windblown microbial and mineral particles accumulate on a glacier surface, and due to the low albedo of the dark coloured granular aggregates, melt down into the ice. Cryoconite harbours rich, biodiverse microbial communities which experience numerous cryospheric stresses and extreme conditions. Previously, the majority of cryoconite biological studies examined community productivity during the summer or focused on the primary producer Cyanobacteria. Few studies examined the stress response and physiological abilities of the community or of individual taxa under differing cryospheric stressors, or indeed the genomic foundations of such responses. Here, the cryoconite community and individual isolates were subjected to two cryospheric stressors, light and temperature. Both 24-hour dark and 24-hour light conditions as well as temperatures above (+2 °C) and below (-5 °C) freezing were applied. The community demonstrated a rapid recovery following a diurnal freeze-thaw (a return to pre-freeze levels of net O_2 production within 48 hours). Additionally, isolates were able to produce increasing CFU/ml $^{-1}$ values following incubation over a period of weeks at -5 °C, indicating an ability to not only withstand and recover from sub-zero temperatures but potentially to multiply at such temperatures. Furthermore, UV exposure as a form of light stress was applied to a selected cold-adapted heterotrophic representative, isolate A18.2, and although non-significant at this stage, results indicate the pigment produced by the isolate may confer some protection against UV irradiation. Sequencing and assembly of metagenomes and genomes followed by annotation and surveying of shock, stress, cold-adaption associated, light-sensing and carotenoid biosynthesis genes provided additional insight to the responses observed to the given cryospheric stresses. As well as genes previously associated with cold-adaption, the gene encoding gsp69 (yhdN) was identified as one of the core shock, stress or cold-adapted genes. yhdN was one of the most abundant stress genes and was present in every metagenome and genome, which indicates its potential, previously unknown link to cold-adaption. Moreover, the prevalence of light-sensing and carotenoid biosynthesis genes as well as the light-induced increase in pigment production demonstrated in both the community and the A18.2 implies this response to light stress could be a common tactic in cryoconite communities. By uncovering these adaptive abilities and responses to light and temperature stress as well as gaining genomic insight into the basis of these abilities, understanding how members of the cryoconite community, and further, how microbes overcome life in the cryosphere, has been furthered.

1 – Thesis Introduction

1.1 The cryosphere and the microbial habitats of glaciers

Around a fifth of the surface of the Earth is frozen, known collectively as the cryosphere, regions include permafrost, frozen parts of the ocean as well as massive glacial ice sheets and glaciers, which by themselves cover about 10% of the land surface of the Earth (Lutz *et al*., 2015; Boetius *et al*., 2015). These ice sheets and glaciers represent the largest freshwater reservoir, accounting for 75% of all freshwater on the Earth, the vast majority of which is present in the ice in the Antarctic and Greenland ice sheets (99.5%) with the remaining frozen freshwater stored in glaciers and ice caps (Jansson *et al*., 2003). Glacial ice is slowly formed over hundreds to thousands of years as fresh snow falls onto the underlying snow layer, compacting into firn, creating solid ice with an average thickness of 2 km (Boetius *et al*., 2015). Glacial ice consists of zones or layers (**Figure 1**) often covered by a layer of fresh snow (cm thickness), the topmost layer of glacial ice at the surface is termed the supraglacial layer (metres thick). Underneath this is the middle section, the bulk of the glacial ice, the englacial layer which can be kilometres deep in ice sheets. Lastly where the glacier meets the sediment rich till layer, bedrock or a subglacial lake, the final layer, the subglacial layer, can be metres thick (Hodson *et al*., 2008; Boetius *et al*., 2015).

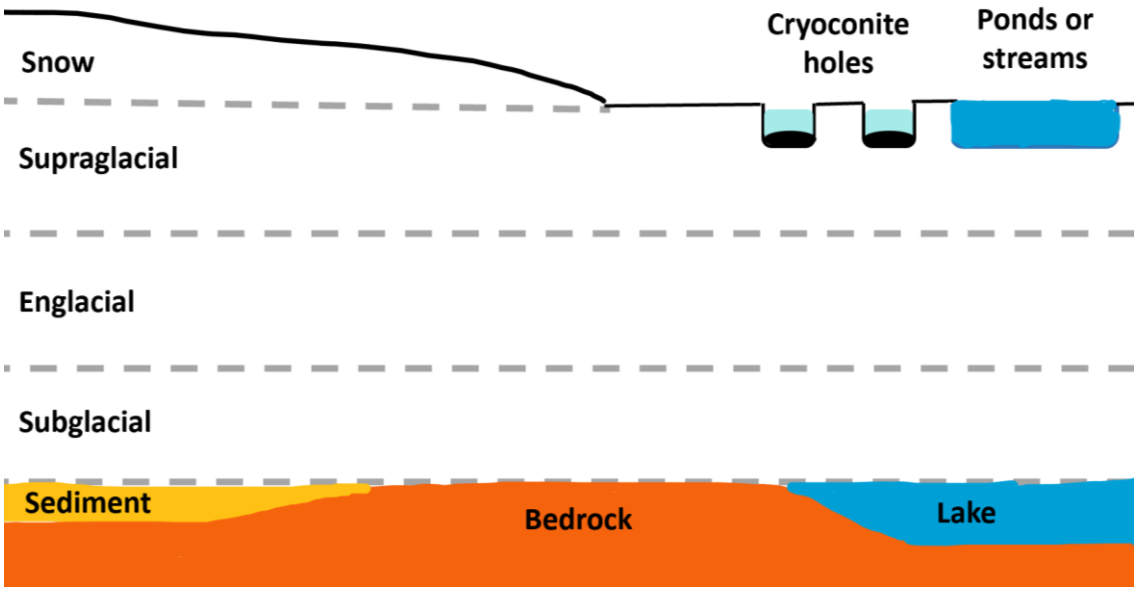

Figure 1. Glacial zones. Glacial zones or layers comprise; the topmost layer of glacial ice, the supraglacial layer (metres thick and often covered with a layer of snow) which provides a number of microbial habitats including wet snow, cryoconite holes, ponds and streams, the middle section, the englacial layer (can be kilometres deep in ice sheets) and the final layer, the subglacial layer (can be metres thick) which meets the sediment, bedrock or a subglacial lake (Hodson *et al*., 2008; Boetius *et al*., 2015). Schematic adapted from Boetius *et al*., 2015.

In these frozen forms, water is not easily available for the necessary cellular processes of life and as such these extreme glacial environments were not thought to house much life until relatively recently (Hodson *et al*., 2008). However, most of these frozen habitats do contain liquid water, including within interstices of the porous matrices (Fountain and Walder, 1998) and in streams or ponds (Boetius *et al*., 2015). All three domains of life are represented in glaciers (Anesio and Laybourn-Parry, 2012) and fascinatingly, microbial life here is not merely persisting, it is responsible for helping shape these habitats. Microbial ecosystems influence biogeochemical cycles (Vincent *et al*., 2011; Hodson *et al*., 2015), ice surface albedo and to some extent the topography of the ice (Ryan *et al*., 2017; Cook *et al*., 2018).

The supraglacial zone provides a number of microbial habitats including wet snow, ponds, streams and cryoconite holes (**Figure 1**). Cryoconite holes can be open, submerged or in the Antarctic, closed (lidded) (Fountain *et al*., 2004; Hodson *et al*., 2008) (**Figure 2**). Cryoconite, known as the ''microbial hotspot'' of surface glacial ice,

hosts ~1x10^8 microbial cells per ml (Hodson *et al*., 2008; Boetius *et al*., 2015) and covers approximately 1% of the ice surface (in Arctic regions) (Hodson *et al*., 2007). As such, cryoconite holes are one of the most studied microbial habitats of the cryosphere. Cryoconite holes, typically dominated by bacteria (Kaštovská *et al*., 2005), also house algae, fungi and various other eukaryotic, archaeal, and viral organisms, supporting a multi-tropic level community (Hodson *et al*., 2008). Community composition and productivity are discussed in Chapter 2, predominant taxa are discussed in Chapter 3.

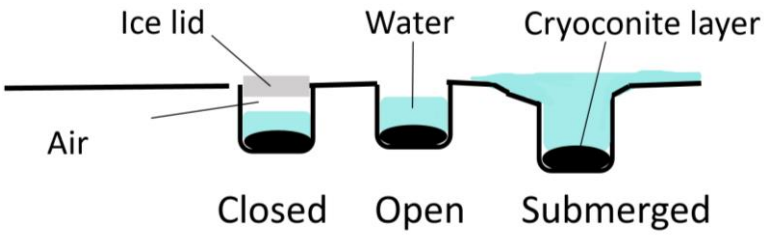

Figure 2. Cryoconite holes. The three types of cryoconite hole, closed, open and submerged are depicted. The closed type has an ice lid covering the hole. Schematic adapted from Hodson *et al*., 2008.

1.2 Cryoconite

The dark coloured, bio-engineered granular aggregates termed 'cryoconite' (from the Greek 'kryos' and 'konis' meaning 'cold dust') form after the deposition of both inorganic particulates and organic matter (OM) from a combination of aeolian, mass movement, fluvial, and melt sources (Takeuchi *et al*., 2001; Hodson *et al*., 2008; Langford *et al*., 2010; Edwards *et al*., 2014; Cook *et al*., 2016a). Cryoconite granule growth is promoted by the filamentous *Cyanobacteria*, which entangles minerals and OM (Stibal and Tranter, 2007) (**Figure 3**). Cryoconite granule size varies according to location, typically ranging from 0.3 – 10 mm, however in Aldegondabreen (Svalbard) individual granules of over 100 mm have been reported (Zarsky *et al.,* 2013).

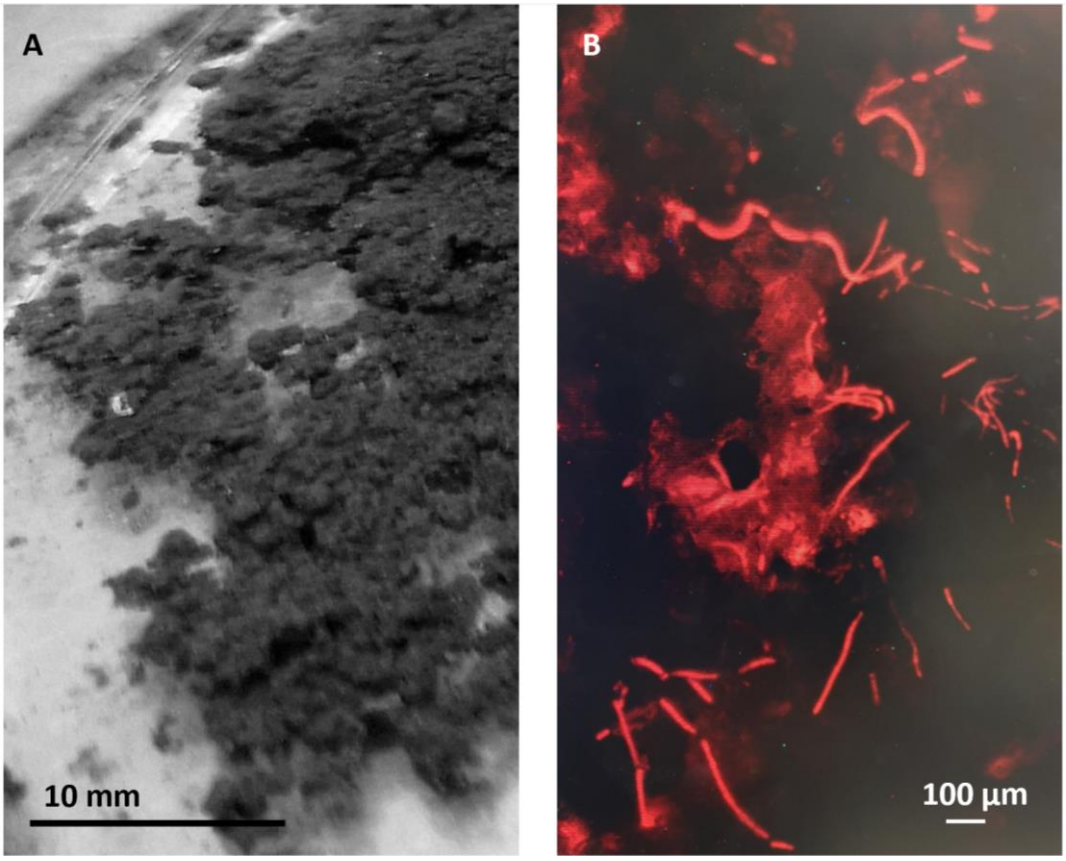

Figure 3. Cryoconite granules. Photographs of the S11 (Svalbard 2011) cryoconite sample. A) granules in the sample can be seen as darkly coloured aggregates. B) autofluorescence microscopy image of cyanobacterial filaments covering granules taken using a green filter, the chlorophyll present auto-fluoresces red.

The low albedo of cryoconite causes melt down into the ice, forming a hole filled with meltwater. The holes are dynamic and as well as being unstable in areas of high melt, leading to the cryoconite being washed into streams, accumulating in new deposits and the formation of new holes (Takeuchi *et al*., 1998; Hodson *et al*., 2008), they are also self-regulating. Self-regulation includes optimising the depth of the cryoconite granule layer, which is maintained at a single grain layer of between 0.04 and 0.2 $g.cm^{-2}$ via the redistribution of excess granules via widening of the hole, thus ensuring optimal solar radiation for the autotrophic members (Cook *et al*., 2010; Cook *et al.*, 2016b), indeed irregular shaped holes signify migration away from topographic shade (Cook *et al*., 2018).

1.3 Cryospheric stresses

Low temperature stress is the immediate stress that comes to mind when considering a cryospheric habitat indeed, last year (2019) the Arctic (North of 80°N) experienced mean temperatures between -28 °C to ~1 °C (http://ocean.dmi.dk/arctic/meant80n.uk.php), however the archipelago of Svalbard although at a latitude of 78°N experiences milder temperatures in comparison, due to the influence of the gulf stream, with the average annual temperature in Isfjord (for example) at -7.5 °C, even so temperatures of -30 °C occur in Svalbard regularly and occasionally even lower temperatures are recorded (https://www.spitsbergen-svalbard.com/spitsbergen-information/climate.html). The structure and heat absorbing properties of cryoconite holes provide some protection from air temperature fluctuations (Hodson *et al*., 2010; Bagshaw *et al*., 2016), indeed, Svalbard cryoconite holes temperatures are ~0 °C in the summer, a temperature often several degrees warmer than air temperature, however in the winter temperatures in the holes drop to below -16 °C (Säwström *et al*., 2002).

Microorganisms that are active in cold, icy environments are known as psychrophilic, psychrotolerant or cold-adapted (D'Amico *et al*., 2006) and require specialist strategies to manage the extreme habitat. Mechanisms to counter cold temperature and other cryospheric stresses include the production of; proteins and peptides to control ice-crystal formation and growth (called ice-binding proteins such as anti-freeze proteins (AFPs) which prevent the formation of large ice grains inside the cells (Białkowska *et al*., 2020)), secreted protective exopolymeric substances (EPS), cold-shock proteins (CSPs), (Boetius *et al*., 2015) pigments and biosurfactants (Sajjad *et al*., 2020) among other mechanisms (**Figure 4**).

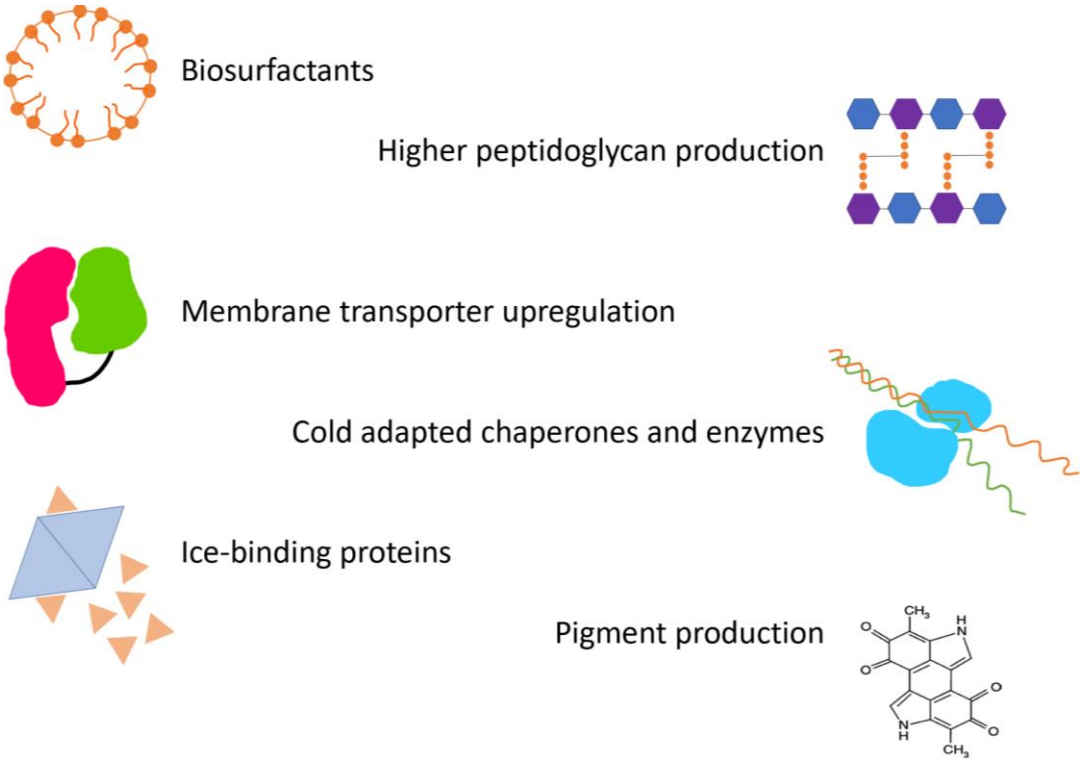

Figure 4. Selection of mechanisms to counter cold temperature and other cryospheric stresses. Microorganisms living in cold habitats use a range of specialist strategies and mechanisms to withstand and counter cryospheric stresses. A selection of some of the mechanisms used are depicted and include the production of ice-binding/antifreeze proteins (AFPs), biosurfactants, pigments, upregulated membrane transporters and increased peptidoglycan production as well as cold-adapted proteins. Schematic adapted from Sajjad *et al*., 2020.

Further discussion on sub-zero temperature stress and the strategies to counter it can be found in Chapter 3. However, multiple other cryospheric stresses impact microbial life in the cryosphere other than sub-zero temperature and as such, microbial inhabitants typically show several adaptations to overcome these (D'Amico *et al*., 2006). Additional cryospheric stresses include low nutrient and water availability, high levels of UV irradiation and oxidative stress (Margesin and Collins, 2019). Mechanisms to counter general cryospheric stresses are discussed in Chapter 2 and UV irradiation stress specifically is discussed in Chapter 3. A number of these stresses fluctuate seasonally, for example two opposing stresses such as 24-hour dark or 24-hour light conditions are experienced by the cryoconite community. Seasonal cryospheric stress variation is discussed further in Chapter 2.

1.4 Relevance of research

Extremophiles such as thermophiles have largely received far greater attention than the cold-loving psychrophiles or cold-tolerant microorganisms, however in the past two decades, the microbial inhabitants of the cryosphere have begun to be given more consideration for a number of reasons.

Cryospheric microorganisms represent a large proportion of the total biomass of the cryosphere and participate in the cycling of key elements, such as nitrogen and carbon, with potentially significant effects on the productivity of these systems (Maccario *et al*., 2015; Makhalanyane *et al.,* 2016). For example, the contribution from microbial communities in restricting carbon losses from permafrost which stores approximately 1600 Pg of carbon, is unclear, however if released this amount of carbon would cause a considerable rise in global CO_2 levels (Makhalanyane *et al.,* 2016).

As well as the impact on global nutrient cycling, microbial ecosystems influence glacial melt. For example, Zygnematophyceae micro-algae of the Greenland icesheet have the potential to considerably influence the ice surface, including the level of melt due to its dark colour lowering the albedo of the ice. Given that the melting of the Greenland ice-sheet is singularly the biggest cryospheric donor to global eustatic sea-level rise, understanding the level of contribution that the ice-algae make to this melt is key in projecting impact (Williamson *et al*., 2018). Williamson and colleagues found that phenolic pigmentation permits extreme irradiance of up to ∼4,000 µmol photons·m^{-2}·s^{-1} to be tolerated by the ice-algae whilst captured ultraviolet and short-wave radiation drives melt generation, contributing up to an additional ∼1.86 cm water equivalent ice surface melt per day (Williamson *et al*., 2020). This equates to a final overall melt attributed to the algae of ~14%.

Cryospheric microorganisms are also studied for their biotechnological applications, such as the eco-friendly advantages and potential application of their cold-adapted proteins and enzymes, which are capable of performing at lower temperatures and for their bioremediation capabilities (Singh *et al.,* 2015; Methé *et al.,* 2005). Cryospheric

microbiology is additionally valuable as an astro-biological model and for the fundamental exploration of ecology of life at the extremes (Martins *et al.,* 2017).

Clearly cryospheric microorganisms are of great relevance, surprisingly however, relatively little about cryospheric microbial life is known. As well as being conceptually difficult to understand (Cavicchioli, 2016), less than a hundred microbial genomes from the Arctic are currently available in public databases (Edwards *et al.,* 2020), in contrast to the tens of thousands from human associated habitats. Furthermore, rapid environmental changes due to global warming and glacial ice thawing will alter the microbial biodiversity of the cryosphere and crucially, could lead to potential extinction of endemic psychrophilic species. The preservation of endangered species needs to be extended to include microorganisms which have fundamental impacts on ecosystems and potentially harbour rich biotechnological resources (Griffith, 2012; Cockell and Jones, 2009). As such, the isolation, testing of the abilities and sequencing of cryospheric microorganisms needs to be a priority. Cryoconite in particular is a useful habitat to focus on due to the abundance of sample sources (cryoconite holes) and the biodiverse, densely populated communities that they harbour.

1.5 Thesis aims and objectives

The overarching aim of this thesis is to further the knowledge and understanding of cold-adapted microorganisms, specifically cryoconite inhabitants by identifying their physiological abilities, their responses and mechanisms for combating two cold-region stresses (temperature and light) and to gain genomic insight into these capabilities and therefore, the cryospheric microbial way of life. By examining both individual isolates and the microbial community, an understanding of the role and contribution discrete taxa provide within the wider community can begin to be constructed thus providing awareness of taxon-specific abilities and how they fit in to the inter-reliant cryoconite ecosystem.

Aims

1) To determine how individual cryoconite isolates respond to temperatures above and below 0 °C (+2 °C and -5 °C) and to assess the microcosm community response to diurnal freeze-thaw conditions by combining both temperature (+2 °C and -5 °C) and light stress (24-hour light and 24-hour dark).

2) To establish how both an individual isolate and the community revealed in culture respond to different light conditions (24-hour light and 24-hour dark) and whether the production of pigment offers any protection against light stress (UV irradiation).

3) To establish taxonomic distribution of the samples and to identify shock, stress and cold-adaptation genes as well as stress countering mechanisms, such as pigment production from assembled and annotated genomes and metagenomes.

Objectives

1) To assess the response from individual cryoconite heterotrophic isolates to temperatures above and below 0 °C , isolates from Svalbard 2011 cryoconite (S11) will be incubated in axenic culture at -5 °C. Colony Forming Unit per ml (CFU/ml^{-1}) and attenuance (at a wavelength of 600 nm) will be compared to that of pre-freeze values (+2 °C). To assess the community response to different temperature and light conditions (a simulated diurnal freeze/thaw cycle), the dissolved oxygen (DO) concentration of S11 microcosms will be measured periodically at +2 °C in 24-hour light then again following incubation at -5 °C in 24-hour dark.

2) To assess how the community revealed in culture responds to different light conditions and whether pigment production is constitutive or in response to illumination, Svalbard 2016 cryoconite (S16) replicates (using velvet stamping) will be placed under continual dark / light conditions. The proportion of conspicuously pigmented colonies in each condition will be recorded. To assess the response of an individual cold-adapted representative isolate (A18.2) to different light conditions,

A18.2 will be grown in axenic culture under 24-hour light and 24-hour dark conditions. Pigment produced by A18.2 will be extracted and using a range of wavelengths (350 – 525 nm) peak absorbance will be established. Additionally, cultures of A18.2 grown axenically under both light and dark conditions will be subjected to UV irradiation from 20,000 – 200,000 µ Joules. The resulting growth will be compared to growth pre-exposure.

3) Assembly and annotation will be performed on both a Svalbard 2019 (S19) and Greenland 2018 (G18) cryoconite metagenome as well as the A18.2 isolate. Representative genomes for S11 isolates will be obtained from National Center for Biotechnology Information (NCBI) and annotated. All genomes and metagenomes will be assessed for the presence of shock, stress and cold-adaptation genes as well as light detection and stress countering mechanisms, including pigment production and carotenoid biosynthesis genes. To establish taxonomic distribution of the community, both the metagenome and culturable representatives obtained from each sample type will have their 16S rRNA gene sequenced and identified. The A18.2 genome will also be assessed for identity.

1.6 Thesis overview

Using a combination of both wet laboratory and bioinformatics research approaches, cryoconite samples from both Svalbard and Greenland are assessed for their response and adaptive abilities to withstand and overcome cryospheric stresses. Two main types of stress are used, light and temperature. Both 24-hour dark and 24-hour light conditions are applied as well as temperatures above and below freezing (+2 °C and -5 °C) to both the cryoconite community as a whole and to individual isolates. Additionally, UV exposure as a form of light stress is applied to a selected cold-adapted representative, a heterotrophic isolate (A18.2) previously isolated by colleagues. The production of pigment as a predominant mechanism to counter cryospheric stress is assessed. Assembly and annotation of metagenomes and genomes followed by

surveying of shock, stress, cold-adaption associated, light-sensing and carotenoid biosynthesis genes is undertaken.

Hitherto, biological studies of cryoconite concentrated on either summer or winter communities. However, snapshots of community productivity do not acknowledge the capacity to recover and adapt rapidly to the transition between the seasons, day or night, or between freeze/thaw cycles, or indeed the potential mechanisms behind these responses. Here, the microcosm community tested demonstrated a rapid recovery following a freeze/thaw cycle. Furthermore, few studies examined the stress response and physiological abilities of individual taxa from cryoconite and primarily focused on the primary producer *Cyanobacteria*, specifically the *Phormidesmis spp*. Here, the heterotrophic bacterial isolates tested were able to produce increased CFU/ml $^{-1}$ after incubation at a sub-zero temperature. Moreover, previously, a limited number of studies examined cold-adaption in general or indeed the genomic ability of cryoconite microorganisms. Here, surveys of genes and stress response mechanisms from both individual taxa and the community identified a gene not previously recognized in cold-adaption. Additionally, the prevalence of light-sensing and carotenoid biosynthesis genes as well as the light-induced increase in pigment production demonstrated in both the community and an individual isolate reveals previously unstudied adaptive mechanisms of the cryoconite microbial community to cryospheric stresses.

By isolating, sequencing and identifying genomic mechanisms, as well as testing and identifying physiological abilities and responses to light and temperature stress not previously documented in cryoconite microorganisms, knowledge of the cryospheric microbial way of life has been extended.

2 - How does the cryoconite microbial community respond to different temperature and light stresses, and what mechanisms to counter these stresses are employed?

2.1 Introduction

2.1.1 Community composition

Numerous studies compare cryoconite from across the globe, including the Arctic and Antarctic, from glaciers in China to Alpine regions and beyond. Although a range of subtle differences are observed, be they biological, physical, mineralogical, or geochemical, many common characteristics and similarities are found giving cryoconite a fairly typical taxonomic profile (Mueller *et al.,* 2001; Mueller and Pollard, 2004; Langford *et al.,* 2010; Pautler *et al.,* 2013; Edwards *et al.,* 2014). Cryoconite harbours a diverse community of several trophic levels (Cook *et al.,* 2016a), bacteria dominate (Kaštovská *et al.,* 2005) but various other eukaryotic, archaeal, and viral organisms are found (Hodson *et al.,* 2008). Both culture dependant and culture independent analysis of the bacterial diversity with the communities confirm the dominance of the Proteobacteria, Actinobacteria, Cyanobacteria, Bacteroidetes, Chloroflexi, Gemmatimonadetes and Acidobacteria (Margesin *et al*., 2002; Edwards *et al*., 2011; Gokul *et al*., 2016; Anesio *et al*., 2017). Food webs are supported by photoautotrophic primary producers which use solar energy to fix atmospheric CO_2 into organic matter (OM). The main primary producers are the Cyanobacteria which as well as fixing C, promote cryoconite granule growth by entangling minerals and OM. Remarkably, 75% - 95% of the available C in cryoconite has been attributed to cyanobacterial photosynthesis alone (remaining C fixation due to heterotrophic uptake) (Stibal and Tranter, 2007). In Arctic regions *Phormidesmis spp.* represent the majority of the *Cyanobacteria* in cryoconite, indeed a single species, *P. priestleyi* dominates (Segawa *et al.,* 2017). Heterotrophic organisms metabolise the OM fixed by primary producers in addition to OM deposited from external sources (Boetius *et al.,* 2015; Cook *et al.,* 2016a).

Although the mineral particles deposited by the wind tend to be retained from season to season (Boetius *et al.,* 2015), the structure of the microbial community, especially the

heterotrophic genera, varies depending upon environmental factors and as such the community composition evolves during the melt season (Anesio and Laybourn-Parry, 2012; Anesio *et al.,* 2017) likely due in part to the continuous flushing by meltwater as well as the increase in light levels, temperature and water availability (Hodson *et al.,* 2008). Though the heterotrophic bacterial community are diverse compared to the autotrophic community (Anesio *et al.,* 2017), a dominant core of bacterial phyla is apparent, as described, thus a central community structure exists; the Cyanobacteria, both filamentous ecosystem engineer and primary producer, and the heterotrophic Proteobacteria and Actinobacteria, the latter of which are thought to humify OM, darkening the cryoconite and lowering albedo (Gokul *et al.,* 2016). However, relatively little is known about the cryoconite heterotrophic taxa and the role they play within the community, although they are clearly abundant, participating members.

2.1.2 Community productivity

Measurements of respiration and bacterial carbon production reveal that this cosmopolitan cryoconite community of autotrophs and heterotrophs has the capacity to contribute significantly to carbon cycling (Säwström *et al.,* 2002; Hodson *et al.,* 2007). The rates of photosynthesis are comparable to Arctic lakes, where temperatures can reach 15 °C (cryoconite hole temperature ~0.1 °C) and to microbial activity in the soils and sediments of temperate regions (Hodson *et al.,* 2008; Anesio *et al.,* 2009; Hodson *et al.,* 2010). Anesio and colleagues estimated that globally, cryoconite (on all the glacial surfaces in total, except Antarctica) has the potential to fix as much as 64 Gg of C per year (calculated by subtracting 34Gg of carbon released by community respiration from 98 Gg of carbon fixed by photosynthesis) (Anesio *et al.,* 2009). During the summer months, the net autotrophic nature of the community is thought to be due to both this positive balance between photosynthesis and respiration and to the ability of organisms to trap or transform the OM derived from allochthonous sources (Anesio and Laybourn-Parry, 2012).

2.1.3 Seasonal and diurnal variation

Evidently the cryoconite community demonstrates high levels of microbial activity during the summer months. Less in known about the levels of activity in cryoconite communities over winter, due partly to the difficulty accessing the field sites during that time of year, although some remote sensing efforts are made (Takeuchi, 2002; Chandler *et al.,* 2014). In studies of Arctic soil, there is evidence that the microbial communities remain active during the winter at <-10 °C (Oechel *et al.,* 1997), whilst it is thought around 20% of the permafrost microbial community can still grow at temperatures as low as –10 °C (Rivkina *et al.,* 2018). However, in other cold regions, such as an Antarctic lake, the microbial community was found to over-winter, returning to an active metabolic state once spring melt begins (Foreman *et al.,* 2011). During the day in the summer months whilst cryoconite holes experience positive temperatures (~0.2 °C water in cryoconite holes in Svalbard (Säwström *et al.,* 2002; Zawierucha *et al.,* 2019) at night, negative, sub-zero temperatures are observed (–0.1 °C Säwström *et al.,* 2002). Nevertheless, these low temperatures are often warmer by 5 °C or more than the air temperature due to the insulative properties of the hole and internal heating (Fountain *et al.,* 2008). Although several studies examine the diurnal activity of the cryoconite community at low temperatures under light or dark conditions (Stibal and Tranter, 2007; Telling *et al.,* 2010; Bagshaw *et al.,* 2016; Franzetti *et al.,* 2017; Hodson *et al*., 2017) to my knowledge, none monitor the speed of the response. How quickly can the community respond and adapt when presented with changing cryospheric stresses?

2.1.4 Mechanisms to counter cryospheric stresses

Even during the summer when environmental conditions are more favourable, the microbial inhabitants face additional stressful conditions such as exposure to high levels of ultraviolet (UV) irradiation (Boetius *et al.,* 2015). As mentioned in Chapter 1, microorganisms in these extreme environments need to employ specialist strategies. These include tactics such as the release of protective EPS, CSPs, AFPs, pigments and alternate membrane lipid compositions to ensure that the outer membrane is an efficient, flexible interface and protect it against rigidity (Varin *et al.,* 2012; Boetius *et al.,* 2015; Ram *et al.,* 2020). It is thought that EPS production by the cryoconite

cyanobacterial *P. priestleyi* BC1401 is a significant factor in its efficient survival in cold environments (Chrismas *et al.,* 2016). Several AFP producing bacteria have been isolated from Arctic cryoconite (Singh *et al.,* 2014a), as well as isolates with CSP genes (Singh *et al.,* 2015). Pigment-production, specifically carotenogenesis is well documented in bacteria from cold environments where these secondary metabolites have a dual purpose; they perform a photoquenching role for the high levels of UV radiation experienced and they are found in the lipid bilayer to stabilise the membrane (Mueller *et al.,* 2005; Dieser *et al.,* 2010; Shen *et al.,* 2018; Vila *et al.,* 2019). Heterotrophic carotenoid producing bacteria from cold environments are shown to tolerate higher levels of environmental stresses compared to non-pigment producing community members (Dieser *et al.,* 2010). However, although some pigmented species have been isolated from cryoconite (Zhang *et al.,* 2011; Schumann *et al.,* 2012) to my knowledge, just a single study on the pigmentation by the phototrophic (primary producers) of the community has been conducted (Perkins *et al.,* 2017) and no studies on the heterotrophic bacterial pigmentation of cryoconite communities to date.

2.1.5 Summary

Clearly the cryoconite community, comprised of biodiverse multi-trophic taxa, is very active during the day in the summer months. Less in known about community activity at night or during the winter when light levels and temperature decrease. Less still, if anything, is known about the mechanism and speed of the response to these changing conditions, the transition stage and adaptive response. Furthermore, pigmentation although evidently extremely useful and common in cold bacterial communities, is scarcely understood in the cryoconite autotrophic community and not at all within the heterotrophic community. Thus, this work is an effort to further knowledge and understanding of the community's abilities and responses to cryospheric stresses experienced by Arctic cryoconite (i.e., continual, 24-hour dark vs continual light, and frozen, sub-zero temperatures vs thawed, positive temperatures). Additionally, the taxonomic distribution of the community and the genes involved in such responses and stress countering mechanisms are investigated using metagenomics.

2.1.6 Aims and Objectives

Aims

1) To establish how the cryoconite microbial community responds to temperatures above and below 0 °C (+2 °C and -5 °C) and to different light conditions (24-hour light and 24-hour dark) and identify how quickly responses occur.

2) To test whether the production of pigment under different light conditions is a prevalent response among the heterotrophic community revealed in culture and to determine whether pigment production differs in response to illumination.

3) To identify taxonomic distribution of the samples, both isolation and axenic culture of viable bacteria as well as metagenomic sequencing of the 16S rRNA genes will be performed. Then, in order to investigate the community metagenomics and identify cryospheric stress countering mechanisms, such as pigment production, a survey of predicted genes will be completed.

Objectives

1) The dissolved oxygen (DO) concentration of Svalbard cryoconite microcosms as a measure of net photosynthesis/respiration will be recorded. Firstly, a baseline for both light and dark conditions at +2 °C will be established. Then a diurnal freeze/thaw cycle will be set up where microcosms will be subjected to a shift from thawed, lit conditions to sub-zero, dark conditions before finally returning to thawed, lit conditions. Microcosms will experience +2 °C in the light to -5 °C in the dark and back again to +2 °C in the light. The DO concentration will be recorded periodically throughout.

2) Svalbard cryoconite sample dilutions will be plated on solid media, incubated +2 °C in dark conditions for four weeks, replicated using velvet stamping before being placed under continual dark and light conditions at +2 °C for four weeks. The

proportion of conspicuously pigmented and non-pigmented colonies produced following light and dark conditions will be recorded by eye.

3) Metagenomic assembly and annotation will be performed on both the Svalbard 2019 and Greenland 2018 cryoconite metagenomes (these samples were previously sequenced by colleagues), the cryoconite samples of which were also used for isolation purposes. Both metagenomes will be assessed for functionality, specifically their stress response and the presence of cold and heat shock genes to determine the putative mechanisms behind the responses to cryospheric stresses and therefore adaptability. Additionally, the metagenomes will be assessed for light detection and pigment biosynthesis genes to determine the capacity of each community to respond to light and produce or up-regulate pigment. Lastly to establish taxonomic distribution of the community, both the metagenome and culturable representatives obtained from each sample type will have their 16S rRNA gene sequenced and identified.

2.2 Materials and Methods

2.2.1 Sample details and preparation

All samples used for this research were kindly made available by Arwyn Edwards, Joseph Cook and Melanie Hay, who collected them from cryoconite holes on glacier surfaces in either Svalbard or Greenland. All were subsequently transported and stored frozen at -20 °C and when needed, were allowed to thaw slowly (24-72 hours depending on sample size) surrounded by crushed ice in a polystyrene box at +2 °C. All samples were then used as quickly as possible. **Table 1** provides an overview of the sample source and experimental work.

After thaw, the S11 cryoconite sample (approximately 250 g, contained in double bagged whirl bags, collected from Svalbard, Foxfonna in 2011), was distributed evenly in a single grain layer in sterile Petri dishes, covered with 15 ml of sterile Milli-Q® water

and placed in light conditions (on a surface 2 feet under an array of ten natural white, 18W LED = 40W standard 1200 mm tubes ((1800 lumens ± 10%)) at +2 °C (throughout all reference to culture or microcosms placed in the light refers to under the same light array at the same distance). The sample was kept in the light at +2 °C and a further 5 ml of sterile Milli-Q® water was added to the Petri dishes as often as needed to retain moisture levels. The S11 sample was used for both microcosm experiments.

A small amount of additional cryoconite sample (S16, sub-samples FIC05, FIC07 and FIC10, collected from Svalbard, Foxfonna in 2016 was used for another community-based experiment.

The remaining samples (S19, G17 and G18) were used for isolation and metagenomic purposes only. Once thawed, due to the small volume, samples were kept in either 2 ml microcentrifuge or larger 50 ml conical centrifuge tubes with sterile Milli-Q® water to cover, rather than placed in Petri dishes. They were also stored in the light at +2 °C and used as quickly as possible.

Table 1. Sample source and experimental work. The cryoconite sample of the largest volume collected from Svalbard in 2011 (S11) was used for the two microcosm community experiments and for isolation. The remaining samples which were of smaller volume, were used for a single community experiment (S16), for isolation only (G17) and for isolation and metagenomics (S19 and G18).

Sample ID	Source	Experiment
S11	Svalbard, Foxfonna, summer 2011 (78.1333/16.2000)	*Microcosm oxygen production under dark and light conditions* *Microcosm recovery under simulated winter condtions* *Isolation & sub-zero growth with S11 isolates (Chapter 3)*
S16 (sub-samples FIC05,FIC07 and FIC10)	Svalbard, Foxfonna, summer 2016 (78.1333/16.2000)	*Pigmentation under dark and light conditions*
S19	Svalbard, March 2019 (78.91047/11.71736)	*Isolation & metagenome*
G17	Greenland summer 2017 (67.119/47.878)	*Isolation*
G18	Greenland winter 2018 (67.119/47.878)	*Isolation & metagenome*

2.2.2 Microcosm dissolved oxygen concentration under dark and light conditions

A 1000X stock solution of Artificial Melt Water Solution (AMWS) (Gokul, 2017) was prepared by adding the following to sterile Milli-Q® water to obtain the final concentration; 0.7 mg/L $^{-1}$ NaCl, 0.015 mg/L $^{-1}$ NH_4NO_3, 0.06 mg/L $^{-1}$ KH_2PO_4, 1 mg/L $^{-1}$ $MgSO_4$, 0.5 mg/L $^{-1}$ $CaCl_2$, 0.2 mg/L $^{-1}$ Na_2CO_3, with the following carbon sources, 0.1 mg/L $^{-1}$ sodium acetate, 0.1 mg/L $^{-1}$ glucose and 0.2 mg/L $^{-1}$ galactose. The pH was adjusted to pH 6 before topping up to a litre with additional sterile Milli-Q® water. The AMWS was then filter sterilized. 1 ml of 1000X AMWS was added to 99 ml of sterile Milli-Q® water to create a 1X working solution.

2 g of cryoconite was added to each of eight sterile glass 100 ml sized reagent bottles with necks and stoppers. 1X AMWS was added to the cryoconite at a ratio of 50:1, thus 100 ml was added per bottle. For controls, 100 ml of 1X AMWS only (2 bottles) were set up. Each bottle was swirled gently to mix, left to settle for five seconds, before being stoppered slowly to avoid air bubbles. All 10 bottles were incubated in the light at +2 °C for 24 hours. Then using a polystyrene box filled with crushed ice to maintain temperature, the microcosms were withdrawn, opened slowly in a laminar flow hood and the dissolved oxygen (DO) concentration was recorded using a calibrated Orion DO probe (Thermo Scientific Orion Star™ A329 RDO/DO portable meter with an Orion optical cap probe, polarized then calibrated using the water-saturated air method as per manufacturer's instructions). DO percentage saturation, DO mg/ml and temperature were recorded. In between each measurement, the probe was swirled in Milli-Q® water to cleanse it. After each DO measurement, the stopper was returned slowly to its bottle, avoiding air bubbles. Four of the microcosm bottles and one of the controls were then wrapped in foil and all ten were then placed back in the light at +2 °C for a further 24 hours. Again, using a polystyrene box filled with crushed ice to maintain temperature, all 10 bottles were withdrawn and DO readings were recorded in the same manner.

2.2.3 Microcosm recovery after freeze/thaw

2 g of cryoconite was added to each of four sterile glass reagent bottles with necks and stoppers. 1X AMWS was added to the cryoconite at a ratio of 50:1, thus 100 ml was added per bottle. As a control, AMWS only (four bottles) were set up. Each bottle was swirled gently to mix, left to settle for five seconds, before being stoppered slowly to avoid air bubbles. All eight bottles were incubated in the light at +2 °C for 24 hours. Then using crushed ice in a polystyrene box to maintain temperature, the microcosms were withdrawn, opened slowly in a laminar flow hood and the dissolved oxygen (DO) concentration was recorded. In between each measurement, the probe was swirled in Milli-Q® water to cleanse it. After each DO measurement, the stopper was returned slowly to its bottle, avoiding air bubbles. All eight bottles were placed back into the light at +2 °C for a further 24 hours. Again, the bottles were withdrawn and DO readings were taken in the same manner as described. All eight bottles were placed back into the light at +2 °C for a further five days before being withdrawn again in the same manner as described and DO readings were taken (day 7). The bottles were then placed into the dark in the freezer at -5 °C for 24 hours. All eight bottles were then withdrawn and placed back into the light +2 °C to thaw. Once they were thawed enough, DO readings were taken periodically (day 9, day 10 and day 14) using the same method detailed, until the end of the experiment (day 14).

2.2.4 Pigmentation under dark and light conditions

Standard dilution series procedure was conducted for each of the S16 sub-samples (FIC05, FIC07 and FIC10). Briefly, 1 g of cryoconite was added to 99 ml of sterile Milli-Q® water, vortexed, and while still in suspension, 1 ml was withdrawn and added to a further 9 ml of sterile Milli-Q® water. These steps were repeated to produce a dilution series up to 10^{-4} for each sub-sample. A 500 µl volume of each 10^{-2}, 10^{-3} and 10^{-4} dilution was plated and spread (in triplicates) using sterile glass beads onto Reasoner's 2A (R2A) agar (LAB M; Yeast Extract 0.5 g/L, Meat Peptone 0.5 g/L, Casamino Acid 0.5 g/L, Glucose 0.5 g/L, Starch 0.5 g/L, Dipotassium Hydrogen Phosphate 0.3 g/L, Magnesium Sulphate 0.05 g/L, Sodium Pyruvate 0.3 g/L) (Reasoner and Geldreich.,

1985) incubated at +2 °C in dark conditions and checked periodically for signs of growth. Once multiple colonies had emerged (at four weeks of growth) plates were selected for the velvet stamping transfer experiment. Briefly, plates were chosen that had enough spaced out, discrete colonies and were chosen from each of the sub-sample types (FIC05, FIC07 and FIC10) as well as from different dilutions to ensure a full representation of the sample. The selected plates were marked with an * to use as a point for orientation and using sterile velvet swatches tied to wooden blocks, the plates were copied onto the velvet using gentle pressure (Lederberg and Lederberg, 1952), before being transferred to two fresh R2A plates. The plates were then incubated at +2 °C in both light and dark conditions for four weeks (one in dark and one in light from each 'stamp'). The mean ratio (as a percentage) of conspicuously pigmented vs. non-pigmented under both light and dark conditions was determined for each "stamp set" (replica set of plates, one of each placed under dark and light) and for the sample as a whole. Colony counts were taken by eye from each of the plates. Visibly pigmented colonies were deemed pigmented whereas colonies not visibly pigmented were deemed non-pigmented.

2.2.5 Isolation

Due to the likely low biomass nature of the S11 cryoconite, just a 10^{-1} dilution was prepared (assigned as full strength). Both that and a 50:50, 10^{-1} dilution: Milli-Q® water (assigned as half strength) were used with no further dilution steps required. Briefly, 1 g of cryoconite was added to 9 ml of sterile Milli-Q® water and vortexed to create the 10^{-1} dilution. 500 µl volume of each (full and half strength) were plated and spread (in triplicates) using sterile glass beads onto R2A agar and incubated at +2 °C, placed in light and dark conditions, and checked periodically for signs of growth. Once colonies emerged, morphologically distinct appearing colonies were gently 'picked' with an inoculating loop and the biomass was spread using the streak plate method onto fresh R2A. The resulting streak plates were assessed, and isolates were re-picked and sub-cultured as necessary until fully isolated. Once fully isolated, glycerol stocks were prepared (500 µl of culture was added to 500 µl of 50% glycerol in a 2 ml screw top

microcentrifuge tube) and the isolates were stored at –80 °C. The same method of isolation and storage was used for S19, G17 and G18 samples.

2.2.6 Isolate identity

To determine the identity of the 35 isolates (S11 A-M, S19 A-K, G17 A-E and G18 A-F), a colony polymerase chain reaction (PCR), using universal 16S rRNA gene primers was conducted. Following PCR, agarose gels to visualize the size of PCR products were conducted. After confirmation that the PCR was successful, an amp-pure bead clean-up was performed before sequencing. Once complete, the sequences were used to establish identity.

2.2.6.1 Colony PCR

The isolates were subjected to colony PCR, a method to directly perform PCR on isolates without the need for DNA extraction (Sebastião, *et al.,* 2015) using universal 16S rRNA gene primers (Invitrogen, 27F; AGAGTTTGATCMTGGCTCAG and 1389R; ACGGGCGGTGTGTACAAG). Briefly, a master mix was prepared with 10 µl of OneTaq® (NEB OneTaq® Quick-Load® 2X Master Mix M0486) 0.25 µl of 27F primer, 0.25 µl of 1389R primer, topped up with PCR grade nuclease free water to a final volume of 20 µl per reaction. Using a pipette tip, a small colony was added to 20 µl of master mix per PCR tube. Using a G-Storm pcr2 machine a PCR was ran with the following conditions: heated lid at 112 °C , hot start at 95 °C for 5 minutes, before 35 cycles of a denature step at 94 °C for 35 seconds, followed by an annealing step at 55 °C for 35 seconds and then an elongation step at 72 °C for 1 minute. To finish, the final elongation step at 72 °C was held for 5 minutes. PCR products were then stored at – 20 °C.

2.2.6.2 Gel electrophoresis

To visualize the PCR products, a 1.5% agarose (SYBR safe 1000X DNA stain) gel electrophoresis was run for an hour at 100 Volts. 5 µl of PCR product was loaded per

well. The gel was then viewed using a gel doc XR (Quantity One program, auto expose setting).

2.2.6.3 SPRI bead clean up

Beckman Coulter Solid Phase Reversible Immobilisation beads (SPRI) AMpure beads were left to come to room temperature before use, the PCR products were allowed to thaw slowly surrounded by crushed ice in a polystyrene before use. 15 µl of PCR product was transferred per well to a 96-well plate and the SPRI bead solution was shaken gently by hand to re-suspend all beads before being added to the wells in a ratio of 12 µl: 15 µl SPRI beads: PCR product. The wells were pipette mixed until homogenous and left at room temperature for 5 mins. The 96-well plate of PCR-bead solution was then placed on a magna-rack until all magnetic beads had been drawn to the magnets. This was left at room temperature for 5 mins for maximum recovery, until the supernatant was almost clear. A pipette was set to 25 µl and the supernatant removed at an angle to avoid beads. The beads were then washed twice with 200 µl of 70% ethanol, letting the ethanol incubate for 30 secs each time. The 96-well plate was then removed from the magna-rack and left to air dry. Finally, the PCR amplicons were eluted using elution buffer (10 mM Tris-HCl pH8) by adding 15 µl to each well and pipette mixing thoroughly. The elution buffer was left for 2 mins. Lastly, the 96-well plate was placed back over magna rack. The supernatant containing the amplicons (15 µl per sample) was pipetted up at an angle avoiding the beads. The cleaned-up PCR amplicons were then stored at -20 °C.

2.2.6.4 Sanger sequencing preparation

Using a 96-well plate, 8 µl of DES buffer, 1 µl of dilute primer (dilute primer is prepared in the ratio of 1 µl 16F primer:99 µl nuclease free water) and 1 µl of cleaned-up PCR amplicon were added per reaction. The sample was then sent for DNA sequencing. Briefly, a Terminator Ready Reaction Mix was used in the sequencing reaction

(Terminator Ready Reaction Mix 4 µl, 1.6 pmol primer, template PCR product 5-20 ng, deionised water q.s. up to a total volume of 10 µl). A PCR reaction was performed with the Big Dye Terminator kit and samples were ran on the ABI 3730 DNA analyser by Aberystwyth University IBERS staff member Caron Evans.

2.2.6.5 BioEdit and NCBI BLASTn

The sequences produced by the ABI 3730 DNA analyser were opened and edited in BioEdit (Hall, 1999). Briefly, the chromatograms from each isolate were viewed and the sequence trimmed before being submitted to the National Centre for Biotechnology Information (NCBI)'s Basic Local Alignment Search Tool for nucleotides (BLASTn) (Zhang *et al.,* 2000 ; Morgulis *et al.,* 2008) to establish closest identity.

2.2.7 Maximum likelihood tree construction

A Maximum likelihood bootstrap consensus tree comprising the partial 16S rRNA gene sequences obtained from isolates and the FASTA sequence of the closest species (highest % identity) available from NCBI (https://www.ncbi.nlm.nih.gov/) was generated using the phylogeny.fr platform (http://www.phylogeny.fr/) (Dereeper *et al.,* 2010; Dereeper *et al.,* 2008; Edgar, 2004; Castresana., 2000; Guindon and Gascuel, 2003; Anisimova and Gascuel, 2006; Chevenet *et al.,* 2006) and comprised the following steps; sequences were aligned with MUSCLE (v3.8.31) configured for highest accuracy, ambiguous regions were removed with Gblocks (v0.91b), the phylogenetic tree was reconstructed using the maximum likelihood method in the PhyML program (v3.1/3.0 aLRT) and lastly the tree was graphically represented and edited with TreeDyn (v198.3).

2.2.8 Metagenomic base calling and assembly

Shotgun metagenomes (G18 and S19) were kindly made available from fieldwork by Arwyn Edwards, Melanie Hay, Joseph Cook and Francesco Sauro in Greenland (G18) where cryoconite was extracted and sequenced using lyophilized chemistry as described

in Edwards *et al.,* 2019 and using LSK108 library preparation and sequencing in Svalbard (S19) by Arwyn Edwards. The Greenland (G18) metagenome FASTQ was assembled using wtdbg2 (Ruan and Li, 2019). Wtdbg2 is a *de novo* sequence assembler that assembles long, noisy reads. Briefly, the assembler component assembles raw reads and generates the contig layout and edge sequences, then the consenser produces the final consensus in FASTA. The Svalbard (S19) metagenome was not base called during sequencing and as such the FAST5 files from the sequencing run were base called using Guppy (version 3.3.0, Oxford Nanopore Technologies), which was the same version on the GPU base caller used by the MinIT to base call live when sequencing the G18 metagenome. The resulting FASTQ files generated from Guppy (S19) were also assembled using wtdbdg2. The pre- and post-assembly statistics were assessed using NanoPlot (De Coster *et al.,* 2018).

2.2.9 Metagenomic analysis

2.2.9.1 KAIJU

Kaiju, available at http://kaiju.binf.ku.dk/ (Menzel *et al.,* 2016), is a taxonomic classification program for metagenomic sequencing reads. Reads are translated into amino acid sequences and using protein-level classification, taxonomy is assigned in NCBI taxonomy by comparing to a reference database. To assign taxonomy for both metagenomes (S19 and G18), Kaiju, with the following parameters, was used; SEG low complexity filter: yes, Run mode: greedy, Minimum match length: 11, Minimum match score: 75 and Allowed mismatches: 5.

2.2.9.2 MG RAST

MG RAST, available at (https://www.mg-rast.org/) (Meyer *et al.,* 2008), was used for both taxonomic classification and functional analysis of the metagenomes (S19 and G18). MG RAST has a maximum length cut off (500,000 bp), as such, of the 8,991 contigs generated by the wtdbg2 assembler for the S19 metagenome, six (>500,000 bp) needed to be fragmented, whilst ensuring the fragments remained as large as possible, thus a

total of 9,000 sequences were submitted to MG RAST. The G18 metagenome did not contain any contigs over the threshold. The distribution of taxa were determined using a contig LCA (Lowest Common Ancestor) algorithm finding a single consensus taxonomic entity for all features on each individual sequence. Predicted protein functions annotated to each category (Clusters of Orthologous Groups (COGs), Non-supervised Orthologous Groups (NOGs), KEGG Orthology (KOs) and Subsystems) were generated. The following parameters were used in both taxonomic and functional assignment; alignment length: 15bp, e-value: e-5 and percent identity: 60%.

2.2.9.3 PROKKA

PROKKA, an annotation tool that locates open reading frames (ORFs) and RNA regions on contigs, translates ORFs to protein sequences and searches for protein homologs (Seemann, 2014), was used to annotate both metagenomes.

2.2.10 Statistical analysis

The IBM SPSS Statistics for Windows, Version 25.0. Armonk, NY: IBM Corp was used for statistical tests and analysis. Independent samples t-tests were performed. Microsoft Office Excel was used for standard calculations, such as dilution factors and percentages.

2.3 Results

2.3.1 Microcosm dissolved oxygen concentration under dark and light conditions

After incubation at +2 °C in the light for 24 hours, the mean dissolved oxygen (DO) concentration (mg/ml) in both microcosms (n=8) and controls (AMWS only) (n=2) was a consistent 7.5 mg/ml. This baseline DO concentration is shown in **Figure 5 A**). Following a further 24 hours in either light (n=4) or dark (n=4) conditions, the mean increase in DO concentration in dark and light microcosms is 0.085 and 2.325 mg/ml respectively. The change in DO concentration following the separation into light and dark conditions, once blank corrected (subtracting the control (AMWS value) from the microcosm value), is

shown in **Figure 5 B**). A significant difference between the dark and light microcosm DO concentration is seen. An independent samples t-test returned a Levene's value of $p>0.05$ ($F=2.607$, $p=0.157$) thus equal variances were assumed and with a two-tailed significant value of $p<0.05$ ($t_6 = -3.198$, $p=0.019$), we can conclude that there is a statistically significant increase in DO concentration and therefore net oxygen production in light compared to dark microcosms in the 24-hour period assessed. Furthermore, the significant decrease in DO concentration in dark microcosms compared to light microcosms demonstrates net oxygen consumption by the heterotrophic community.

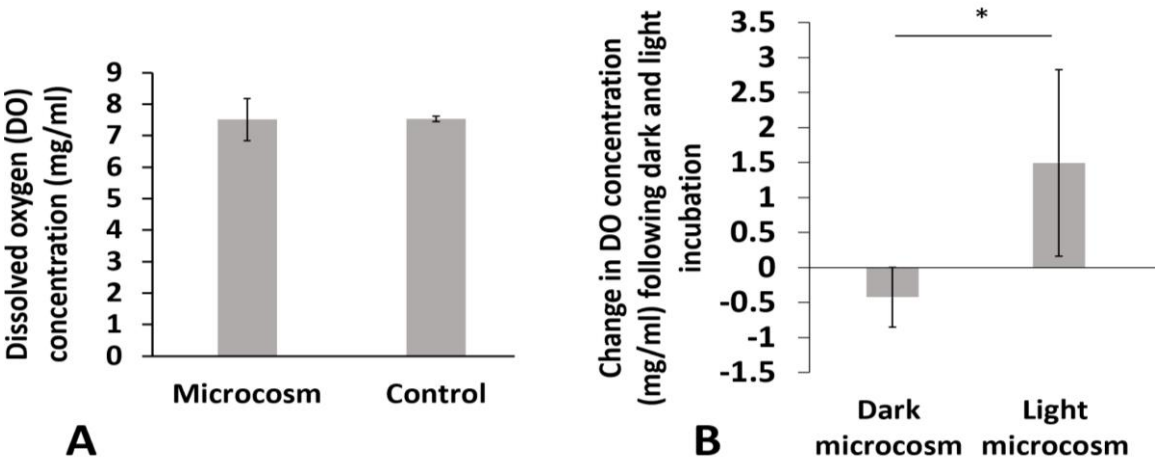

Figure 5. Microcosm community oxygen production. **A)** Average (mean) DO concentration (mg/ml) in microcosms (n=8) incubated at +2 °C in light conditions for 24 hours vs controls (n=2) were plotted in Excel. After 24 hours of incubation, the mean DO concentration was 7.5 mg/ml for both. **B)** Following the initial 24-hour incubation, microcosms were returned to the light (n=4) for a further 24 hours or placed in dark conditions (n=4) for 24 hours. The average (mean) increase or decrease of DO (mg/ml) produced in the 24-hour period in both conditions is plotted. Light microcosms showed a significant ($p<0.05$) increase in DO concentration compared to dark microcosms ($t_6 = -3.198$, $p=0.019$). (Errors bars shown are ± one standard deviation). (Statistical significance, where present, is designated with a horizonal bar and asterisk; $p<0.001$ ***, $p<0.01$ ** and $p<0.05$ *).

2.3.2 Microcosm recovery following freeze/thaw

Following a 24-hour incubation in the dark at -5 °C, the microcosms placed back into +2 °C light conditions recovered and reached pre-freeze DO concentration levels within 48

hours (**Figure 6**). On day 7 prior to being frozen, both microcosm (n=4) and control (n=3) mean DO concentration were ~13 mg/ml, with microcosm slighlty higher. Post-freezing and once thawed, the mean microcosm DO concentration at day 9 was 11.15 mg/ml compared to the control DO concentration of 13.83 mg/ml, which is a highly significant difference in microcosm vs. control ($p<0.001$). An independent samples t-test returned a Levene's value of $p>0.05$ ($F=5.642$, $p=0.064$) thus equal variances were assumed and with a two-tailed significance value of $p<0.001$ ($t_5= -10.719$), we can conclude that there is a highly statistically significant decrease in DO concentration and therefore oxygen production post-freezing in the microcosm compared to the control at day 9. By day 10 however no significant statistical difference between control and microcosm is found (Levene's $F=3.115$, $p=0.138$) ($t_5= -1.210$, $p=0.28$) thus the rapid community response and corresponding increase in net oxygen production in the 24 hour period post-thaw (day 9-10) brought the mean microcosm DO concentration almost level with the control (13.6 mg/ml) and back to the same microcosm pre-freeze level of 13.4 mg/ml. By day 14 the mean microcosm DO concentration was again slightly higher than that of the control at 13.7 mg/ml, vs. the control of 13.5 mg/ml. The gradual increase in the DO concentration of the control (AMWS only) over the 14 day period could be due to disequilibrium with the atmosphere and is discussed further in the discussion.

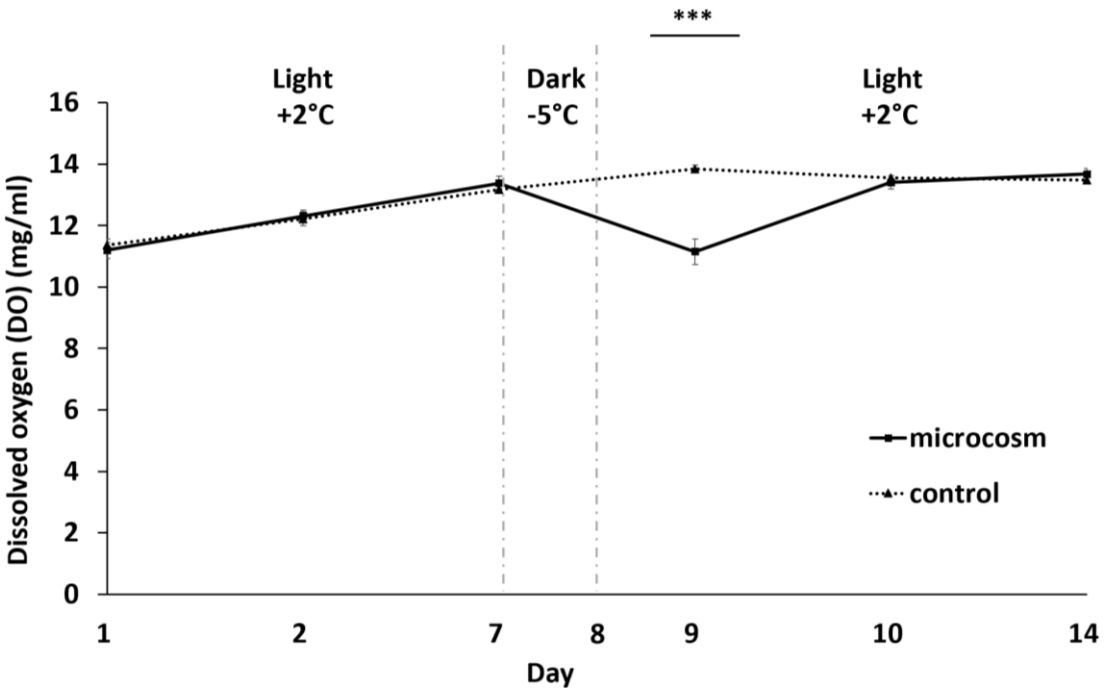

Figure 6. Microcosm community recovery following freezing, dark conditions. Following incubation at +2 °C in light conditions for 7 days, microcosms (cryoconite and 1X AMWS (Artificial Melt Water Solution)) were frozen at -5 °C (in the dark) for 24 hours (n=4). Placed back into +2 °C light conditions, once thawed (day 9), mean Dissolved Oxygen (DO) readings (day 9, day 10 and day 14) are plotted (n=4) using Excel. Controls (1X AMWS only) (n=3) are also plotted (Excel). On day 7 prior to being frozen, both microcosm and control mean DO concentration were ~13 mg/ml. Post-freezing and once thawed, the mean microcosm DO concentration at day 9 was 11.15 mg/ml compared to the control DO concentration of 13.83 mg/ml, a statistically significant reduction in DO ($p<0.001$). A day later (day 10) the mean microcosm DO concentration had increased to 13.4 mg/ml, just below the control mean (13.6 mg/ml). By day 14 the mean microcosm DO concentration was slightly higher than that of the control (13.7 mg/ml and 13.5 mg/ml respectively). (Errors bars shown are ± one standard deviation). (Statistical significance, where present, is designated with a horizonal bar and asterisk; $p<0.001$ ***, $p<0.01$ ** and $p<0.05$ *).

2.3.3 Pigmentation under dark and light conditions

The proportion (mean percentage) of conspicuously pigmented colonies in the culturable community under light and dark conditions at three and four weeks of growth are plotted in **Figure 7.** At three weeks of growth **Figure 7 A**) a significantly higher proportion of pigmented colonies on plates under light conditions compared to plates under dark conditions was observed. An independent samples t-test returned a Levene's value of $P>0.05$ ($F=0.222$, $p=0.646$) thus equal variances were assumed with a two-tailed significance value of $p<0.01$ ($t_{12} = 4.121$, $p=0.0014$). By week four **Figure 7 B**), the

proportion of pigmented colonies under light conditions compared to dark conditions increased further. An independent samples t-test returned a Levene's value of P>0.05 (F= 0.076, p=0.788) thus equal variances were assumed and a two-tailed significance value of p<0.001 (t_{12} = 4.765) was determined.

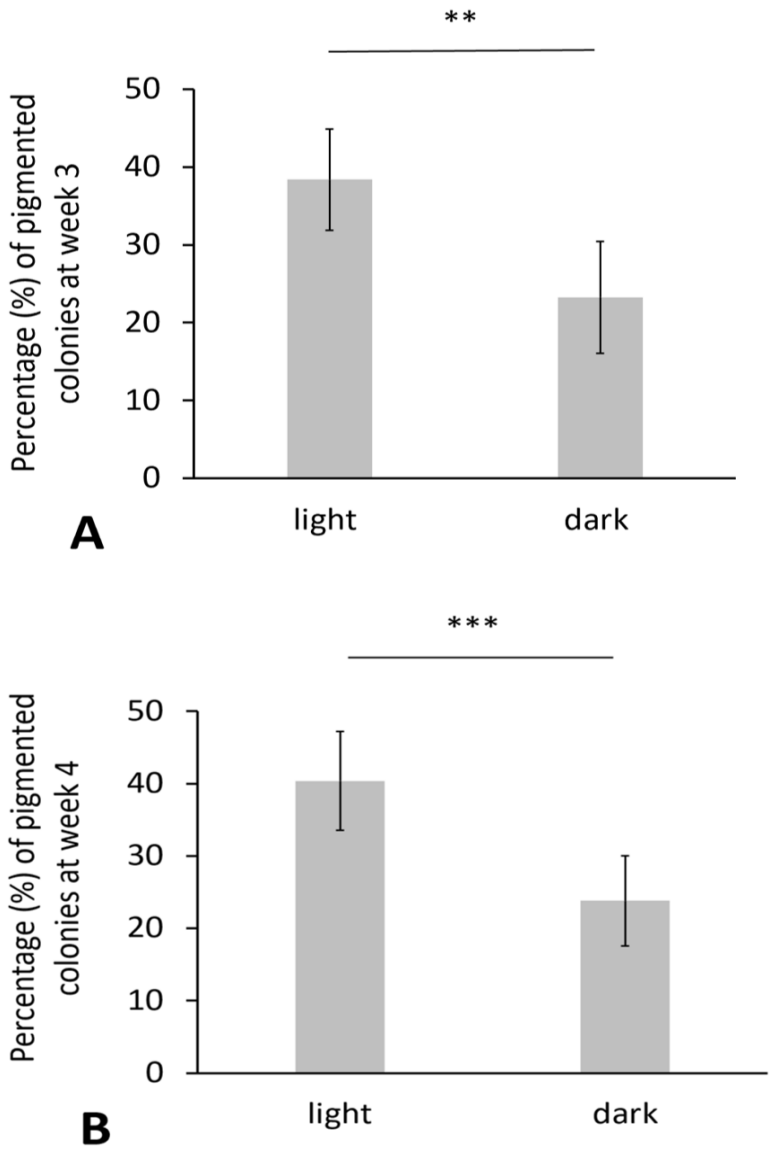

Figure 7. The proportion of conspicuously pigmented colonies in the culturable community under light and dark conditions. The mean pigmented colony percentage (%) in light (n=7) and dark (n=7) conditions were plotted in Excel. **A)** Three weeks of growth. Duplicate plates placed under both light and dark conditions grown for three weeks showed a significantly higher proportion (p<0.01) of pigmented colonies in the light. **B)** By week four, the abundance of pigmented colonies in light vs dark conditions increased further (p<0.001). (Errors bars shown are ± one standard deviation). (Statistical significance, where present, is designated with a horizonal bar and asterisk; p<0.001 ***, p<0.01 ** and p<0.05 *).

The higher proportion of visibly pigmented colonies in the culturable community under light conditions was due to the absence of visible pigmentation in counterpart colonies under dark conditions (**Figure 8**), however of note is the intensity of pigmentation. Plates under light conditions frequently had more intense pigmentation (**Figure 9**) compared to counterpart colonies grown in the dark, although they too were pigmented.

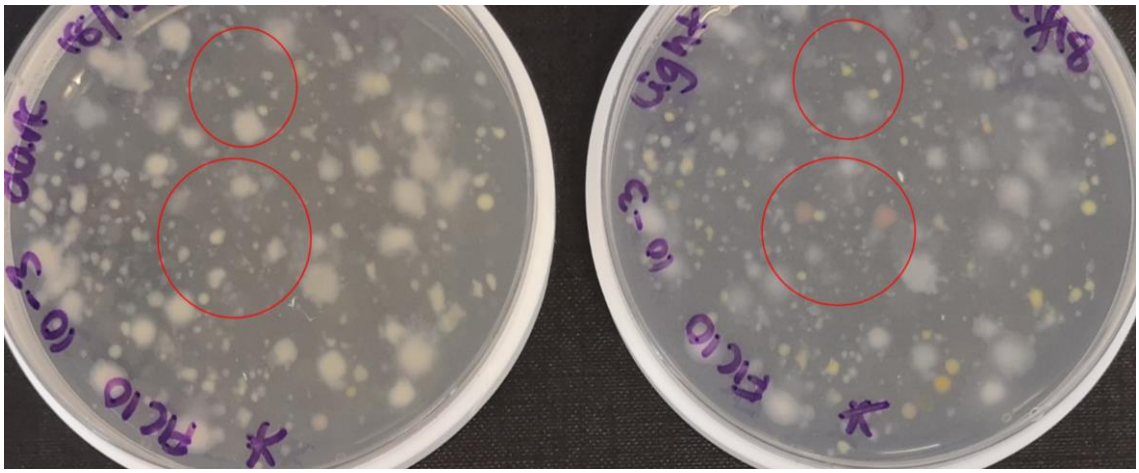

Figure 8. Plates grown in the light have pigmented colonies which (by eye) in the dark counterpart colony is lacking. In many cases no pigmentation was visible by eye in corresponding dark counterpart colonies, seen here (some examples are circled) at four weeks of growth. Also note the abundance of cloudy looking white cream colonies (suspected overgrowth of the yeast *Mrakia* or *Mrakiella spp*.). Dark plate on the left, light plate on the right. The asterisk * was used for orientation. Image taken with plates side by side, same lighting and capture conditions.

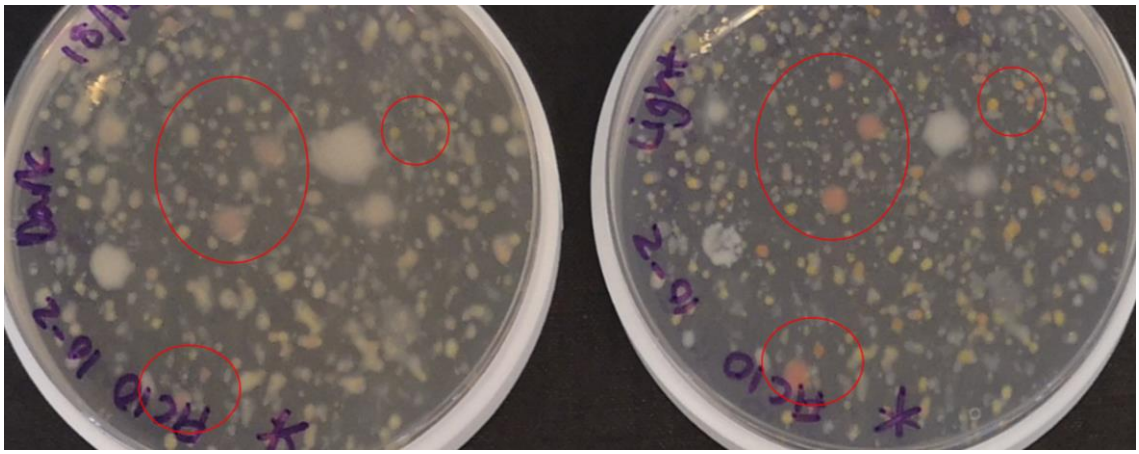

Figure 9. Plates grown in the light have more intense pigmentation in colonies compared to counterpart colonies grown in the dark. The brightness or intensity of the pigmented colonies in the light compared to their counterparts in the dark, seen here at four weeks growth (some examples are circled), is increased. Also note the abundance of cloudy looking white cream colonies (suspected overgrowth of the yeast *Mrakia* or *Mrakiella spp*.). Dark plate on the left, light plate on the right. The asterisk * was used for orientation. Image taken with plates side by side, same lighting and capture conditions.

2.3.4 Isolate identity and phylogeny

Of the colony PCR products obtained from the 35 isolates (13 isolates from cryoconite sample S11, 11 isolates from sample S19, five isolates from sample G17 and six isolates from sample G18) and checked for success using gel electrophoresis, 18 were cleaned up and sent for sequencing. Of the sequences retrieved following sequencing, 17 were complete enough to be used in BLASTn to identify the genus/species (**Table 2**).

Table 2. Isolate identity. The 16S rRNA gene of 17 isolates were successfully sequenced following colony PCR using universal 16S rRNA gene primers. The sequences obtained were trimmed using BIOEDIT and submitted to NCBI BLASTn. The resulting nearest match identity and percentage, query cover, length and E-value are shown in the table below. Where E-value is given as 0.0, the value for E is $<1x10^{-20}$

Source	Isolate ID	Isolate colour	Closest match	Identity (%)	Query cover (%)	Query length (bp)	E -value
Svalbard 2011	S11C	White	*Polaromonas* sp. strain EXB-L-2565	99.86	100	718	0.0
	S11F	Cream	*Polaromonas glacialis* strain HCR18h	100	100	847	0.0
	S11I	Peach	*Variovorax* sp. HW81	99.84	100	641	0.0
	S11L	Pale orange	*Polaromonas* sp. strain EXB-L-2565	94.16	100	253	7e-102
	S11M	Bright orange	*Pseudomonas* sp. strain ANT_J9B	92.06	100	701	0.0
Svalbard 2019	S19B	Yellow	*Flavobacterium* sp. CGMCC 1.09831	98.18	99	933	0.0
	S19C	Bright orange	*Cryobacterium psychrotolerans* strain BMP52	99.69	100	954	0.0
	S19D	Red	*Hymenobacter* sp. strain Co722	98.88	100	892	0.0
	S19E	Cream	uncultured Oxalobacteraceae	95.39	99	457	0.0
	S19F	Cream/pale peach	*Polaromonas* sp. strain EXB-L-2565	95.35	100	171	5e-69
Greenland 2017	G17A	Cream/pale pink	*Massilia eurypsychrophila* strain cACR1c.1	99.67	100	909	0.0
	G17B	Cream/pale pink	*Massilia eurypsychrophila* strain cACR1c.1	99.89	100	875	0.0
	G17C	Cream	*Massilia eurypsychrophila* strain cACR1c.1	100	100	743	0.0
	G17D	Cream	*Duganella* sp. strain FT134W	91.07	93	239	7e-82
	G17E	Cream	*Massilia eurypsychrophila* strain cACR1c.1	100	100	781	0.0
Greenland 2018	G18A	Cream/pale pink	Oxalobacteraceae bacterium strain EXB-L-2132	98.53	100	612	0.0
	G18D	Yellow	*Undibacterium* sp. strain EXB-L-2060	99.55	100	666	0.0

The phylogeny of the 16S rRNA gene sequences obtained from the isolates and the closest species (% identity) sequence FASTA available from NCBI were examined by constructing a maximum likelihood bootstrap consensus tree **(Figure 10).** The tree is dominated by the Proteobacteria phyla. The Gammaproteobacteria are shown in green and two families within the Betaproteobacteria are shown (blues), the Comamonadaceae family in dark blue and the Oxalobacteraceae family in light blue. The Bacteroidetes shown in pink and Actinobacteria in orange are also represented.

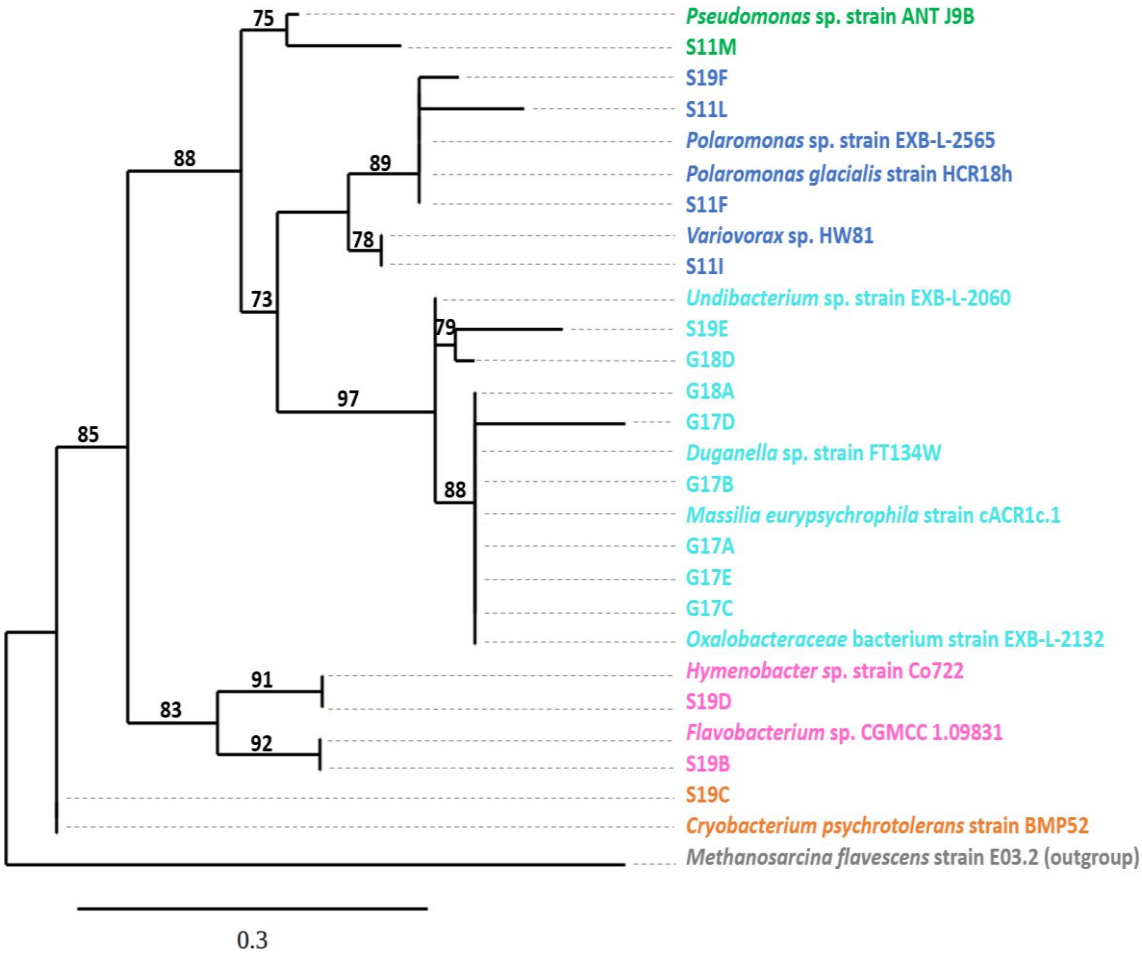

Figure 10. Maximum likelihood bootstrap consensus tree. The tree comprises the partial 16S rRNA gene sequences obtained from isolates and the closest species (% identity) sequence available from NCBI. Tree generated using PhyML (v3.1/3.0 aLRT) (bootstrap 100). Bootstrap values (greater than 70%) are displayed at the nodes. Scale shows nucleotide substitutions per site. The Proteobacteria phyla dominate the tree; Gammaproteobacteria are in green with the Betaproteobacteria in blues; the Comamonadaceae family in dark blue and the Oxalobacteraceae family in light blue. The Bacteroidetes in pink and Actinobacteria in orange are also represented.

2.3.5 Metagenomic assembly

The pre- and post-assembly metagenomic data for each sample type (location) compared in **Table 3.** Prior to assembly, the Svalbard metagenome had more than twice as many reads as the Greenland metagenome and over twice as many base pairs in total. Following assembly, Svalbard similarly had a little under double the number of total base pairs compared with the Greenland metagenome, however Greenland had two-thirds the number of contigs that Svalbard had. Yet, both the average contig length and N50 value for the Greenland metagenome were shorter, so although the Greenland metagenome had relatively more contigs for its size compared to the Svalbard metagenome, these contigs were shorter.

Table 3. Metagenome pre- and post-assembly statistics. Both the Svalbard 2019 and Greenland 2018 metagenome FASTQ reads were assembled using the wtdbg2 fuzzy bruijn graph assembly program. The output at each stage is compared using NanoPlot in the table below.

Pre-Assembly	**Svalbard**	**Greenland**
Number of reads	1,337,380	660,512
Mean read length (bp)	2,835	2,355
Median read length (bp)	2,586	1,796
Read length N50	4,125	3,592
Total bases (bp)	3,791,435,694	1,555,431,073
Post-Assembly	**Svalbard**	**Greenland**
Number of contigs	8,991	5,853
Mean contig length (bp)	11,591	10,273
Median contig length (bp)	7,550	7,344
Contig length N50	13,082	11,063
Total bases (bp)	104,211,852	60,125,399
Shortest contig (bp)	1,395	3,486
Longest contig (bp)	1,858,116	175,214
Average GC content (%)	56.62	56.24

2.3.6 Taxonomic distribution and abundance within the metagenomes

The domain distribution within the metagenomes using both MG RAST and KAIJU classification tools are given in **Table 4**. Bacteria are the dominant domain in both locations using both methods of classification. Some consdierable variation is apparent for Archaea and Eukaryota between location and classification method. Eukaryotes account for between 0.56% - 2% of the Greenland metagenome (MG RAST and KAIJU respectively) and a more consistent 0.72% - 0.8% within Svalbard. Archaea abundance is roughly three times as high using the KAIJU classification compared to MG RAST for both metagenomes. Viruses are the least abundant taxonomic category and only detected in the Svalbard metagenome by MG RAST. KAIJU had a greater number of unclassified sequences compared to MG RAST.

It should be noted though, KAIJU and MG RAST use different methods to classify reads. KAIJU uses a protein level classification approach by translating reads into amino acid sequences whereas MG RAST uses the nucleotide (LCA algorithm) approach.

Table 4. Domain classification in the Svalbard and Greenland metagenome. The percentage of cellular organisms are given in the table below for both locations using both MG RAST and KAIJU taxonomic classification. KAIJU figures are rounded by the KAIJU pipeline.

	MG RAST		KAIJU	
	Svalbard	Greenland	Svalbard	Greenland
Bacteria (%)	99.19	99.09	99	98
Eukaryota (%)	0.72	0.56	0.8	2
Archaea (%)	0.07	0.25	0.2	0.6
Viruses (%)	0.01	0	0	0
Unclassified / other sequences (%)	0.01	0.11	0.1	0.3

The top ten most abundant phyla within each metagenome using both MG RAST and KAIJU taxonomic assigment are shown in **Figure 11**. Variation between classification method and sample location is apparent, however trends are visible, specifically the dominance of the *Proteobacteria*. The distribution of phyla in the Svalbard metagenome is fairly consistent across both MG RAST and KAIJU methods. However, Greenland has more disparate distribution between classification methods. The proportion of the Cyanobacteria, Actinobacteria, Firmicutes, Chloroflexi, Gemmatimonadetes and the Planctomycetes differs substanially across classification method in the Greenland metagenome.

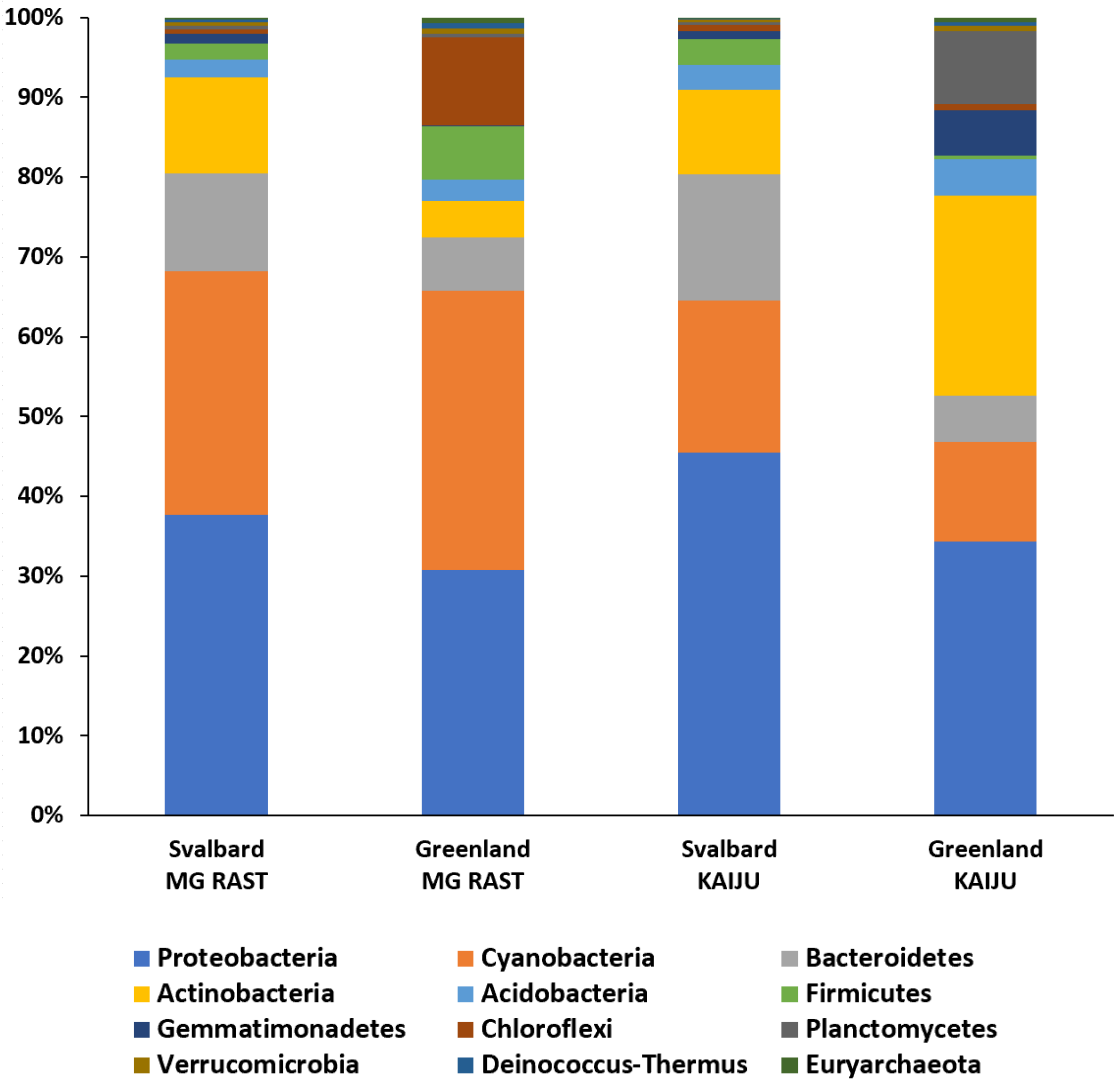

Figure 11. Distribution of the most abundant phyla in the Svalbard and Greenland metagenome. Two methods of taxonomic classification, MG RAST and KAIJU were used to assign phyla. The top 10 most abundant phyla in each sample are plotted in Excel with an 100% stacked bar chart.

Using MG RAST, the α-diversity of the Svalbard data set was found to be 291 species and for Greenland, 223 species. The top fifty most abundant phyla within each metagenome using MG RAST taxonomic assignment are shown in **Figure 12**. Proteobacteria and Cyanobacteria are the dominant phyla in both locations, accounting for ~65% of all distribution, however Cyanobacteria is predominant in Greenland. In Svalbard, other dominant phyla include the Bacteroidetes and Actinobacteria whereas in Greenland Chloroflexi and Firmicutes phyla make up the top most abundant taxa.

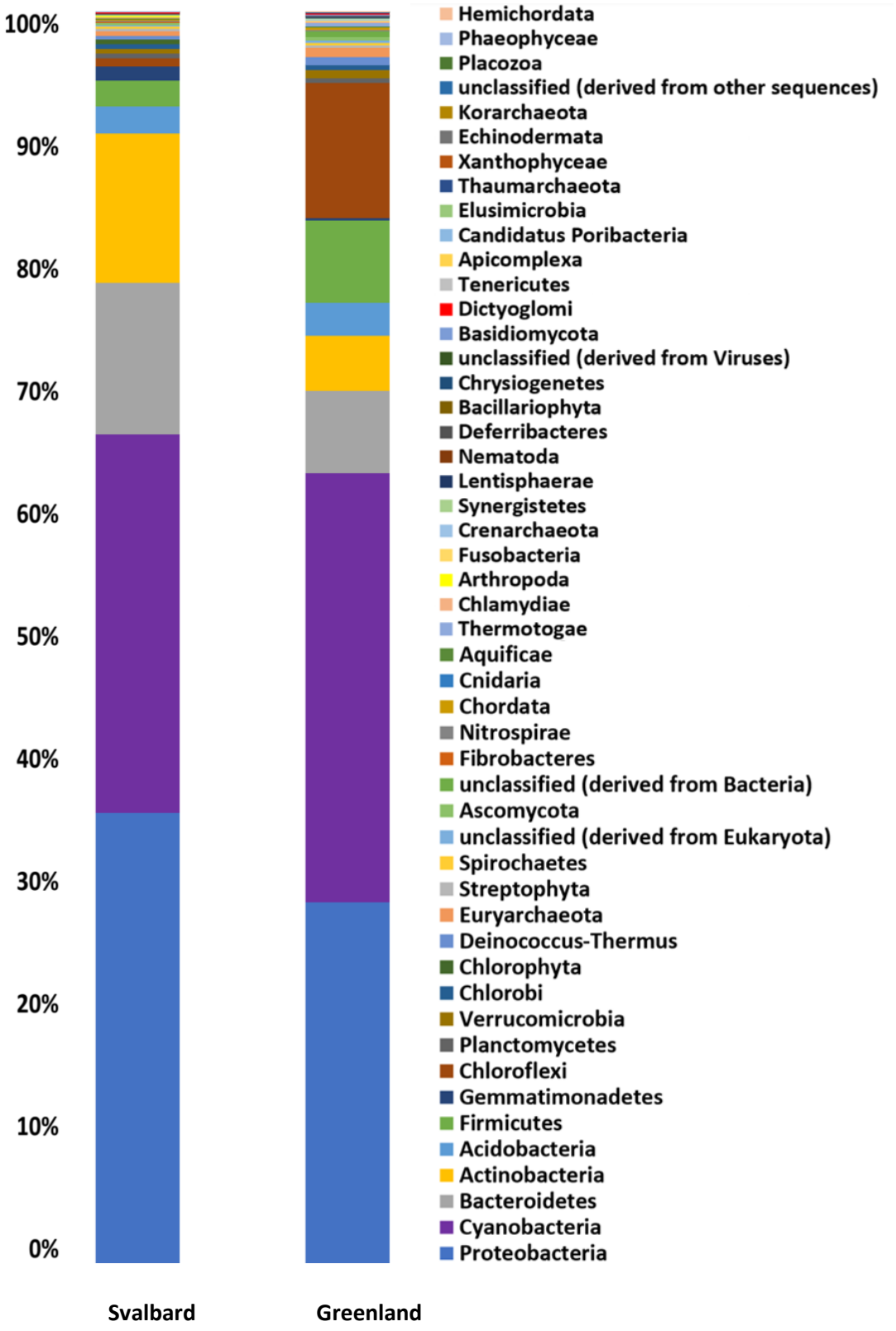

Figure 12. Distribution of top 50 phyla in Svalbard and Greenland metagenome. The 50 most abundant phyla using MG RAST taxon assignment are plotted in Excel using an 100% stacked bar chart.

In order to explore the presence of the culture dependent (isolates obtained) and culture independent (the dominant genera in sequence only form) genera, for each location and using each taxonomic tool (both MG RAST and KAIJU), taxonomic assignment down to genera level is assessed (**Table 5**). MG RAST and KAIJU use different approaches for the classification of taxa. In the KAJIU method, reads are first translated into amino acid sequences and using protein-level classification, taxonomy is assigned, whereas MG RAST uses a contig LCA (Lowest Common Ancestor) algorithm asssigning taxonomic classification directly for each individual sequence.

The genera identifed via isolation and 16s rRNA gene sequenicng (culture dependent) accounted for a substantial proportion of the reads (culture independent) classified in the metagenome by the taxaonmic tools. For example, the *Polaromonas spp.* accounted for almost 2% of all reads in the Svalbard metagenome (both taxonomic tools) (**Table 5**).

When the most abundant genera in the metagenomes (culture independant only) were assessed for abundance, on six occasions the count was >5%, with the highest seen in the Greenland metagenome (using MG RAST tool) - a sizeable 12.38% of all reads were *Ktedonobacter*. Interestingly, the genera *Polaromonas*, *Variovorax* and *Flavobacterium* (isolated from Svalbard samples) were detected by both tools in both locations across the board, whereas *Duganella* for example, was only detected in Svalbard (using KAIJU) even though it was isolated from a Greenland sample.

Table 5. Genera abundance in each metagenome. The abundance (%) of the specified genera within the metagenomes are given in the table below. The genera listed are the isolates obtained from the Svalbard and Greenland samples and the top two most abundant genera in each metagenome from each taxonomic classification method.

	MG RAST		KAIJU	
	Svalbard	**Greenland**	**Svalbard**	**Greenland**
Isolate genera	**Abundance (%)**	**Abundance (%)**	**Abundance (%)**	**Abundance (%)**
Polaromonas spp.	1.92	0.33	1.89	0.22
Variovorax spp.	0.7	0.65	1.15	0.33
Pseudomonas spp.	0	0.98	0.45	0.46
Massilia spp.	0	0	0.31	0.09
Duganella spp.	0	0	0.21	0
Cryobacterium spp.	0	0	0.64	0
Hymenobacter spp.	0	0	0.37	0
Flavobacterium spp.	0.26	0.33	0.5	0.46
Top genera in metagenome				
Ktedonobacter spp.	0.35	12.38	0.04	3
Phormidesmis spp.	0	0	2.03	8.28
Gemmatimonas spp.	9.88	0.49	2.64	0.1
Spirosoma spp.	7.26	0.98	3	0.2
Candidatus Solibacter spp.	5.06	8.14	1	0.9

2.3.7 Functional profile within the metagenomes

The highly similar distribution of sub-system functional categories within each metagenome as assigned by MG RAST is shown in **Figure 13**. The communities appear to function in a very similar manner with near identical proportions of reads allocated to each catergory.

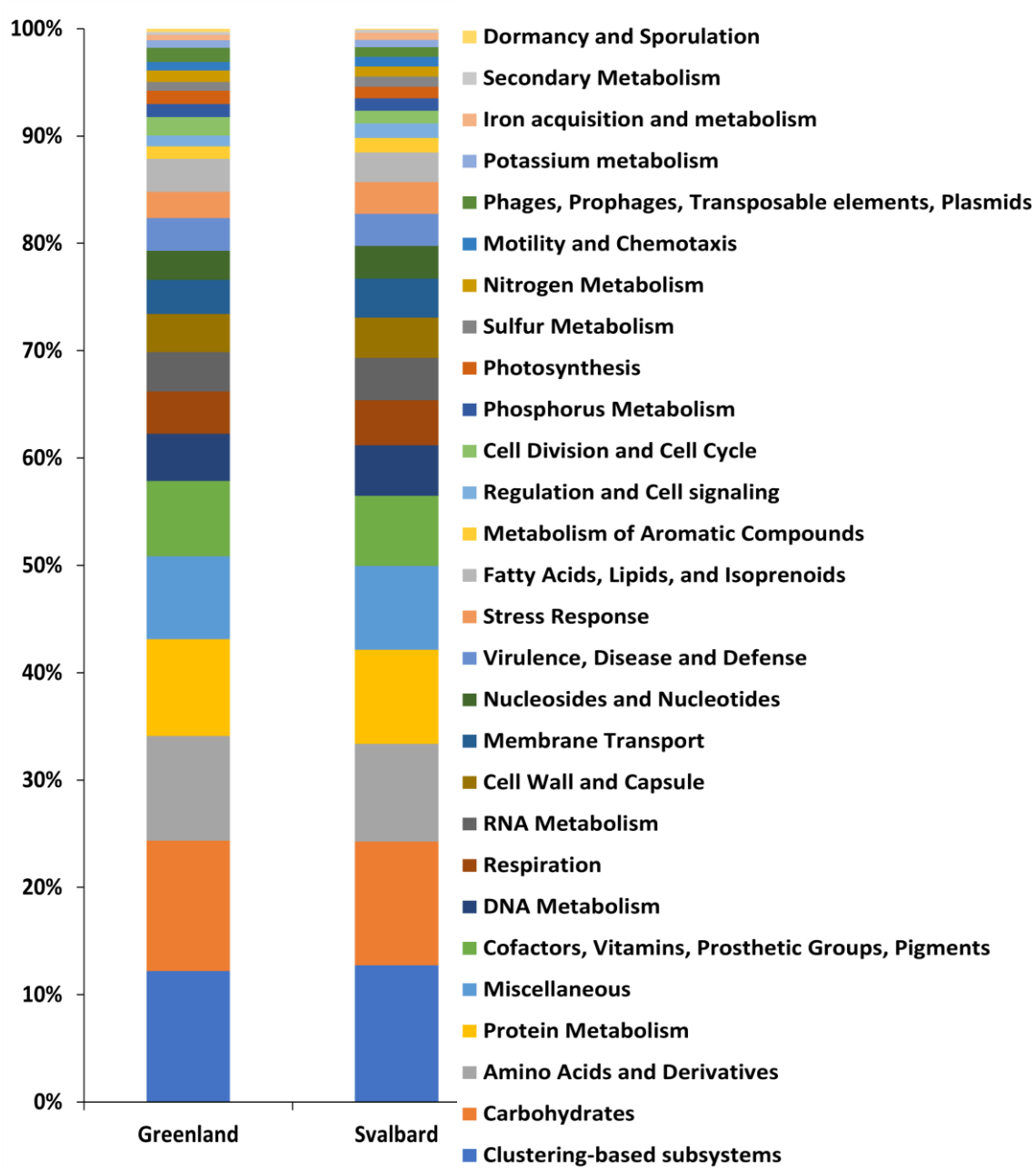

Figure 13. Sub-system functional category. The distribution of functional categories from each metagenome is plotted in the 100% stacked bar chart. The functional profile of each location is aligned in Excel using MG RAST output.

2.3.8 Stress response within the metagenomes

The similar stress response functional profile of each metagenome, as assigned by MG RAST, is shown in **Figure 14**. In both metagenomes oxidative stress accounts for almost half of all the stress response, while heat and cold shock combined account for ~20% of the stress response profile.

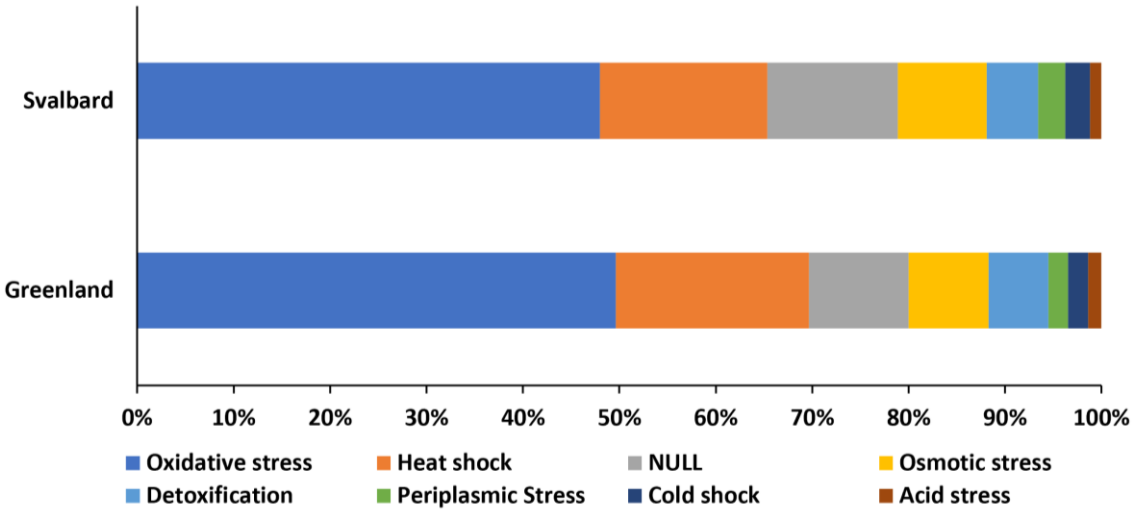

Figure 14. Stress response functional profile. The 100% stacked bar chart displays the stress response distribution from each location. The functional profile of each location is aligned in Excel using MG RAST assignment.

The abundance of heat and cold shock genes from the metagenomes assigned using MG RAST and PROKKA are examined in **Table 6**. PROKKA identified more heat shock genes than MG RAST whereas MG RAST identified more cold shock genes than PROKKA.

Table 6. Heat and cold shock genes. MG RAST and PROKKA annoations are compared in the table below for each metagenome.

	MG RAST		PROKKA	
	Svalbard	Greenland	Svalbard	Greenland
Heat Shock				
Chaperone protein DnaJ	16	0	52	3
Chaperone protein DnaK	41	15	97	11
Cold Shock				
Cold shock protein CspA	11	1	6	0
Cold shock protein CspC	2	0	0	0
Cold shock protein CspD	0	0	2	0
Cold shock protein CspE	0	1	0	0
Cold shock protein CspG	6	1	4	0

Other stress and cold-adaption genes present in both metagenomes (assigned by PROKKA) include : - the general stress protein 69 (yhdN) (**Appendix Table 14**), the cold-adaption genes; Pyruvate dehydrogenase E1 component (aceE), Chromosomal replication initiator protein (DnaA), DNA primase (DnaG), DNA gyrase subunits A and B

(gyrA and gyrB), Translation initiation factors IF-2 and IF-3 (infB and infC), Transcription termination/antitermination protein (nusA), Polyribonucleotide nucleotidyltransferase (pnp), Ribonuclease R (rnr) and Protein RecA (**Appendix Table 15**) and lastly the cold and heat shock genes; Heat-inducible transcription repressor (HrcA), Ribonuclease PH (rph), Translation elongation factor 4 (lepA), Xanthosine/inosine triphosphate pyrophosphatase (MMALV_14540) and tmRNA-binding protein SmpB (smpB_1) (**Appendix Table 16**).

2.3.9 Carotenoid biosynthesis within the metagenomes

Pigment production was assessed in both metagenomes and carotenoid biosythesis was by far the prominent system. The distribution of terpenoid and polyketide metabolism within each metagenome is examined in **Figure 15**. Terpenoid backbone biosynthesis accounts for over half the profile in each location. Carotenoid biosynthesis in Greenland makes up over 20% of the functional profile, in Svalbard around 15% of the profile is allocated to carotenoid biosynthesis.

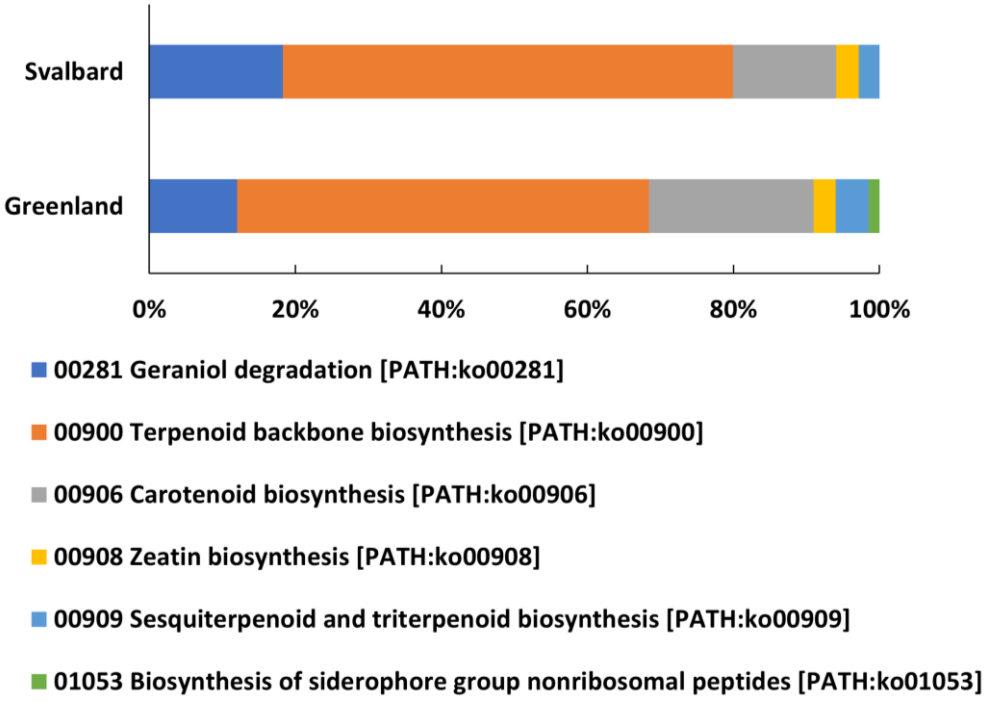

Figure 15. Metabolism of terpenoids and polyketides. The 100% stacked bar chart displays the distribution of terpenoid and polyketide metabolism from each location. The functional profile of each location is aligned in Excel using MG RAST output.

When carotenoid biosynthesis alone is examined, some functional differences between the metagenomes are evident (**Figure 16**). Although there are similarities in the profiles, the Svalbard metagenome has a greater diversity of carotenoid (*crt*) genes than Greenland. The three *crt* genes crtI, crtO and crtQ dominate the Greenland carotenoid biosynthesis profile accounting for over 65% of the profile. The three genes most dominant in the Svalbard profile are the crtI, crtP and crtF genes, accounting for over 50% of the profile.

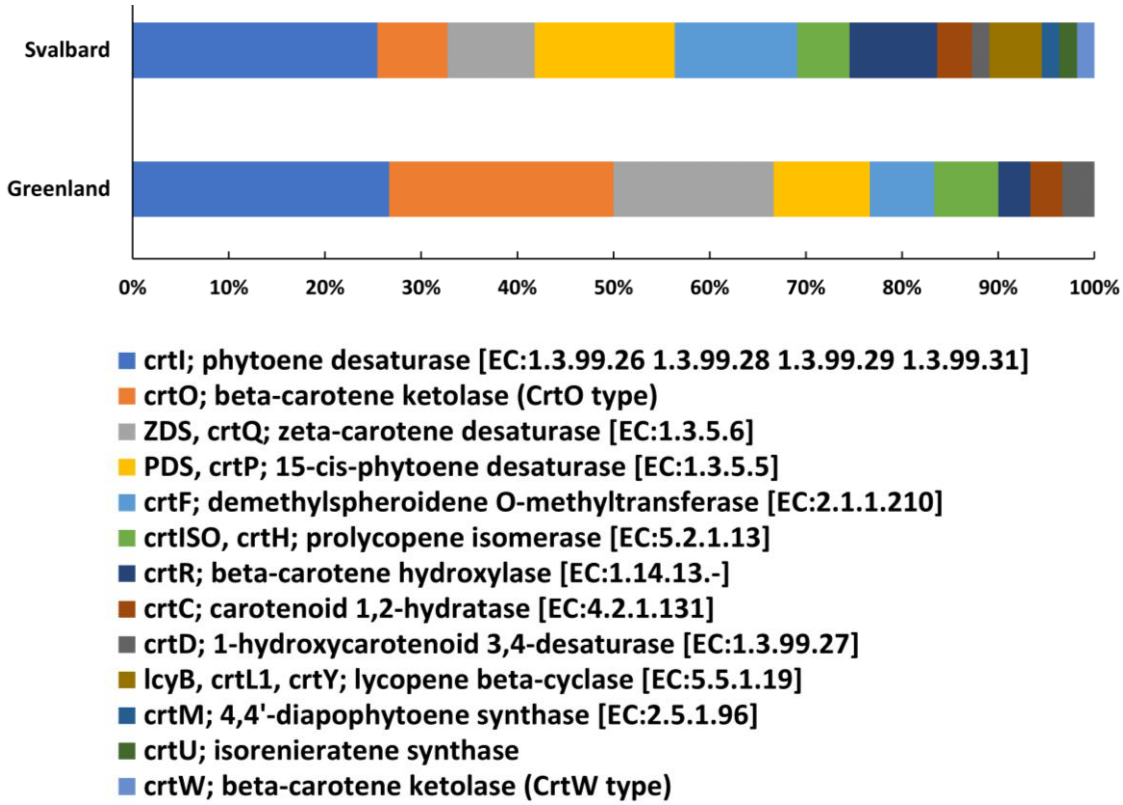

Figure 16. Carotenoid biosynthesis. The 100% stacked bar chart displays the distribution of carotenoid biosynthesis gene assignment from each metagenome. The profile of each metagenome location is aligned in excel using MG RAST output.

There are two naturally occurring carotenoid biosynthesis pathways, the 2-C-methyl-D-erythritol 4-phosphate (MEP) pathway, which is the pathway used by bacteria in most cases, and the mevalonate (MVA) pathway which is mainly used by eukaryotes and archaea (Zhang, 2018). Carotenoids are considered the most widely produced and diverse pigment class (Malik *et al*., 2012; Kirti *et al*., 2014; Sajjad *et al*., 2020), currently

in excess of 1100 carotenoid pigment structures are known (Sajjad *et al*., 2020). **Figure 17** shows the carotenoid pigment biosynthesis diversity and complexity.

Figure 17. Carotenoid biosynthesis pathway. The complexity and diversity of carotenoid pigment biosynthesis. KEGG map produced using RAST SEED viewer.

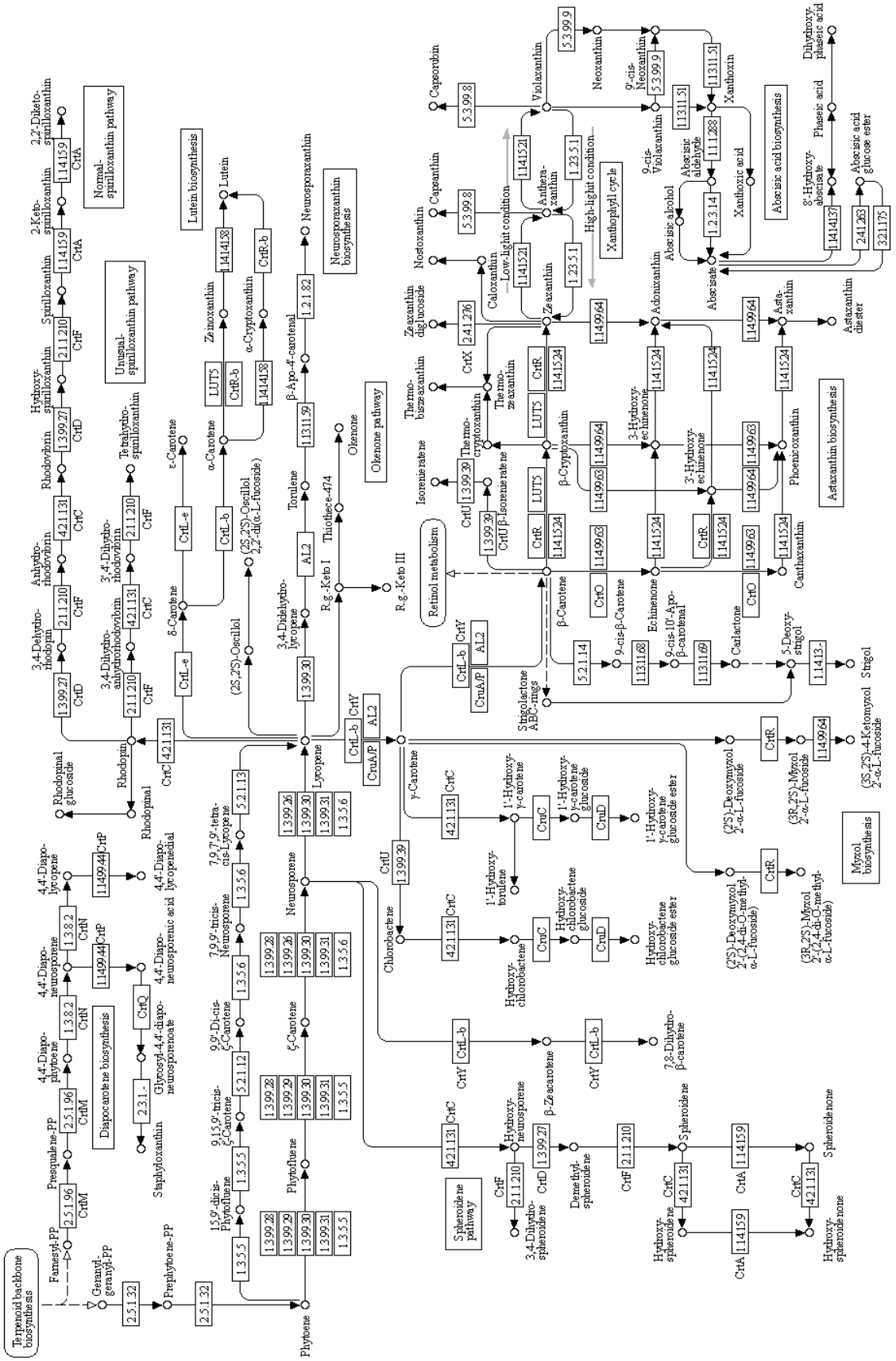

2.3.10 Light sensing and carotenoid biosynthesis genes within the metagenomes

Additional types of *crt* genes not identified by MG RAST were detected by PROKKA. The *crt* genes identified by both methods and the light sensing phytochromes (light-regulated two-component histidine kinases) (identified by PROKKA only) in each metagenome are shown in **Figure 18**. In the Greenland metagenome, **Figure 18 A**) two types of phytochrome and 11 types of *crt* genes are present. In the Svalbard metagenome, **Figure 18 B**) three types of phytochrome and 18 types of *crt* genes are present.

The **Appendix** contains full detail on all the carotenoid and light sensing genes within the metagenomes **i**) **Table 17** carotenoid biosynthesis **ii**) **Table 18** light sensing genes.

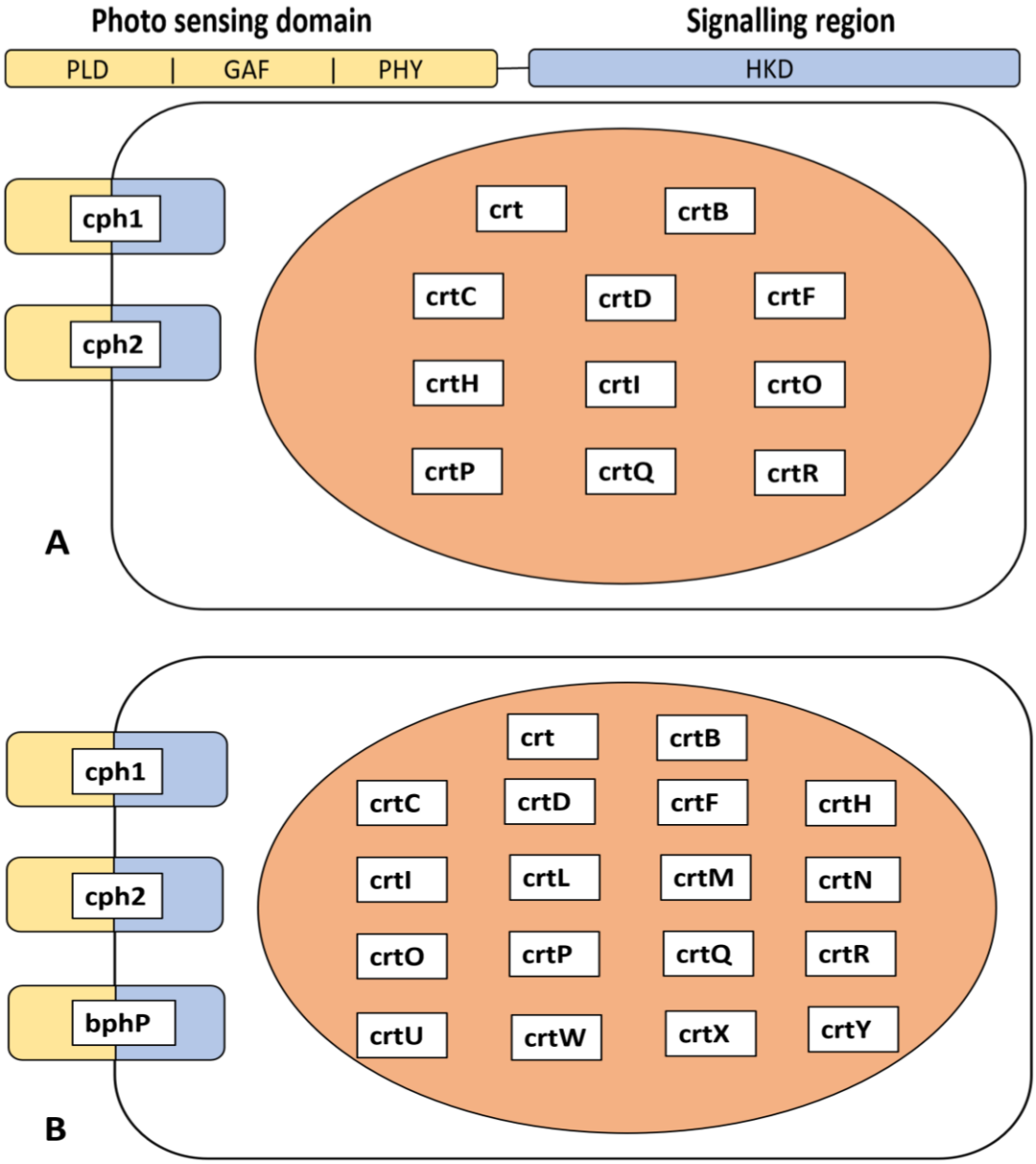

Figure 18. Phytochrome and carotenoid biosynthesis genes in the metagenomes. Phytochromes (cph1, cph2 and bphP) consist of two distinguishable regions, an amino-terminal photo sensing (yellow) and a carboxy-terminal signalling (blue) domain. Conserved sensing domains consist of a PAS-like domain (PLD) and two domains distantly related to PAS (GAF) (PHY). Conserved signalling regions consists of a histidine kinase domain (HKD) (Sharrock, 2008). Carotenoid biosynthesis (crt) genes, both regulatory and enzymatic, are displayed in the orange zone. Genes were assigned using PROKKA and MG RAST. **A) Greenland metagenome.** Both cph1 and cph2 phytochromes are present and a total of 11 types of crt genes. **B) Svalbard metagenome.** All three types of phytochrome are present and a total of 18 types of crt genes.

2.4 Discussion

The cryoconite community showed considerable adaptive responses following subjection to opposing extreme stresses, i.e., frozen vs thaw and dark vs light. Following dark, freezing conditions, the community recovered within 48 hours. The community revealed in culture displayed a substantial increase in conspicuous pigmentation when exposed to continual illumination. Additionally, the metagenomic functionality reflected the adaptive, defensive responses exhibited by the community to such stressors. Furthermore, the taxonomic distribution of isolates and the metagenome for both Svalbard and Greenland samples agree with previous taxonomic distributions and are suggestive of the contribution different community members offer to coping with such extreme environments.

2.4.1 Baseline community productivity at +2 °C

A baseline for net community oxygen production under dark and light conditions was established (**Figure 5**). The light microcosms showed a statistically significant increase in DO concentration within a 24-hour period compared to dark microcosms (t_6 = -3.198, p=0.019). DO concentration however is not just a function of biotic processes but of both abiotic and geological processes (Bagshaw *et al.,* 2016). Nevertheless, compared to controls, the DO concentration in microcosms was indicative of the increase in oxygen consumption under dark conditions (net heterotrophy) and the increase in oxygen production via primary productivity (net autotrophy) under light conditions. This shift is likely to occur more gradually seasonally with the peak photoautotrophic activity expected in mid-summer, although until further *in situ* field experiments can be conducted a level of uncertainty remains (Hodson *et al.,* 2007). This laboratory experiment could be further extended by both increasing the temperature and length of time that microcosms are incubated under dark and light conditions to establish if even higher levels of oxygen consumption or production are observed and by testing additional samples from different regions and sources to compare and contrast communities.

2.4.2 Community recovery

While the cryoconite in the freeze/thaw (second microcsom) experiment took longer than expected to achieve higher DO levels than that of controls (day 7 vs day 2 in first microcosm experiment, potentially due to extended age of sample), and a gradual increase in the DO concentration of the control (AMWS only) over the 14 day period was seen, which could be due to disequilibrium with the atmosphere, indeed substainal changes in oxygen disequilibrium under cold climate stress has been noted in other studies (Eggleston and Galbraith, 2018), microcosm recovery occurred rapidly (**Figure 6**). Indeed, the community had a statistically significant reduction in oxygen production immediately following freezing, dark conditions compared to controls ($t5= -10.719$, $p<0.001$) but was able to return to pre-freeze levels of O_2 production within 48 hours. This rapid recovery is testament to the ability of the cryoconite community to respond and adapt to undoubtedly the major stressors of the cryospheric environment – the transition from day to night (as well as summer to winter), the shift, which in itself brings both stresses tested in this thesis, opposing temperature and light stress.

To establish how prevalent this ability to bounce back following freezing, dark conditions is and to determine if it can occur even quicker with fresher samples, cryoconite from different locations and of different age (since collection) should be used. Additionally, by adjusting the periods of incubation from days, to weeks or longer, diurnal cycles can be lengthened to model seasonal cycles and in combination with testing different temperatures, perhaps down to – 10 °C and -15 °C, the extent of the community's ability to recover following such stresses can be determined. In Addition, the pre- and post-freeze temperature could be raised from +2 °C to a higher temperature as it has been shown that higher temperatures improve cryoconite community productivity. For example, Stibal and Tranter found that at +18 °C the uptake rates of dissolved inorganic carbon by cryoconite debris were significantly higher than at +3 °C. As such, a higher, physiological optimum temperature could improve the rate of recovery seen in this work further. This higher optimum temperature is thought to be due to the cryoconite community largely not being truly psychrophilic but psychrotolerant instead (Stibal and Tranter, 2007). Furthermore, *in situ* monitoring during different seasons and at the shift

between day or night or between seasons would further expand understanding. Alternatively, experimental cryoconite holes that mimic naturally formed cryoconite holes could be used (Sommers *et al.,* 2019).

2.4.3 Cold tolerance and adaptibility - metagenomic insights

The metagenomes assembled and annotated for this study give insight into the ability of the community to repsond to light/dark and freeze/thaw in such a rapid manner. It should be noted that the nanopore MinION platform was used for sequenicng. This technology is useful for long reads but co-assembly using standard sequencing reads to create a hybrid assembly may be a more robust process. However, the assembly produced contigs comparable to other cryoconite sequence data and the use of nanopore-only sequence data is a useful approach to obtaining fast, acuarate metagenomic information (Edwards *et al.,* 2016). Furthermore, different sized metagenomes were assembled and annotated in this study. To ensure fully representative comparisons and conclusions between samples can be drawn, sequence data of more similarly matched samples should be used.

While the presence of a functional gene does not assure functionality (Brankatschk *et al.,* 2010), metagenomic analysis of cold stress and cold-adaption genes in cryospheric communities as a means to survey implicit functionality is pervasive (Varin *et al.,* 2012; Koo *et al.,* 2016; Mackelprang *et al.,* 2017; Koo *et al.,* 2018). Since the first metagenome from cryoconite was assembled (Edwards *et al.,* 2013) metagenomic and metabolomic functionality analyses of cryoconite continue to emerge (Edwards *et al.,* 2014; Edwards *et al.,* 2016; Franzetti *et al.,* 2016), although to my knowledge, limited cold stress or cold-adaption surveys of the cryoconite community exist to date. Here, metagenomes from Svalbard and Greenland cryoconite are assessed for their stress response and for the presence of stress, cold and heat shock genes.

The distribution of sub-system functional categories within each metagenome (**Figure 13**) was remarkably similar and near identical proportions within each category were observed. The Arctic locations have comparable environmental conditions, thus along with the dominant distribution of key phyla (*Proteobacteroia* and *Cyanobacteria*

accounting for >60% of taxa in each location, **Figure 12**), it is relatively unsurprising the sub-system functional catergories are so alike. Similarly, the stress response was mirrored within the metagenomes (**Figure 14).** Oxidative stress accounted for nearly half of each stress profile, whilst heat and cold shock make up ~20% of stress response.

The identity and abundance of heat and cold shock genes using differing annotation methods were contrasted **(Table 6)**. Heat shock genes were more abundant than cold shock genes in all cases. The protein folding chaperone proteins DnaJ and DnaK, although named heat shock genes, are associated with cold-adaption and are frequently predominant over cold shock genes in cryospheric metagenomes (Varin *et al.,* 2012; Koo *et al.,* 2018). Specifically, the DnaK and DnaJ genes have been identified in the Cyanobacteria, the Proteobacteria, the Actinobacteria and the Bacteroidetes phyla within Arctic microbial mat metagenomes (Varin *et al.,* 2012). PROKKA was better able to identify heat shock genes (DnaK and DnaJ combined total) than MG RAST in the Svalbard metagenome (149 genes in total vs 57, PROKKA and MG RAST respectively) whereas no real difference in the Greenland data was observed (14 genes vs 15, using PROKKA and MG RAST respectively).

Less incongruity was observed between the MG RAST and PROKKA annotation of cold shock genes. For Svalbard and Greenland respectively, a total of 19 genes vs 3 using MG RAST and 12 genes vs 0 using PROKAA were detected. CspA and CspG were the most frequent in both number and distribution. Additonally, the light and temperature sensing genes such as the Blue light- and temperature-regulated antirepressor (bluF) among other light activated and photoreceptive proteins, phytochromes and histidine kinases detected (**Appendix Table 18**) likely play a role in detecting light and temperature stimuli resulting in the rapid and adaptive repsonses observed in the microsom experiements within this study.

Upon analysis of the metagenome gene annotations, a core set of stress, shock and cold-adaption genes was identified **(Appendix Tables 14, 15 and 16**). The majority of genes in this set have been previously identified as associated with cold-adaption and include; the aceE gene, a protein with pyruvate dehydrogenase, decarboxylase activity (Varin *et al*., 2012; Jones and Inouye, 1994; Mihoub *et al*., 2003), recA, a protein with general,

homologous recombination, DNA repair activity and involved in the induction of the SOS response (Jones and Inouye, 1994; Jones *et al*., 1987; Varin *et al*., 2012), infB, a protein chain initiation factor IF2 for translation initiation (a fMet-tRNA binding and protein chaperone) (Caldas *et al*., 2000; Jones and Inouye, 1994; Jones *et al*., 1987), infC, another protein chain initiation factor (IF3), involved in translation initiation, initiation site selection, RNA binding and in stimulating mRNA translation (Giuliodori *et al.,* 2007; Gualerzi *et al*., 2003), nusA, a transcription termination /antitermination /elongation L factor (Bae *et al*., 2000; Han *et al*., 2005; Jones and Inouye, 1994; Jones *et al*., 1987) pnp, (purine nucleoside phosphorylase) is a cold shock protein required for growth at low temperatures (3'–5' exoribonuclease and component of RNA degradosome) (Beran and Simons, 2001; Jones and Inouye, 1994; Jones *et al*., 1987; Marchi *et al*., 2007; Varin *et al*., 2012) gyrA, DNA gyrase, subunit A, involved in DNA cleaving/binding/re-joining subunit of gyrase (Jones *et al*., 1992; Grau *et al*., 1994; López-García and Forterre, 1999; Varin *et al*., 2012), GroES (Ting *et al*., 2010) and GroEL (Ting *et al*., 2010; Mykytczuk *et al*., 2011) the synergistic chaperone proteins involved in protein folding (Gragerov *et al*., 1992). DnaJ and dnaK, synergistic proteins with chaperone function and previously connected to cold-adaption (Varin *et al., 2012)* were also prevalent although not present in every sequence (metagenome and genome), as were DnaG genes. DnaG is a protein with primase activity and has been previously linked to cold-adaption (Han *et al*., 2005). DnaA, a protein with DNA binding, replication initiation and global transcription regulator roles also previously connected to cold-adaption (Han *et al*., 2005; Varin *et al*., 2012; Atlung and Hansen, 1999) was also identified in many instances (both genome and metagenome). A gene not previously linked to cold-adaption, the general stress protein 69 gene yhdN was also detected in both metagenomes. Currently, little is known about the function and role of gsp69 other than that it has aldo/keto reductase activity (Chandrangsu *et al.,* 2014) and is involved in stress response (Höper *et al.,* 2005).

Although the different annotation tools used (PROKKA and MG RAST) gave slightly differing results, the presence and abundance of cold-adaption, shock and stress genes within the metagenomes are indicative of the mechanisms employed, broadly, cold-adapted enzymes and chaperones, to withstand cold temperature stress. It is likely that

a combination of both generalized and specific mechanisms are employed, thus producing the cold adaptation ability profile of the community as a whole (Tribelli and López, 2018). The diversity and abundance of such genes within the sequences substantiate the ability to recover so swiftly following freezing conditions, as demonstrated by the microcosm recovery experimental findings.

2.4.4 Pigmentation

The community revealed in culture showed marked differences in visible pigmentation levels under dark and light conditions (**Figure 7**), despite the replica plates being more crowded than intended. When replica stamps were taken and transferred (at four weeks of growth following the initial dilution plating), colonies were spaced out and discrete. However, the replica plates by the third week of growth under both light and dark conditions had higher numbers of colonies than the initial master plates and as such were more crowded than intended. Cold-adapted micro-organisms tend to be slow-growers and therefore potentially continued to emerge after the replica transfer (seven weeks to emerge in total, given four weeks on first dilution plate with further three weeks on replica plate). For example, *Mrakia spp.* are psychrophilic yeast that have been isolated from cryoconite, grow on R2A, are butyrous, white cream in colour and can be surrounded by hyphae, and take ~3 weeks to grow at +6 °C (Thomas-Hall *et al.,* 2010; Tsuji *et al.,* 2018). The *Mrakiella spp.* are yeast very similar physiologically to *Mrakia (*Margesin and Fell., 2008). The excess growth on the replica plates appeared to fit the morphology described for such yeasts (**Figures 8 and 9**) and given that the plates were incubated at +2 °C it is feasible that the yeasts took longer to emerge. However, the excess colonies were not characterized. If repeated, the addition of a fungicide, for example cycloheximide to prevent fungal growth could be applied if the heterotrophic bacterial community alone wanted to be assessed.

Nevertheless, a statistically significant increase in the number of conspicuously pigmented colonies on plates under light conditions compared to their dark counterparts was evident. After three weeks of growth (**Figure 7 A**), a significantly higher proportion of perceptibly pigmented colonies were apparent ($t_{12} = 4.121$, $p<0.01$), with

a mean 38.4% of all colonies being pigmented in the light compared to 23.3% in the dark. A week later, at four weeks of growth (**Figure 7 B**), the proportion of pigmented colonies in the light had risen to 40.4% whereas the dark proportion remained at a significantly lower level of 23.8% (t_{12} = 4.765, p<0.001). In addition to the higher proportion of pigmentation evident in the culturable community under light conditions due to the absence of noticeable pigmentation in counterpart colonies under dark conditions (**Figure 8**), of note is the intensity of pigmentation. Plates under light conditions frequently showed more intense pigmentation (**Figure 9**) compared to counterpart colonies grown in the dark, although they too were pigmented. For these reasons, it appears two mechanisms could potentially be in action, both an upregulation of pigment production in constitutive producers and a light-induced production in non-constitutive producers. Various environmental factors influence the regulation of the carotenoid biosynthesis pathway and the accumulation of carotenoids is often seen as a response to stress (Ram *et al.,* 2020). Carotenogenesis can occur in a constitutive, light-induced or a cryptic manner. Whilst most microorganisms reported thus far produce carotenoids in a constitutive manner, some have been shown to do so only when illuminated (Takano *et al.,* 2006). Light-induced carotenogenesis requires a light-sensing mechanism coupled to the genetic regulation for carotenoid biosynthesis gene expression (Takano *et al.,* 2006).

The abundance of conspicuously pigmented colonies in response to illumination indicates light-induced pigmentation as a counter mechanism to light stress could be a tactic in stress response. However, the current literature does not reflect this and further experimentation to establish if this mechanism is taking place is needed. Carotenoids are evidently the most widely produced and diverse pigment class (Malik *et al*., 2012; Kirti *et al*., 2014; Sajjad *et al*., 2020) and whilst a range of environmental factors are known to influence the regulation of the carotenoid biosynthesis pathway and the accumulation of carotenoids is often seen as a response to stress (Ram *et al*., 2020), the majority of carotenoid producing microorganisms are reported to do so constitutively and only a limited range of genera demonstrate light-induced pigment production (Takano *et al*., 2006.). The bulk of documented light-induced carotenogenesis studies focus on *Myxococcus spp.* (Hodgson and Murillo, 1993;

Whitworth and Hodgson, 2001) though light-induced carotenoid production is also reported in other genera including *Streptomyces (*Takano *et al.,* 2005), *Cephalosporium* (Seviour and Codner, 1973)*, Agromyces* (Weeks and Garner, 1967), *Rhodopseudomonas (*Zhou *et al*., 2014), *Sulfolobus* (Grogan, 1989) and *Mycobacterium (*Rilling, 1962). Whilst pigment production in the cold-adapted algae is well studied (Remias *et al*., 2005; Williamson *et al*., 2019; Williamson *et al*., 2020), the potential of cold-adapted bacteria and fungi to produce pigments is currently relatively neglected, potentially due to a number of reasons such as the distinctive physiological and nutritional requirements of such microorganisms (Sajjad *et al*., 2020). High light conditions have been reported to induce the overproduction of pigments in microalgae (Lamers *et al*., 2010; Mulders *et al*., 2014) however this has not to my knowledge been reported in bacterial or fungal taxa in cold-adapted or cryospheric microorganisms.

Although potentially two differing mechanisms of pigment production were observed, specifically upregulation of pigment production by constitutive producers and light-induced production by non-constitutive producers, in order to confirm the mechanism of production and gather quantitative data, further approaches would need to be applied. These include single point microscopy, the use of a software package like ImageJ or whole plate extraction and quantification of total pigment concentration. Additionally, different temperatures, sample and media types would likely result in a variety of culturable community responses to light stress. It should be noted that, due to the small volume of archived sample available for this study, all the community experimentation used Svalbard sample only.

2.4.5 Carotenoid biosynthesis genes

The incidence of carotenoid biosynthesis genes within the metagenomes substantiates the widespread pigmentation response seen in the replica plating experiment.

Terpenoid and polyketide metabolism within each metagenome is comparable (**Figure 15**). Terpenoid backbone biosynthesis constitutes over half of each profile whilst carotenoid biosynthesis in Greenland makes up over 20% and in Svalbard around 15%

of the profile. Nevertheless, when carotenoid biosynthesis alone is assessed, some perceptible differences between the metagenomes are evident (**Figure 16**). The Svalbard metagenome has a greater diversity of carotenoid (*crt*) genes than that of Greenland, potentially due to the size difference of the metagenomes **(Table 3)** (Svalbard pre-assembly size of 3.8Gbp and post-assembly 104Mbp vs Greenland 1.6Gbp pre- and 60Mbp post-assembly) or due to the differing distribution of phyla and corresponding diversity of carotenoid biosynthesis. It is possible that the organisms in Svalbard use pigmentation more so than that of Greenland organisms. Certainly, the isolates obtained from Svalbard had a higher rate of diversely coloured pigmented representatives compared to Greenland isolates **(Table 2)**, however, further isolation and characterization in combination with additional metagenomic assembly of matched sizes would explore this in greater detail.

Furthermore, the abundance of light-sensing genes within the metagenomes corroborates the light-induced pigment over-production witnessed in the replica experiment. It seems reasonable to suggest that a considerable proportion of the cryoconite population has the capacity to both detect light and synthesise carotenoids in response to light stress and therefore counter UV irradiation. Additionally, pigments often perform a dual purpose and also stabilise membranes as a protective tactic against low temperature stress (Mueller *et al.,* 2005; Dieser *et al.,* 2010; Shen *et al.,* 2018; Vila *et al.,* 2019) and as such, pigment production is undoubtedly an extremely useful adaption for cryospheric life. The types and proportions of crt genes within the metagenomes and genomes differed, suggestive of the highly varied carotenoid compounds generated in this class of pigments (Sajjad *et al.,* 2020). Using samples from different locations and habitats to produce additional genomic sequences and isolates followed by 24-hour illumination incubations to identify conspicuous light-induced pigment producers will establish how widespread this response is within the cryospheric microbial inhabitants. Additionally, I propose that existing isolate collections from cryospheric regions are grown under illumination for a minimum of three weeks to establish if they too are unknown pigment producers.

Furthermore, I noted an increase (albeit observational and not quantified) in pigment intensity in isolates following sub-zero incubation. Interestingly this was especially so in

isolates that produced an increase in colony count following the sub-zero incubations, indicating that pigment production may be linked to an ability to grow at low temperatures. It has been demonstrated previously that colder temperatures can be optimal for pigment production and induce over-production of pigments (Pandey *et al*., 2018; Chattopadhyay *et al*., 1997), likely for the purpose of cryoprotection or to maintain membrane fluidity at these low temperatures, although the role these compounds play in cold adaption is yet to be confirmed (Collins and Margesin, 2019) as such, further experiments to quantify the amount of pigment produced by isolates at different temperatures should be conducted, in combination with assessing if pigmented strains fair better at coping with sub-zero temperature stress.

2.4.6 Photoreceptor genes

All six of the main forms of photoreceptor were detected within the metagenomes (**Appendix Table 18**); the light, oxygen, voltage protein (LOV), the blue light sensing protein (BLUF), the photoactive yellow protein (PYP), the cryptochrome, phytochrome and the rhodopsin (Gomelsky and Hoff, 2011). The most abundant photoreceptor class were the phytochromes with a substantial 0.07% of all coding sequences (CDS) assigned to phytochromes alone in the Svalbard metagenome. When the presence of both *crt* and phytochrome genes in each metagenome is evaluated using a combination of annotation methods (**Figure 18**), additional diversity is apparent in the Svalbard metagenome (**Figure 18 A**) where three types of phytochrome and 18 types of *crt* genes are present. Still, in the Greenland metagenome, **Figure 18 A**) two types of phytochrome and 11 types of *crt* genes are present which given that the assembled size is 60Mbp compared to the Svalbard 104Mbp is substantial. Phytochromes are light-regulated two-component histidine kinases which in cyanobacteria and eubacteria regulate pigmentation, phototaxis and synthesis of the photosynthetic apparatus (Sharrock, 2008). Undoubtedly the cryoconite community are sensing and responding to changing light levels and do so in a rapid manner. It is probable that the phytochrome photoreceptors sense light, generate an output signal and regulate responses such as pigmentation in the community. The Svalbard metagenome showed more variety and a

higher frequency of light sensing and *crt* biosynthesis genes, although it was a larger size than the Greenland one. Additionally, the Svalbard samples produced more pigmented representatives in the isolate collection compared to the Greenland samples. Further culture dependant and independent analysis is required to confirm the manner of pigmentation, be it light-induced or constitutive and to ascertain the different pigmentation strategies to light stress in different communities.

2.4.7 Taxonomic distribution

The dominance of bacteria that was observed in the communities was expected (Kaštovská *et al.,* 2005; Hodson *et al.,* 2008), although it should be noted that metagenomic databases have a bacterial bias due to the fact that metagenome taxonomy has to date focused on bacteria and as such the greater proportion of the databases consist of bacterial genomes, however discrepancy between taxonomic classification method was observed (**Table 4**) and phylum distribution varied considerably between the tools also (**Figure 11**).

There was however discrepancy between the taxonomic classification tools used for the metagenomes (KAIJU and MG RAST). Different proportions of phyla were produced from each of the tools, the largest disparity seen in the Greenland metagenome. As mentioned, KAIJU and MG RAST use different methods to classify reads. KAIJU uses a protein level classification approach by translating reads into amino acid sequences whereas MG RAST uses the nucleotide (LCA algorithm) approach. Additionally, MG RAST uses an alignment length of 15bp, e-value of e-5 and percent identity of 60% whereas KAIJU uses a shorter minimum match length of 11, the same number of allowed mismatches of 5 but has a higher minimum match score of 75%. The disparity between classification tools, especially in the Greenland metagenome, could also be due to the fact that the Greenland metagenome was smaller (approximately half the size of the Svalbard metagenome) or due to the fact that the reads identified as a particular phylum using one tool then another phyla using the other tool were reads from phyla not well represented in taxonomic databases. Potentially, metagenome assembled

metagenomes (MAGs) (Parks *et al.,* 2017) using those reads that give variable results (depending on tool used) could improve taxonomic classification.

The taxonomic distribution of both metagenomes and isolates, which revealed the dominance of the Proteobacteria, Cyanobacteria, Actinobacteria, Bacteroidetes, Chloroflexi, Gemmatimonadetes and Acidobacteria phyla, were consistent with previous Arctic cryoconite microbial taxonomic findings (Margesin *et al.,* 2002; Edwards *et al.,* 2011; Gokul *et al.,* 2016; Anesio *et al.,* 2017), although it should be noted that community structure has been found to differ between years, even when sampled in the same month at the same location, thought to be driven by temperature (Pittino *et al.,* 2018). As such, taxonomic distribution although useful to establish dominant members is a snapshot of the community structure at a given time point and is expected to be variable. Additionally, geographic location has been shown to have a bigger effect on the bacterial community distribution when compared to the eukaryotic community, which further substantiates the need to appreciate the snapshot nature of a sample, especially in regard to the bacterial community (Lutz *et al.,* 2019).

Of the top ten most abundant phyla (**Figure 11**), Proteobacteria dominated the Svalbard sample with 38% of the relative abundance (RA) assigned using the MG RAST tool and 45% RA assigned using KAIJU. In the Greenland data set, KAIJU also assigned the Proteobacteria as the most dominant phyla with 34% RA, however using MG RAST, Cyanobacteria at 35% RA were the most dominant phyla in Greenland. Conversely, Cyanobacteria in Greenland using KAIJU were just 13% RA, whereas the Cyanobacteria were the second most abundant phyla in all other cases, i.e., 31% RA in Svalbard using MG RAST and 19% RA in Svalbard using KAIJU. The Actinobacteria were the second most dominant phyla in Greenland using KAIJU with a RA of 25%, compared to 5% RA in Greenland using MG RAST and 11% and 12% in Svalbard in KAIJU and MG RAST respectively. In the Svalbard data set, the Bacteroidetes, Acidobacteria, Firmicutes, Gemmatimonadetes and Chloroflexi were all abundant in corresponding proportions between KAIJU and MG RAST tools. More disagreement between the tools in the Greenland data set was apparent. For example, the Chloroflexi constituted 11% RA in

the MG RAST assignment compared to the 0.8% RA using KAIJU and the Planctomycetes had 19% RA in KAIJU compared to a 0.5% RA using MG RAST. Clearly whilst some substantial disparity is evident, the presence of these top ten phyla, especially the predominance of Proteobacteria and the Cyanobacteria agrees with other studies (Edwards *et al.,* 2014; Gokul *et al.,* 2016).

Whilst the metagenomic taxonomic assignment confirmed the dominance of the Proteobacterial phyla, a dominant specific genus was not identified, whereas for the Cyanobacteria a high number of *Phormidesmis* spp. were detected (up to 8.28% of all reads). Although a dominant phylum, a dominant specific genus was not assigned from within the Actinobacteria. However, for the remaining dominant phyla, dominant specific genera were assigned (**Table 5**); within the Bacteroidetes, the *Spirosoma* genus (up to 7.6% of all reads), within the Chloroflexi phylum, the *Ktedonobacter* genus (up to 12.38% of all reads), within the Gemmatimonadetes phylum the *Gemmatimonas* genus (9.88% of all reads) and from within the Acidobacteria the *Candiadtus Solibacter* genus (8.14% of all reads) were detected.

Culture-dependant identities also concurred with other studies, although the full set of isolates were not successfully identified (**Table 2**). The colony PCR performed on the isolate set was not productive in all cases. This could be due to a number of factors such as the need to optimize the colony PCR conditions, for example, the volume of biomass added to reactions (colony PCR is highly sensitive) or due to a cell-wall bias. It should be noted that 16 of the 17 isolates successfully identified were Gram-negative. Additionally, the isolates could have been yeasts and only universal 16S rRNA gene (bacterial) primers were used. Additionally, microscopical observation could have been used to assess the isolates.

Regardless, the typical phylogenetic distribution is well reflected in the isolates obtained from the cryoconite samples (**Figure 10**). The maximum likelihood tree is dominated by the Proteobacteria, especially the Betaproteobacteria, and both the Bacteroidetes and Actinobacteria are represented. Although it should be noted that this dominance of proteobacterial isolates could also be due to culture method bias, Proteobacteria are often the predominant isolate obtained when culturing environmental samples from

cold regions (Panwar *et al.,* 2019). The genera isolated from Svalbard samples in this study, specifically *Pseudomonas, Polaromonas, Cryobacterium and Flavobacterium* agree with previous Svalbard cryoconite isolated genera (Singh *et al.,* 2014b). To my knowledge, no study has yet isolated and identified bacterial strains from Greenland cryoconite, thus no direct comparison can be made, although as stated, the isolates obtained agree with previous metagenomic taxonomy distribution of Greenland cryoconite.

Although the role of the Cyanobacteria in the cryoconite community is relatively well understood, additional investigation of the roles other dominant phyla play within the community needs to be conducted. This is begun to be addressed in chapter 3.

2.4.8 Chapter conclusion

In conclusion, the cryoconite community evidently needs to be highly stress tolerant. The members experience multiple stress factors which could be seen as two different, extreme environments. The summer days brings light, thawed meltwater and higher temperatures whilst the nights and winter are dark, frozen with sub-zero temperatures. When compared to other extremophilic organisms, who are adapted for a set of extreme stresses that remain more constant, the cold-adapted, psychrophilic or psychrotolerant organisms need to cope with opposing, changeable severe stressors. These shifting conditions require sophisticated environmental processing. The ability to respond to changing external stimuli efficiently and rapidly is critical to their survival.

Indeed, when tested the community was able to recover rapidly following a freeze/thaw cycle, and within 48 hours return to net O_2 production. Furthermore, the upregulation and/or light-induced production of pigments within as little as three weeks indicates how swiftly the community responds to external factors. This sensing of changing environmental conditions and corresponding switching off and on of genes needs to be a tightly regulated yet fast, flexible process. The majority of cryoconite studies examine summer community activity. Snapshots of the summer or winter do not identify the mechanisms behind the transition between the shift between day or night or between seasons, or indeed the speed of the response, the switch points between the extreme,

opposing stressors. As well as further *in situ* and laboratory investigation of cryoconite community responses to fluctuating stressors, additional sequencing to compliment the experimental work is needed. One of the limitations of metagenomic analysis, however, is the origin of the microbial community DNA, specifically whether it is from living, dead or indeed dormant cells. As such other –omic technologies are necessary to confirm functionality, such as meta-transcriptomics and meta-proteomics (Margesin and Collins, 2019). However, hopefully this survey in combination with the experimental work goes some way in uncovering the mechanisms and functionality behind the stress responses observed in the cryoconite community. Multiple light-sensing, carotenoid biosynthesis, stress response, cold and heat shock genes were detected and are indicative of the adaptive responses and functions the cryoconite community demonstrated and indeed require in order to conquer its extreme environment.

3 - How do individual taxa from cryoconite respond to sub-zero temperature and light and UV irradiation stress and what mechanisms to counter these stresses are employed?

3.1 Introduction

3.1.1 Dominant members

The dominance of the Proteobacteria, Cyanobacteria, Actinobacteria, Bacteroidetes, Chloroflexi, Gemmatimonadetes and Acidobacteria phyla in the cryoconite bacterial community has been established in previous studies in both culture dependant and culture independent form (Margesin *et al.,* 2002; Edwards *et al.,* 2011; Gokul *et al.,* 2016; Anesio *et al.,* 2017). The findings from Chapter 2, confirmed this composition in both representative isolate and metagenomic sequence form (see Chapter 2, Results). Indeed, the majority of the isolates obtained belonged to the Proteobacteria phyla and included *Pseudomonas, Polaromonas, Variovorax, Massilia* and *Duganella* genera. Isolates from the Actinobacteria phyla (*Cryobacterium* genus) and the Bacteroidetes phylum (*Flavobacterium* and *Hymenobacter* genus) were also obtained. Although the

Pseudomonas, Polaromonas, Cryobacterium and Flavobacterium genera have been isolated from Svalbard cryoconite previously (Singh *et al.,* 2014b), the isolates obtained from Svalbard samples in this study were different species to those isolated previously. Additionally, the isolates obtained from this study (from both Svalbard and Greenland samples), specifically *Massilia*, *Duganella*, *Pseudomonas* and *Flavobacterium* species have been isolated from Alpine glacier cryoconite (Lee *et al.,* 2011), although again, different species were identified in this study. Specific genus were also identified within the metagenomic taxonomic assignment, which confirmed the dominance of the *Phormidesmis spp.* within the Cyanobacteria and the *Ktedonobacter* within the Chloroflexi.

Though it is understood that the diverse heterotrophic members of the community metabolise the organic matter fixed by primary producers (Boetius *et al.,* 2015; Cook *et al.,* 2016a), consequently humifying the organic matter, which in turn darkens the cryoconite and lowers albedo (Gokul *et al.,* 2016), the variety of roles and abilities of individual taxa is relatively poorly understood. Of the limited number of studies that investigate cryoconite bacterial role and function, the majority have focused on the ecosystem engineer and primary producer the *Cyanobacteria*, specifically the *Phormidesmis* genera. This is unsurprising given that as much as 95% of available C within cryoconite holes has been attributed to cyanobacterial photosynthesis alone (Stibal and Tranter, 2007) and that in Arctic regions, *Phormidesmis spp.* represent the majority of the *Cyanobacteria*, as mentioned, a single species of *P. priestleyi* dominates cryoconite communities (Segawa *et al.,* 2017). However, additional study is required to understand the role and function of the heterotrophic taxa of the cryoconite community, especially their response to cryospheric stresses. Indeed, to my knowledge, just a single recent study has looked at the physiological abilities of cryoconite bacterial heterotrophs (Poniecka *et al.,* 2020). In order to begin cryospheric stress experiments on an individual isolate as soon as possible, the A18.2 isolate was chosen as a cold-adapted representative at random from the laboratory's heterotrophic bacterial culture collection. The other isolates used for experimental purposes in this study were isolated from a Svalbard 2011 cryoconite sample.

3.1.2 Sub-zero temperature stress and the adaptive, protective measures to counter it

Of the many stresses endured by the cryoconite community, the sub-zero temperatures experienced are one of the most extreme. At a low temperature, lethal damage from ice crystals rupturing cell membranes (Rivkina *et al.,* 2000) and the solidification of lipid membranes (Methé *et al.,* 2005) can occur. Additionally, freezing can cause severe injury, such as the release and loss of ribonucleic acids, amino acids and peptides (Wu., 2008). The low water potential of frozen environments can be extremely damaging to a cell, indeed, water is fundamental in multiple biotic processes, including the maintenance of the structural order and integrity of the cell, the turgor and osmotic pressure balance, the stabilization of proteins, nucleic acids and lipids, as well as being the basis of the intracellular environment, where essential chemical reactions occur and metabolic systems function (Anderson *et al.,* 2015).

Members of the cryoconite community have been found to use different methods to counter this sub-zero temperature stress and prevent cytoplasmic freezing, including the release of protective EPS, documented in the cyanobacterial *P. priestleyi* BC1401 (Chrismas *et al.,* 2016), the production of AFPs, documented in several bacterial isolates (Singh *et al.,* 2014a) and CSP genes have also been predicted in isolates (Singh *et al.,* 2015). Hence, the distinction between sub-zero temperature and freezing is made due to the fact that many cryospheric microbial communities counter the low temperature stress preventing the freezing process and although at a sub-zero temperature, are not actually frozen. Indeed, a proportion of the microbial community in many cryospheric environments manages to grow at low temperatures, for example in permafrost it is thought around 20% of the microbial inhabitants are growing at −10 °C , whilst at the higher temperature of –2.5 °C, 67% of bacterial isolates from permafrost grew (Rivkina *et al.,* 2018). The lowest temperature that a microorganism has been shown to grow and divide at to date is the *Planococcus halocryophilus* strain Or1, isolated from high Arctic permafrost at –15 °C (Rivkina *et al.,* 2018). However, few studies of growth at sub-zero temperatures using cryoconite isolates has been conducted. Furthermore, many functions, strategies and mechanisms of cold-adaption and low temperature tolerance from cryoconite members remain unknown at present. Identification of the individual

methods different members employ to adapt to, and counter sub-zero temperatures will further knowledge of life within a cryoconite hole.

3.1.3 UV irradiation stress and the adaptive, protective measures to counter it

Cryoconite community members are also exposed to other highly damaging stresses, such as high levels of ultraviolet (UV) radiation (Boetius *et al.,* 2015). UV A (320 to 400 nm) damages membranes and proteins as well as indirectly damaging DNA by generating reactive oxygen compounds, UV B (290 to 320 nm) is directly absorbed by DNA and damages it by generating photoproducts and cyclo-butane pyrimidine dimers which alter nucleotides, UV C (100 to 290 nm) does not reach the Earth as it is entirely blocked by the ozone layer, however it damages in a similar manner as UV B and is used artificially as a bactericide (Elasri and Miller, 1999; Peccia and Hernandez, 2002; Santos *et al.,* 2013). In bacteria, the major DNA repair system, the UV radiation ABC system (UvrABC), repairs damage and mutations (Zion *et al.,* 2006).

One of the main UV protective measures is the production of pigments, such as carotenoids which provide a shielding layer from environmental UV radiation as well as scavenging free radicals (Moeller *et al.,* 2005). Carotenoid production is well documented in bacteria from cold environments. Indeed, up to 95% of ice core isolates from a Tibetan glacier were pigmented (Shen *et al.,* 2018). Carotenoid pigments often perform a dual purpose, a photo-quenching role and the stabilisation of the membrane by reinforcing the lipid bilayer (Mueller *et al.,* 2005; Dieser *et al.,* 2010; Shen *et al.,* 2018; Vila *et al.,* 2019). Cryospheric carotenoid producing bacteria tolerate higher levels of environmental stresses compared to non-pigment producing community members (Dieser *et al.,* 2010). Carotenoid production can occur in a constitutive, light-induced or a cryptic manner, though the majority of microorganisms reported produce carotenoids constitutively (Takano *et al.,* 2006). Although some pigmented bacterial species have been isolated from cryoconite (Zhang *et al.,* 2011; Schumann *et al.,* 2012) no studies on the protective properties of the pigment or the manner of production, be it light induced or constitutive, have been conducted to date to my knowledge.

3.1.4 Summary

It is only by identifying mechanisms and contributions from individual taxa that we can understand the wider cryoconite community and therefore the ability of the cryospheric microorganism to endure harsh cryospheric conditions. Given that to date most studies of cryoconite biology focus on the Cyanobacteria, more understanding of the function and response to cryospheric stresses from the most abundant, dominant heterotrophic phyla, the Proteobacteria and Actinobacteria, is required. Two of the most challenging stresses, sub-zero temperature and light stress (therefore UV radiation) pose significant challenges to life in a cryoconite hole. In Chapter 2 how the community as a whole responded to these two cryospheric stresses was addressed. A fast (48 hour) recovery from sub-zero incubations and the production of pigment in response to continual illumination was observed. Multiple shock, stress and cold-adaption associated genes were identified from within the cryoconite metagenomes, as well as photoreceptors and carotenoid biosynthesis genes. In this chapter, the effort is extended and the individuals' ability to thrive at a sub-zero temperature and the protective properties that pigment confers against UV irradiation are investigated. A fully assembled genome as well as representative isolate genomes are surveyed for the presence of associated genes. In this way, cryospheric stress counter mechanisms and strategies from individual taxa are identified and in combination with the findings from the community investigation, an insight into the basis of the abilities of the members of the cryoconite community to tolerate such an extreme environment can begin to be constructed.

3.1.5 Aims and objectives

Aims

1) To test the ability of isolates obtained from Svalbard cryoconite (S11) to grow following sub-zero temperature incubations
2) To identify shock, stress and cold-adaptation genes in S11 isolate representative genomes
3) To test the manner of isolate A18.2 pigment production and assess if the pigment offers protection against UV irradiation

4) To sequence and assemble the A18.2 genome in order to identify the species and the presence of shock, stress, cold-adaptation and carotenoid biosynthesis genes

Objectives

1) S11 isolates will be incubated in axenic culture at -5 °C for four weeks, eight weeks and twelve weeks. Cultures once withdrawn will be diluted, plated and grown to compare CFU/ml $^{-1}$ to that of pre-freeze levels. The attenuance of cultures at a wavelength of 600 nm will also be measured at each time point and compared to pre-freeze values.
2) Representative genomes for S11 isolates will be obtained from NCBI and annotated. The presence of shock, stress and cold-adaptation genes will be determined using PROKKA.
3) Isolate A18.2 will be grown for three weeks under 24-hour light and 24-hour dark conditions. The pigment produced in each treatment will be extracted and the absorbance value determined at a range of wavelengths between 350 – 525 nm to establish peak absorbance. Additionally, cultures of A18.2 grown under both 24-hour light and 24-hour dark conditions for three weeks will be subjected to increasing doses of UV irradiation from 20,000 – 200,000 µ Joules before being plated. The resulting growth will be compared to growth pre-exposure.
4) DNA from A18.2 will be extracted, sequenced and the reads assembled to produce the genome. The identity of the isolate will be investigated using several methods: NCBI BLASTn, a maximum likelihood tree and ANI methods. The presence of shock, stress and cold-adaptation genes will be determined using PROKKA. Pigment production and carotenoid biosynthesis will be investigated in several ways: the genome will be submitted to a secondary metabolite biosynthesis cluster detection tool (antiSMASH), the presence of genes following annotation will be determined and the KEGG metabolic map constructed (RAST, SEED viewer).

3.2 Methods

3.2.1 Sample preparation

S11 isolates obtained from Svalbard 2011 cryoconite were stored in glycerol at -80 °C and sub-cultured onto fresh R2A (R2A details provided in Chapter 2, methods section *2.2.4*) prior to use.

A18.2 (Isolated from a Storglaciären sample by Sophie Cook) and stored within the laboratory's culture collection (Aliyah Debbonaire) was selected at random as a representative cryoconite heterotrophic bacterial isolate. A18.2 was stored in glycerol at -80 °C and sub-cultured onto fresh R2A prior to use.

3.2.2 S11 isolates – response to sub-zero temperature

The isolates obtained from S11 (13 in total, A-M) were grown in R2A broth, supplemented with glycerol (3% concentration). Briefly, a 10 µl loopful of biomass was swirled into each flask containing 25 ml of 3% glycerol R2A media, a 3% glycerol R2A media only (control) was prepared too, before each flask was incubated in the light at +2 °C for three weeks. (Glycerol was added to inhibit freezing (Mykytczuk *et al.,* 2013)). The flasks were then placed in a polystyrene box surrounded by crushed ice to maintain temperature, withdrawn and aliquoted into 2 ml microcentrifuge tubes, adding 0.5 ml culture and 0.5 ml of fresh 3% glycerol R2A media to account for nutrient depletion. Just 1 ml was added in total per 2 ml tube to allow for expansion upon freezing. Nine microcentrifuge tubes were prepared as described per isolate. A set of nine microcentrifuge tubes from the control were prepared in the same manner. The microcentrifuge tubes (9 X 14, total = 126) were placed in the freezer at –5 °C to incubate.

The remaining culture was also diluted 50:50 with fresh (3% glycerol R2A) media, gently swirled to mix before attenuance readings of each isolate were taken on a spectrophotometer (CECIL CE1010 100 series) at OD_{600}, using 1ml of culture per cuvette and the control as the blank. A standard serial dilution was then prepared from the 50:50 diluted culture. Three dilutions (10^{-2},10^{-3} and 10^{-4}) in triplicate per isolate were plated

onto R2A solid media using the drop plate method (Herigstad *et al.,* 2001). Briefly, individual drops of 25 µl per dilution in triplicate were placed on the corresponding section of the plate (see **Figure 19**). Using this method, seven plates were required as opposed to the 126 plates if each dilution for each isolate was plated in triplicates on individual plates. The control (3% glycerol R2A) was also plated in the same manner. The plates were incubated at 2 °C in dark for five days, withdrawn, colonies counted, before being returned to 2 °C in dark before being withdrawn again at three and a half weeks for the final plate count.

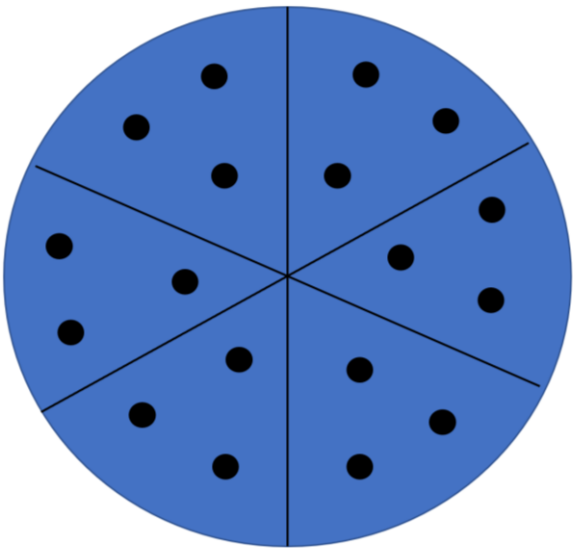

Figure 19. Drop plate arrangement. The plate was divided into six equal segments and triplicates of each dilution were spotted in 25 µl drops.

The microcentrifuge tubes (incubated at – 5 °C) were withdrawn in triplicate sets at three time points for OD_{600} readings and for dilutions and drop plating (for colony counts). i.e. three tubes per isolate were withdrawn from the freezer after four weeks growth, after eight weeks, and lastly at twelve weeks growth. OD readings and dilutions for plate counts were prepared in the same manner as described, however a ~10-20 min wait for thaw was required although the OD_{600} readings, dilutions and drop plating were completed as soon as possible following removal from freezer. In total, for the three sets of readings at the three time points, plus the initial pre-freezer set, the drop plating method resulted in the use of just 28 plates in total as opposed to the 504 which would

have been required using traditional individual plating of each dilution of each isolate in triplicate (4x126=504 vs. 4x7=28).

3.2.3 A18.2 pigment production and extraction

A18.2 was streaked onto R2A and incubated in 24-hour light and in 24-hour dark conditions at +2 °C for three weeks. By the third week of growth the bright yellow pigment was evident in those grown in the light. Quadruplicate sets of flasks (four sets of four=16 total) containing liquid R2A media (50 ml) were inoculated (10 µl loopful) with A18.2 grown in the dark (from the single plate) and A18.2 grown in the light (from the single plate), a set of each then went into both dark and light conditions. Namely, four flasks went into 24-hour light conditions sourced from the plate of A18.2 grown in the dark, four flasks went into 24-hour light sourced from the plate grown in the light, four flasks went into the dark sourced from the plate grown in the dark and lastly four flasks went into the dark sourced from the plate grown in the light. A total of 16 flasks were produced, eight of which were incubated in 24-hour light and the other eight were incubated in 24-hour dark, all were incubated at +2 °C for three weeks.

The flasks were withdrawn and 1 ml from each flask was transferred to a cuvette to read the attenuance at OD_{600} on the spectrophotometer. The remaining culture from each flask (~49 ml) was transferred into large (50 ml) centrifuge tubes and spun at 10,000 g for 5 min on a Hettich Zentrifugen Universal 320 centrifuge. The supernatant was discarded, and the pellet resuspend in 2 ml ethanol (purity 99%) per 50 ml centrifuge tube, a few sterile glass beads were added per tube and the tubes were vortexed to lyse cells and ensure full extraction. Each sample (containing a mixture of the ethanol/cells/pigment) was pipetted into individual 2 ml microcentrifuge tubes, leaving the glass beads behind. The microcentrifuge tubes were then centrifuged at 10,000 G for 5 minutes. The supernatant contained the pigment extract suspended in ethanol. Upon examination of the samples, the pellet (cell debris) was white with all pigment fully extracted. 1 ml of each sample's supernatant was then transferred to a fresh microcentrifuge tube for storage at -20 °C (wrapped in foil to protect the pigment from light). (Note, the stored extracts were intended for pigment characterisation but due to

COVID-19 this could not go ahead). The remaining 1 ml of supernatant was withdrawn and transferred to a cuvette to read on the spectrophotometer. Readings across a range of wavelengths were taken to determine peak absorption. Ethanol was used as the blank.

3.2.4 A18.2 UV tolerance

A18.2 was grown on R2A (in triplicate) for three weeks in both light and dark conditions at +2 °C. Two large 10 µl loopfuls of biomass from each plate were transferred to 50 ml centrifuge tubes with 15 ml of R2A and vortexed briefly (triplicate light, triplicate dark = six centrifuge tubes in total). The OD_{600} was recorded and additional R2A was added as necessary until equal OD was reached for each sample. 25 µl volume were taken in triplicate from each culture and placed in a row **(see Figure 20)** onto R2A media. Then 10 ml of culture from each centrifuge tube was decanted into petri dishes. All dishes (six in total) were simultaneously exposed (lids off while exposed) to increasing doses of UV (µ Joules x100) in a Stratalinker® UV Crosslinker (model 1800 with five 254-nm UV light bulbs, 8 watts each).

After the first dose of 20,000 µ Joules, the plates were lidded, withdrawn and 25 µl drops were taken in triplicate from each dish and placed in a row (see **Figure 20**) onto R2A media. Thus biological triplicates and technical triplicates for A18.2 grown in both light and dark conditions were plated for each dose of UV exposure (a total of six plates, three of which represent A18.2 grown in dark and three of which represent A18.2 grown in light conditions, with each row on each plate corresponding to the technical triplicate for the corresponding dose, with a total of five rows). The plates were returned to the Stratalinker® and exposed to the next dose, withdrawn and triplicates plated as described above. This was repeated to obtain doses of 60,000 µ Joules, 120,000 µ Joules and lastly 200,000 µ Joules, accounting for the accumulation of dose with each additional exposure. All the plates were then incubated wrapped in foil at +2 °C and checked for growth at one week and at four weeks of incubation.

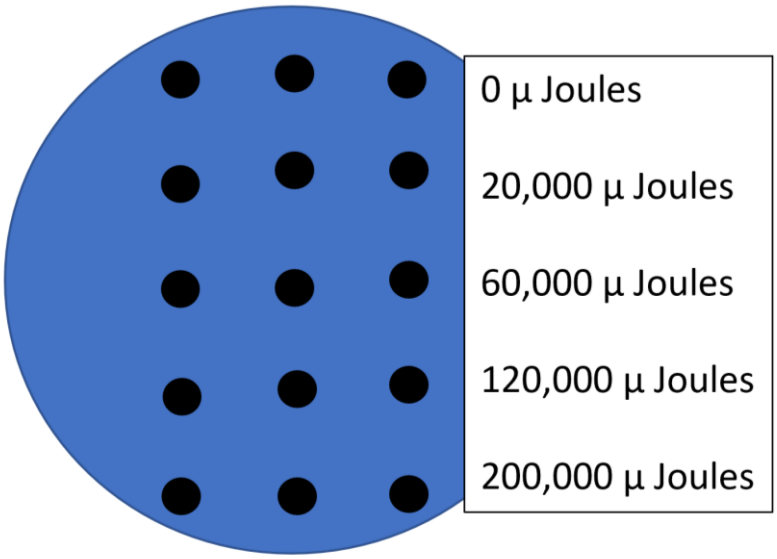

Figure 20. UV plate arrangement. The plate was divided into three columns with five rows. Each row was a technical triplicate and each column represented culture progressively more exposed to UV, starting with zero exposure and culminating in 200,000 µ Joules. Drops of 25 µl were placed spaced apart and evenly.

3.2.5 A18.2 DNA extraction

A18.2 biomass was taken from a streak plate by flooding it with liquid R2A medium and scraping with a sterile spatula until all the biomass was suspended and then transferred to a 50 ml conical centrifuge tube. The tube was spun at 5,000 G for five minutes to pellet the biomass before the supernatant was discarded. A Qiagen DNeasy® PowerSoil® kit was used to extract DNA according to manufacturer's instructions.

3.2.5.1 Qubit® DNA quantification

To quantify the concentration of DNA, a Qubit® 2.0 Fluorometer using a dsDNA HS (high sensitivity) assay kit was performed according to manufacturer's instructions.

3.2.6 A18.2 Nanopore sequencing

The Oxford Nanopore Technologies MinION sequencing platform was used to sequence A18.2 DNA. A (R9.4.1 model) MinION with a 2017 flow cell and a field kit (SQK-LRK001) were used. Briefly, the (freeze dried) field kit comprised vial 1 fragmentation mix, vial 2 rapid adapter and vial 3 sequencing buffer. The flow cell was plugged in to heat up to 37 °C for quality control (34 °C for sequencing run). The flow cell had >300 pores active so could proceed. Two PCR machines were turned on to heat up, one set at 30 °C and one at 80 °C. 10 µl of DNA was transferred to vial 1 and the tube was held for 1 minute 30 seconds at 30 °C then at 80 °C for 1 minute before being placed on ice. The contents of vial 1 were then transferred to vial 2 and left for ~ 5 min at room temperature. Meanwhile, vial 3 was prepared by adding 65 µl of resuspension buffer. After the five minutes had elapsed, the 10 µl from vial 2 was transferred to vial 3, resulting in a 75 µl library. A flush-tether/flush-buffer mix was prepared by adding 30 µl flush tether to 770 µl flush buffer and gently mixing. The flow cell was prepared by opening the priming port cover and extracting away 20-30 µl liquid. Then 600 µl of the flush-tether-buffer mix was added slowly, before the port cover was closed. The priming port was re-opened after five minutes and the last 200 µl was added to complete the flush, before the library was immediately dropped on to the loading port. Sequencing parameters were selected, sequencing with active base-calling (Guppy, version 3.3.0, Oxford Nanopore Technologies) was performed by the MinIT GPU.

3.2.7 S11 representative genomes

The most appropriate (closest phylogenetically, cryospheric where possible and with the most complete assembly) representative genomes for S11 isolates (with identity) were obtained from NCBI.

3.2.8 A18.2 genome assembly

Genome assembly was performed using the CANU pipeline. CANU applies four steps i) it detects overlaps in high-noise sequences using a MinHash alignment process (MHAP)

ii) it generates corrected sequence consensus iii) it trims corrected sequences and lastly iv) it assembles trimmed corrected sequences (Koren *et al.,* 2017; Koren *et al.,* 2018; Nurk *et al.,* 2020).

3.2.8.1 A18.2 genome visualisation

BANDAGE, a Bioinformatics Application for Navigating De novo Assembly Graphs Easily, was used to visualize the assembly (Wick *et al.,* 2015).

3.2.8.2 A18.2 identity

The NCBI BLASTn tool (details provided in Chapter 2, methods section *2.2.6.5*) was used to identify the closest match to the 16S rRNA gene sequence obtained for A18.2.

A Maximum likelihood tree was constructed (details provided in Chapter 2, methods section *2.2.7*) of the A18.2 and relevant 16S rRNA gene partial sequences.

Average Nucleotide Identity (ANI) of A18.2 compared to *C. psychrotolerans* (CGMCC 1.5382) was determined using the online calculator available at http://enve-omics.ce.gatech.edu/ani/ (Rodriguez and Konstantinidis, 2016).

3.2.9 A18.2 annotation

PROKKA (details provided in Chapter 2, methods section *2.2.9.3*) annotation of genomes was performed for the assignment of genes.

3.2.10 A18.2 Carotenoid biosynthesis

The A18.2 and *C. psychrotolerans* type strain 0549^{T} (CGMCC 1.5382) genomes were submitted to antiSMASH: Rapid identification, annotation and analysis of secondary metabolite biosynthesis gene clusters to identify carotenoid biosynthesis where present

(Medema *et al.,* 2011; Blin *et al.,* 2013; Weber *et al.,* 2015; Blin *et al.,* 2017; Blin *et al.,* 2019).

Metabolic KEGG (Kyoto Encyclopaedia of Genes and Genomes) maps of A18.2 and *C. psychrotolerans* (CGMCC 1.5382) were constructed using RAST (Rapid Annotation Subsystem Technology) and the SEED viewer, available at https://rast.nmpdr.org/ (Overbeek *et al.,* 2014)

3.2.11 Statistical analyses

The IBM SPSS Statistics for Windows, Version 25.0. Armonk, NY: IBM Corp was used for statistical tests and analysis. ANOVA, Kruskal-Wallis, the Fisher Exact test and Independent samples t-tests were performed. Microsoft Office Excel was used for standard calculations, such as dilution factors and percentages.

3.3 Results

3.3.1 S11 isolate sub-zero incubations

3.3.1.1 Colony counts

Isolates incubated at -5 °C in triplicate for 4 weeks, 8 weeks and 12 weeks were withdrawn, diluted and plated. The resulting colonies were counted (colony forming units per ml, CFU/ml $^{-1}$) and compared to the number obtained pre-freeze. The observed overall difference in mean CFU/ml $^{-1}$ pre- and post- freeze is shown in **Table 7.** S11D, S11G, S11I and S11L had an increase in CFU/ml $^{-1}$. S11D showed an increase at both week 4 and week 8 then a decrease at week 12 (**Figure 21**), thus a rise in CFU/ml $^{-1}$ before a reduction was observed, however this was still significantly higher than the pre-freeze levels. S11K and S11M had variable responses with no observed trend, with both increases and decreases at different time points in different dilutions. S11C and S11E showed no difference in CFU/ml $^{-1}$ pre- to post- freeze. The remainder of the isolates produced less colonies post freeze compared to pre- freeze counts.

Table 7. CFU/ml $^{-1}$ change in S11 isolates after sub-zero incubation. S11D, S11G, S11I and S11L had an increase in CFU/ml $^{-1}$ following incubation at -5 °C. S11K and S11M had variable increase and decrease in CFU/ml $^{-1}$. S11C and S11E showed no difference and the remainder of the isolates had a decrease in CFU/ml $^{-1}$ following incubation at -5 °C.

Isolate code	Closest match ID (where known)	Decrease	No difference	Variable increase/ decrease	Increase
S11A	-	+			
S11B	-	+			
S11C	*Polaromonas* sp. strain EXB-L-2565		+		
S11D	-				+
S11E	-		+		
S11F	*Polaromonas glacialis* strain HCR18h	+			
S11G	-				+
S11H	-	+			
S11I	*Variovorax* sp. HW81				+
S11J	-	+			
S11K	-			+	
S11L	*Polaromonas* sp. strain EXB-L-2565				+
S11M	*Pseudomonas* sp. strain ANT_J9B			+	

The S11 isolates had different morphologies and growth profiles (**Appendix, Table 19**) therefore, different dilutions (10^{-2} , 10^{-3} and 10^{-4}) and different colony counts (day 5 and at 3.5 weeks) were required to ascertain the change in CFU/ml $^{-1}$ pre- to post- freeze. As such, the data set most informative / illustrative from isolates with increased CFU/ml $^{-1}$ following incubation at -5 °C are plotted in **Figure 21.**

CFU/ml $^{-1}$ of isolate S11D increased for the first two incubation periods then dropped in the final incubation period (**Figure 21, A**). The 10^{-3} dilution, day 5 count data showed a statistically significant difference between groups as determined by one-way ANOVA ($F(3,8) = 38.111$, $p<0.001$). A least significant difference (LSD) post hoc test revealed that compared to pre-freeze (mean CFU/ml $^{-1}$ of 0 ± 0), week 4 (mean CFU/ml $^{-1}$ of 53.34 ± 7.09, $p<0.001$), week 8 (mean CFU/ml $^{-1}$ of 43.67 ± 6.66, $p<0.001$) and week 12 incubation colony counts (mean CFU/ml $^{-1}$ of 18 ± 9.54 $p<0.05$) were all significantly higher than pre-freeze.

CFU/ml $^{-1}$ values for of S11G (**Figure 21, B**) were significantly different pre- to post-freeze. A statistically significant difference (10^{-2}, week 3.5 count data) between groups (was determined by one-way ANOVA ($F(3,8) = 6.403$, $p=0.016$). A LSD post hoc test revealed that compared to pre-freeze (mean CFU/ml $^{-1}$ of 38.34 ± 6.03), CFU/ml $^{-1}$ values

in week 4 incubations (mean CFU/ml $^{-1}$ of 72 ± 12.53, p=0.009), week 8 (mean CFU/ml $^{-1}$ of 74.34 ± 9.07 p=0.006) and week 12 incubations (mean CFU/ml $^{-1}$ of 73.34 ± 17.21 p=0.007) were all significantly higher.

Similarly, CFU/ml $^{-1}$ values of S11I (10 $^{-3}$, day 5 data) were all significantly higher post-freeze compared to pre-freeze (**Figure 21, C**) (one-way ANOVA (F(3,8) = 63.965, p<0.001). A LSD post hoc test revealed that compared to pre-freeze (mean CFU/ml $^{-1}$ of 0 ± 0), week 4 (mean CFU/ml $^{-1}$ of 112 ± 14.93, p<0.001), week 8 (mean CFU/ml $^{-1}$ of 125.34 ± 13.01 p<0.001) and week 12 incubation colony counts (mean CFU/ml $^{-1}$ of 108.34 ± 15.5 p<0.001) were all significantly higher.

Due to a lack of variance between the within group values in the S11L data set (10 $^{-4}$, week 3.5 count data) (**Figure 21, D**), the Kruskal-Wallis test was applied rather than an ANOVA, and a significant difference (H=10.735, df=3, p=0.013) between the mean ranks of at least one pair of groups was observed. Dunn's pairwise tests were carried out for the four pairs of groups. There was a significant increase in CFU/ml $^{-1}$ (p=0.045, adjusted using the Bonferroni correction) from the pre-freeze group to all other groups (weeks 4, 8 and 12 incubation) (median pre-freeze CFU/ml $^{-1}$ value of 13, all other incubations were the same CFU/ml $^{-1}$ at 300).

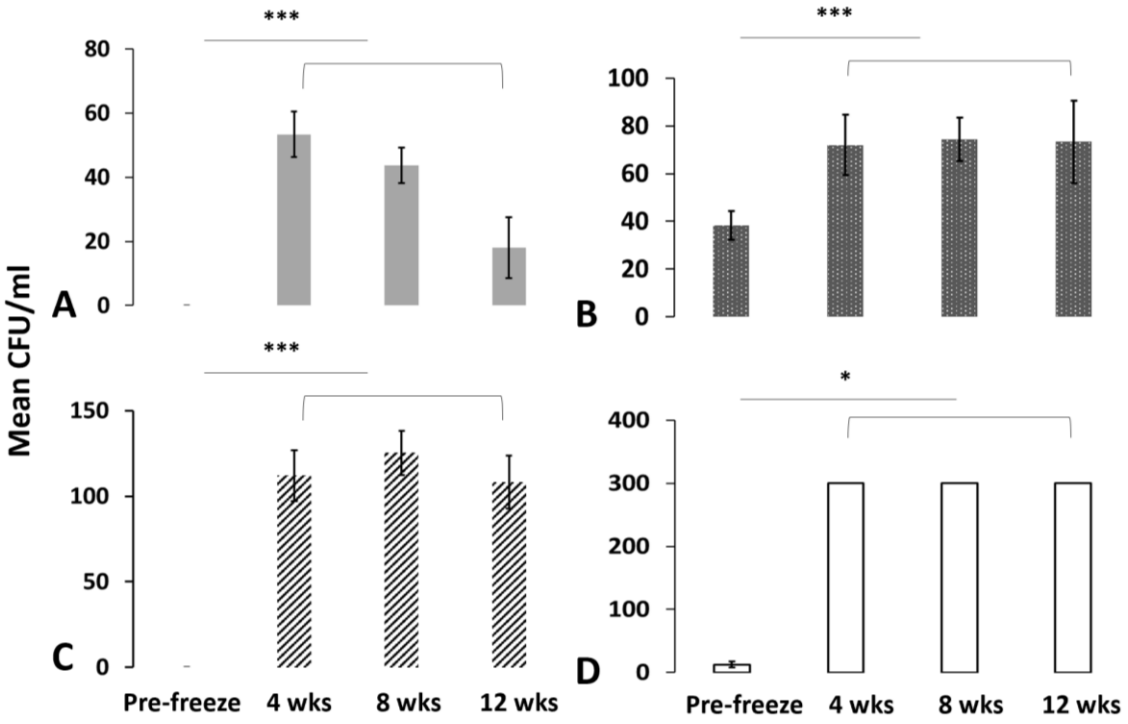

Figure 21. Isolates with increased CFU/ml $^{-1}$ following incubation at -5°C. Colony counts were recorded at day 5 and at 3.5 weeks for each isolate at each dilution in triplicate. The most informative data for each isolate are plotted (mean CFU/ml $^{-1}$ (n=3) for each incubation period). Each isolate showed a statistically significant increase in CFU/ml $^{-1}$ in all incubations compared to the pre-freeze number in each case. Where 300 is plotted this indicates a fully grown confluent field of growth. **A) Isolate S11D**, the 10 $^{-3}$ dilution (CFU/ml $^{-1}$ at day 5) is plotted. **B) Isolate S11G**, dilution set of 10 $^{-2}$ is plotted (CFU/ml $^{-1}$ at 3.5 weeks). **C**) **Isolate SIII**, dilution set of 10 $^{-3}$ is plotted (CFU/ml $^{-1}$ at day 5). **D) Isolate SIIL**, dilution set of 10 $^{-4}$ is plotted (CFU/ml $^{-1}$ at 3.5 weeks). (Errors bars shown are ± one standard deviation). (Statistical significance, where present, is designated with a horizonal bar and asterisk; $p<0.001$ ***, $p<0.01$ ** and $p<0.05$ *).

3.3.1.2 Attenuance

Optical density attenuance readings at 600 nm for each isolate were taken prior to freezing and then as soon as possible (once thawed) following withdrawl from the freezer at each incubation time point. Due to time restrictions and the volume of isolate sample available after dilutions and plating, the triplicate set of incubation samples for each isolate were pooled for the reading. As such, attenuance values plotted (**Figure 22**) represent a mean, pooled average of each isolate at each time point.

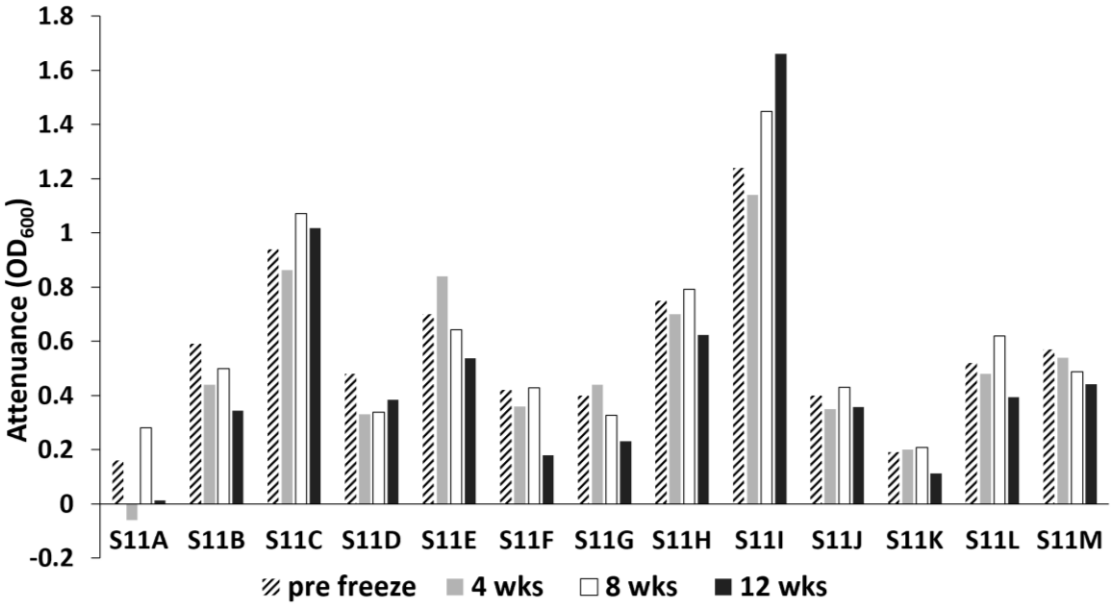

Figure 22. Attenuance (OD_{600}) of S11 isolates pre- and post- incubation at -5°C. Readings were taken pre-freeze and at 4 , 8 and twelve weeks of incubation from pooled (n=3) samples.

Although increases in attenuance are observed at some time points for several isolates, generally values either remained similar to the pre-freeze values, or indeed dropped. However, one isolate did show an overall increase in attenuance, S11I , although the week four value dropped just below that of pre-freeze (down to 1.14 AU from the pre-freeze value of 1.24), attenuance (at OD_{600}) climbed to 1.66 by the 12-week incubation point. This is an increase of 0.24, or ~20% which is the highest increase in attenuance observed in the isolates (pre- to post- freeze). This corresponds to a statistically significant increase in CFU/ml $^{-1}$ following incubation at sub-zero. Indeed, the only isolate to show both increased CFU/ml $^{-1}$ and overall increased attenuance was S11I, the isolate with 99.84% identity to *Variovorax* sp. HW81.

Additionally, it should be noted that an intensification of pigment was observed generally pre- to post- incubation (**Appendix, Figure 35**), especially so in isolates S11I and S11M. However, this was not quantified and is observational only.

3.3.2 A18.2 pigment production

The difference in pigmentation of isolate A18.2 grown under 24-hour dark and light conditions was visually apparent (**Figure 23**). When grown in the dark, the colonies appear cream in colour, in the light they are lemon yellow.

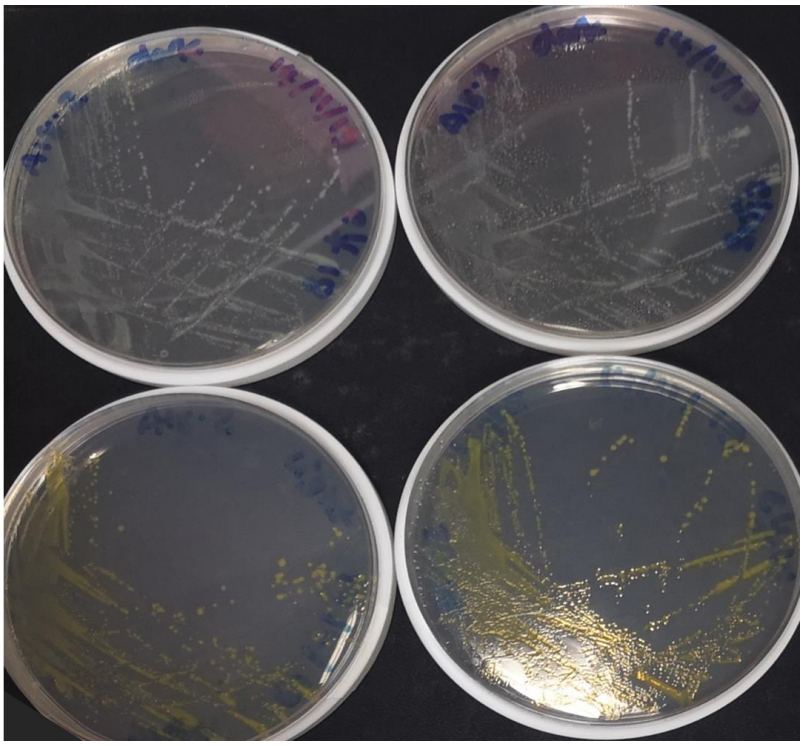

Figure 23. A18.2 on R2A. A18.2 grown on R2A under 24-hour dark condtions (top row) and 24-hour light condtions (bottom row) incubated at +2 °C for three weeks. The bright yellow pigment in those grown in the light is evident.

The level of pigmentation was assessed using sets of quadruplicate flasks of A18.2 grown in 24-hour light and 24-hour dark condtions using both biomass (inoculum) sourced from a dark grown plate and from a light grown plate (n=4 X 4, total of 16 flasks) incubated at +2 °C for three weeks.

To quantify the peak absorbance of the yellow pigment, extracts (**Figure 24**) were exposed to a range of wavelengths (**Figure 25**) (dark plate sourced inoculum into light and dark conditions is shown). Please refer to **Table 20 in Appendix** for the full data set (additional light plate sourced inoculum into light and dark conditions).

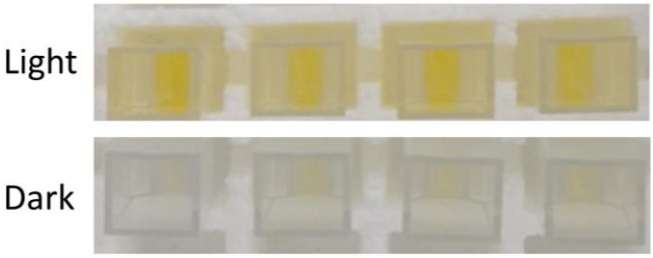

Figure 24. Extracted pigment. The extracts from the culture (dark plate sourced inoculum) grown in the 24-hour light conditions (top row) and 24-hour dark conditions (bottom row).

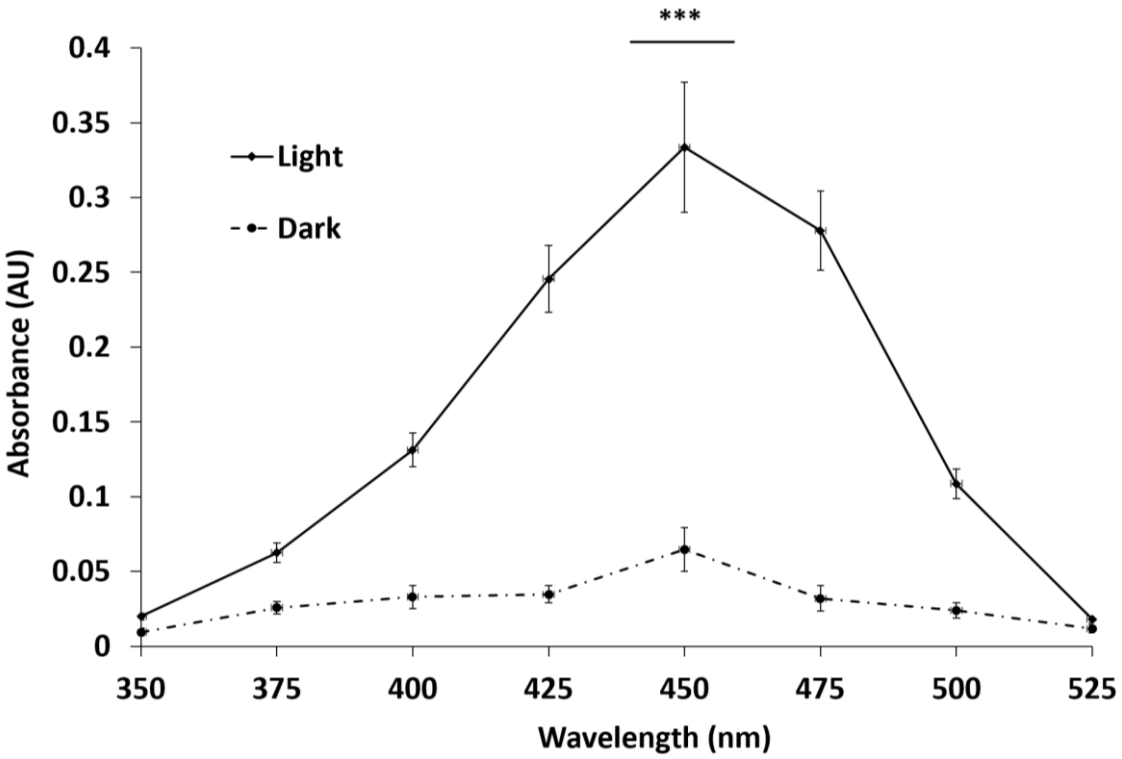

Figure 25. A18.2 pigment absorbance. The absorbance of the extracts from the culture (dark plate sourced inoculum) grown in 24-hour light conditions (n=4) and 24-hour dark conditions (n=4) are plotted. Peak absorbance in both sample sets is 450 nm. The mean AU value for light grown extracts at 450 nm (0.34) is over five times higher than that of the mean for dark grown (0.06) extracts and is statistically significant at $p<0.001$ (t_6 = 11.687). (Errors bars shown are ± one standard deviation). (Statistical significance, where present, is designated with a horizonal bar and asterisk; $p<0.001$ ***, $p<0.01$ ** and $p<0.05$ *).

As well as establishing that the peak absorbance for the extracted pigment is 450nm, a clear difference in the AU values between conditions is apparent. For instance, for the

450nm data an independent samples t-test returned a Levene's value of $p>0.05$ ($F=5.139$, $p=0.064$) thus equal variances were assumed and with a two-tailed significant value of $p<0.001$ ($t_6 = 11.687$), we can conclude that there is a highly statistically significant increase in AU value at 450nm in extracts from cultures grown in the light compared to dark. This indicates a considerable increase in pigment concentration and therefore pigment production under 24-hour light conditions compared to 24-hour dark conditions.

As stated, unfortunately due to COVID-19 restrictions, the extracts were not characterised as intended.

3.3.3 A18.2 UV tolerance

To establish if the pigment produced by A18.2 confers any increased resistance or tolerance to UV light irradiation, light grown and dark grown (pigmented and non-pigmented) cultures were exposed to increasing dosages of UV. The presence or absence of growth following the dosage for each replicate is given in **Table 8.**

Table 8. UV tolerance in light and dark grown A18.2. The presence or absence of growth, donated with **+** or **–** respectively, and sparse growth, **+ s,** for each biological replicate (light n=3, dark n=3) and each technical replicate (n=3 per biological replicate) for each dosage level is given in the table below.

µ Joules	light 1			light 2			light 3		
0	+	+	+	+	+	+	+	+	+
20,000	+	+	+	+	+	+	+	+	+
60,000	+	+	+	+	+	+	+	+	+
120,000	+	+	+	+	+	+	+	+	+
200,000	+	+	+	+	+	+	+	+	+
	dark 1			dark 2			dark 3		
0	+	+	+	-	+	+	+	+	+
20,000	+	+	+	+	+	+	+	+	+
60,000	+	+	+	+	+	+	+	+	+
120,000	+	+	+	+ s	+	+ s	+	+	+
200,000	+ s	+ s	-	-	-	-	+	+	+

For the purpose of binary statistical testing, all growth whether sparse or not, was deemed as growth. A Fishers exact test (alternative to chi square test) of all growth or non-growth following UV dosing for pigmented (light grown culture) vs non-pigmented (dark grown culture) (the full data set) gave a test statistic value of p=0.0556, which although close, is not significant. Using the data from just the strongest dose only (200,00 µ Joules), the Fisher exact test statistic value of p=0.08. Although these values are not significant, the sparser growth and lack of growth was only observed in the dark grown culture. Additionally, the dosage range was not extended far enough (**Figure 26**) to find maximum tolerance levels for each of the dark and light grown cultures.

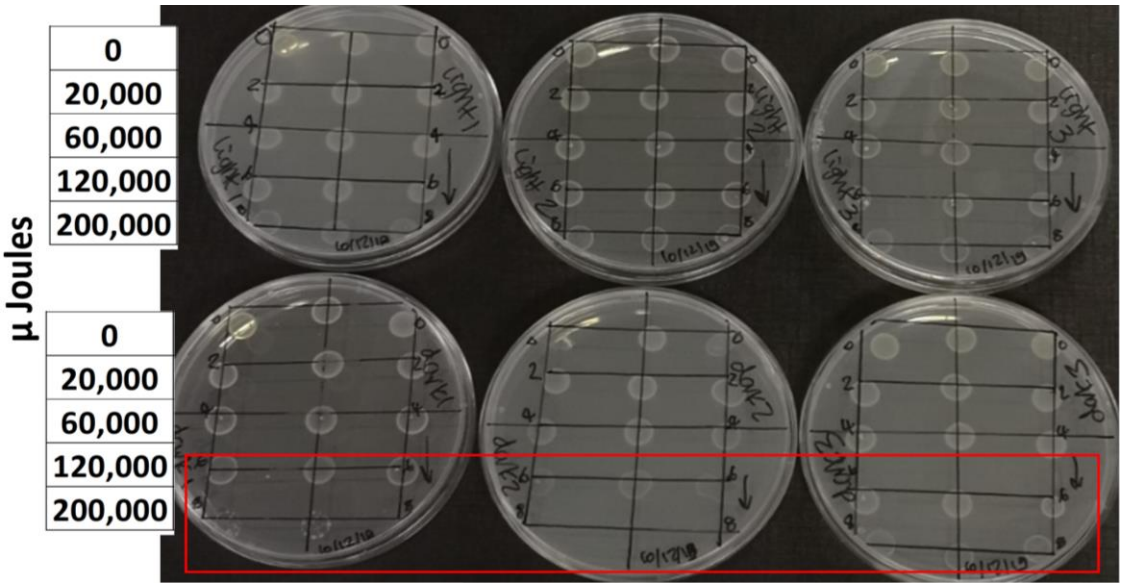

Figure 26. **UV tolerance in light and dark grown A18.2 at week 4**. Light grown cultures (top row of plates, biological replicate 1 to 3, left to right) grew at every single dosage level and in each technical replicate (rows within the plates). The dark grown cultures (bottom row of plates, biological replicate 1 to 3, left to right) grew in the majority of dosage levels, with the beginning of tolerance limit observed at a dosage of 120,000 - 200,000 µ Joules (red rectangle).

3.3.4 S11 isolate representatives

Representative genomes for S11 isolates with 16S rRNA gene sequences (therefore closest identity) were obtained from NCBI. In each case, the most suitable representative was selected, i.e. a cryospheric genome if available, in combination with

selecting for the completeness of assembly whilst being closest phylogenetically. This is understandably not wholly representative of the true variation in the genome that would be obtained from full genome sequencing of individual isolates but is a means of gauging an approximation of the type of genes that may be present in the genera. The three genomes selected (**Table 9**) were submitted to PROKKA for annotation. The annotations were then examined for cold and heat shock genes, stress genes and other genes associated with cold-adaption as well as light-sensing and carotenogenesis genes (full table providing frequency of gene type is available in **Appendix, Table 21**).

Table 9. Representative genome details. Identity, size and number of CDS.

	GenBank/ RefSeq assembly accession:	Contigs:	Bases (Mb):	CDS:
***Pseudomonas psychrotolerans* (ASM638497v1)**	GCA_006384975.1	1	5.4	4,772
***Polaromonas* sp. Pch-P (ASM966422v1)**	GCA_009664225.1	1	4.5	4,209
***Variovorax paradoxus* (M949845v1)**	GCA_009498455.1	1	7.3	6,688

All three representative genomes contained a number of stress, shock and cold-adaption associated genes (**Figure 27**) as well as predicted light-sensing and carotenoid biosynthesis genes (**Appendix, Table 21**). The only genome to contain CSP genes was the *Pseudomonas psychrotolerans* genome, 5 copies of CspA and a single copy of CspD. All three contained multiple stress, cold-adaption associated and heat shock genes.

Pseudomonas psychrotolerans contained all three types of phytochrome (cph1, cph2 and bphP) as well as the Blue light- and temperature-regulated anti-repressor BluF. *Variovorax paradoxus* had the cph2 and BluF genes and *Polaromonas* sp. Pch-P had the cph1 and BluF genes. All three representative genomes contained several carotenogenesis genes.

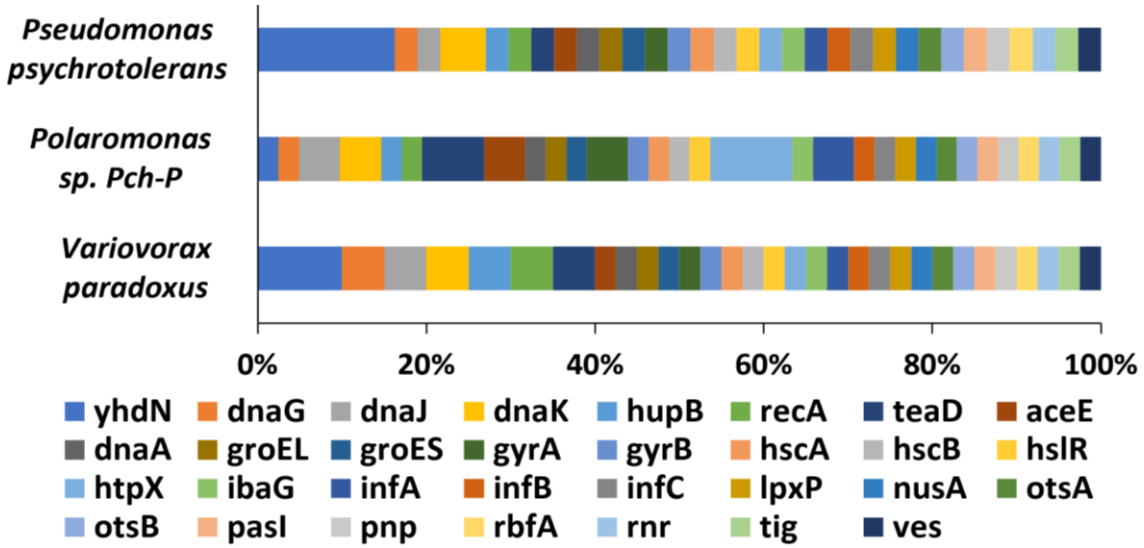

Figure 27. Cold-adaption associated, shock and stress genes in S11 isolate representative species. The genes common in each representative species assigned by PROKKA annotation are shown in the 100% stacked bar chart. The yhdN gene, which codes for general stress protein 69, is the most abundant gene (copy number) (from the identified set of stress/shock genes) in both *Variovorax paradoxus* and *Pseudomonas psychrotolerans*. The HtpX gene (heat shock response) was most abundant in the *Polaromonas* genome. The dnaK gene (chaperone protein) was present in equal proportion across the genomes.

3.3.5 A18.2 genome assembly

3.3.5.1 A18.2 Assembly statistics

The A18.2 FASTQ file generated from sequencing (live base-called) was submitted to the CANU assembly pipeline. The size and number of reads pre-assembly and the size and numer of resulting contigs are listed in **Table 10**. To view the assembly, the .gfa file produced from CANU was visualised in BANDAGE (**Figure 28**). The CANU assembler assigned the smaller contig (pink, 40,269 bp), which overlaps the end of the larger contig (green, 4,079,695 bp), as a repeat section (**Figure 28**, **A**)). When viewed on its own, the large contig forms a circular joined, contig (**Figure 28**, **B**)).

Table 10. A18.2 pre and post – assembly overview. The A18.2 reads pre-assembly, and once assembled are compared in the table below.

	Pre-Assembly
Number of reads	120,876
Mean read length (bp)	5,613
Median read length (bp)	4,059
Read length N50	8,621
Total bases (bp)	678,431,007
	Post-Assembly
Number of contigs	2
Mean contig length (bp)	2,059,982
Median contig length (bp)	4,079,695
Contig length N50	4,079,695
Total bases (bp)	4,119,964
Shortest contig (bp)	40,269
Longest contig (bp)	4,079,695
Average GC content (%)	67.2

3.3.5.2 A18.2 Genome visualisation

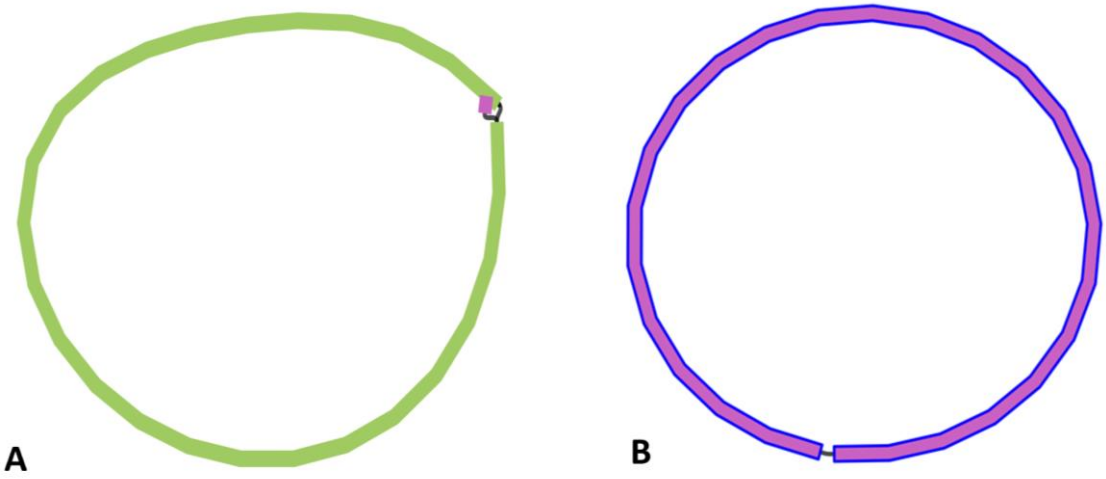

Figure 28. A18.2 assembly contig visualisation in BANDAGE. **A**) Both contigs are displayed, the smaller contig (pink, 40,269 bp) overlaps the end of the larger contig (green, 4,079,695 bp) and appears to be a repeat section as suggested by the CANU assembler. **B**) The large contig on its own forms a circular joined, contig.

3.3.5.3 A18.2 identity

The identity of isolate A18.2 was investigated using several methods. Firstly, the 16S rRNA gene sequence was submitted to NCBI BLASTn (**Table 11).** The query sequence did not cover more than 99% of any match. The top hit was *Cryobacterium* sp. AsdMX-L1 at 98.54% identity with 99% query cover. The top 5 closest matching FASTA 16S rRNA gene sequences and three further *Cryobacterium* spp. 16S rRNA gene FASTA sequences (from NCBI) were used to build a phylogenetic tree (**Figure 29).** The tree ranked *Cryobacterium psychrotolerans* strain 0549^{T} (the type strain) as the closest species to A18.2. Lastly the full genome of A18.2 and the type strain (*Cryobacterium psychrotolerans* strain 0549^{T} =CGMCC 1.5382^{T}, GenBank/RefSeq accession number: GCF_900101115.1) were submitted to an average nucleotide identity (ANI) calculator (http://enve-omics.ce.gatech.edu/ani/). ANI was estimated using both best hits (one-way ANI) and reciprocal best hits (two-way ANI) between the two genomes (**Figure 30**). The ANI between the two genomes was a mean 80.92% identity.

Table 11. **A18.2 16S rRNA gene sequence NCBI BLASTn top 5 results.** Top hits for the A18.2 16S rRNA gene.

Description	Max Score	Total Score	Query Cover	E value	Per. Ident	Accession
Cryobacterium sp. AsdMX-L1	2600	2600	99%	0.0	98.54%	JX123060.1
C. psychrotolerans strain SD-4	2599	2599	98%	0.0	99.13%	MF555698.1
Cryobacterium sp.DR9	2585	2585	99%	0.0	98.28%	FJ464984.1
Cryobacterium sp.ER1	2577	2577	99%	0.0	98.15%	FJ517629.1
Cryobacterium sp.EL1	2576	2576	99%	0.0	98.15%	FJ517614.1

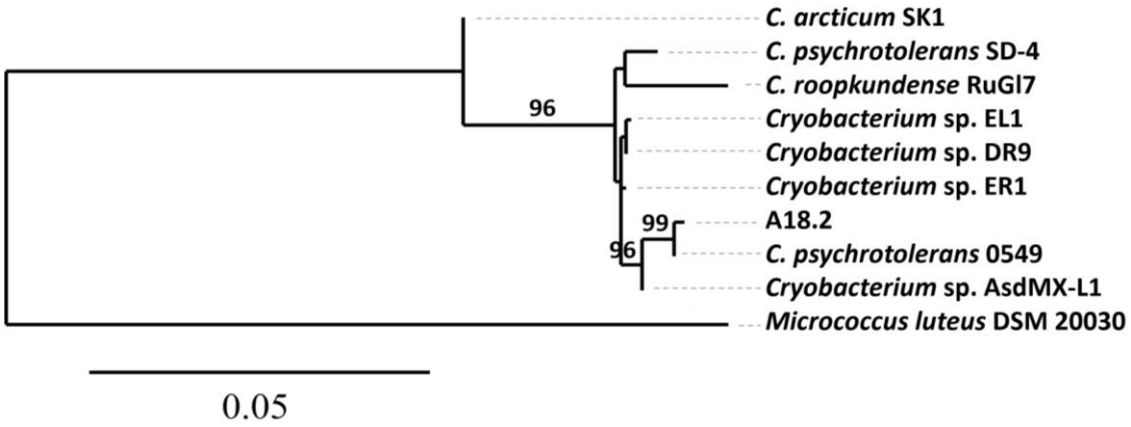

Figure 29. Maximum likelihood bootstrap consensus tree. The tree comprises the partial 16S rRNA gene sequences obtained from the A18.2 isolate, the top five closest species (% identity) sequences and three further *Cryobacterium* spp. sequences (from NCBI, including the type strain 0549). Tree generated using PhyML (v3.1/3.0 aLRT) (bootstrap 100). Bootstrap values (greater than 75%) are displayed at the nodes. Scale shows nucleotide substitutions per site.

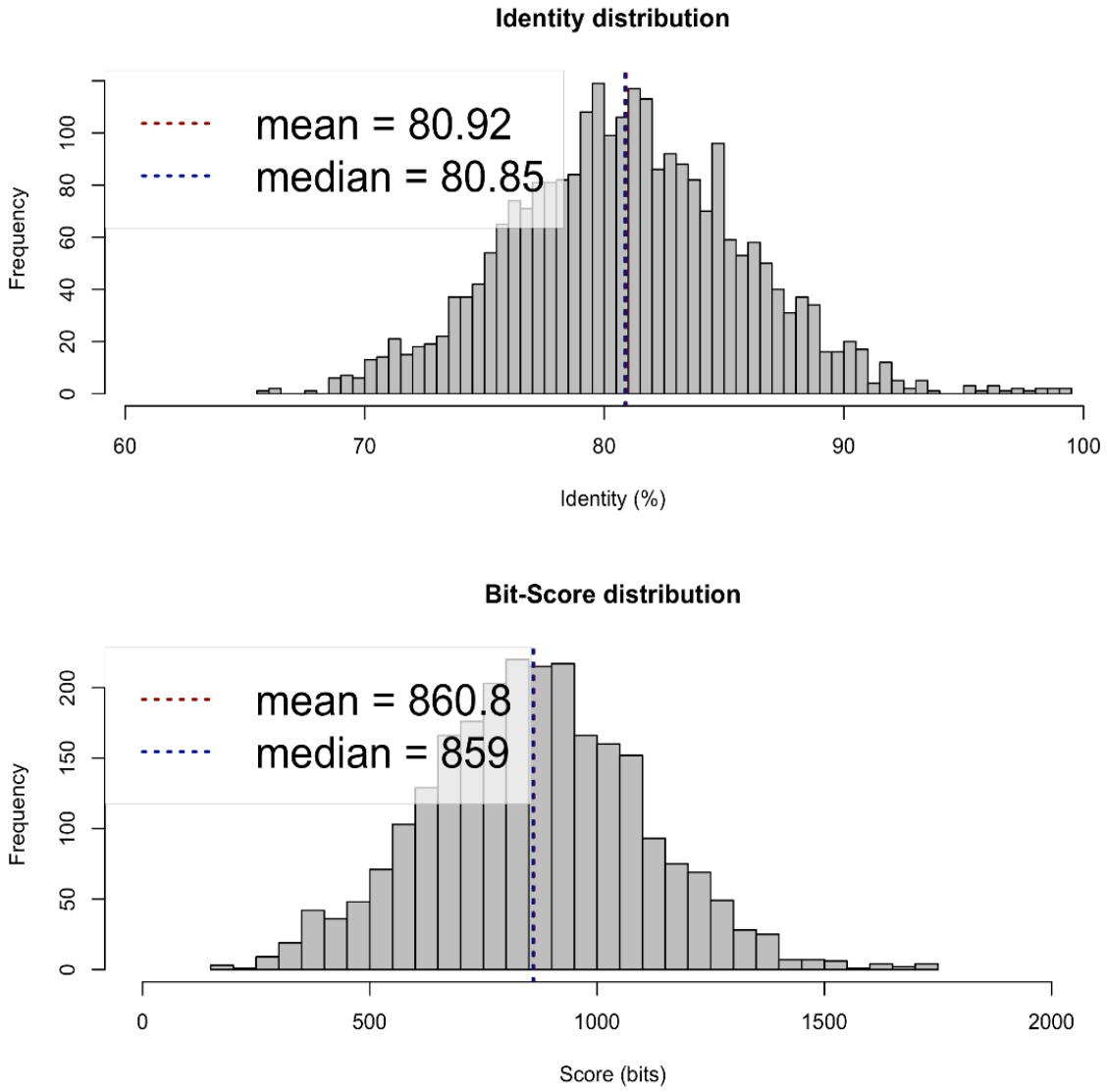

Figure 30. ANI between A18.2 and the *C. psychrotolerans* strain 0549^{T} (type strain) CGMCC 1.5382. Analysis and figure generated by the ANI calculator tool at http://enve-omics.ce.gatech.edu/ani/. The ANI values calculated were as follows – i) One-way ANI 1: 80.42% (SD: 4.83%), from 3743 fragments, ii) One-way ANI 2: 80.56% (SD: 5.14%), from 3811 fragments and iii) two-way ANI: 80.92% (SD: 4.85%), from 2506 fragments.

With a 16S rRNA gene sequence similarity value of 98.5% (<98.7%, the cut-off point regarded to be indicative of a new species) and an ANI value of 80.9% (<95%, the cut-off point regarded to be indicative of a new species) the A18.2 isolate is potentially a new *Cryobacterium* species (Chun *et al.,* 2018) or at the very least a new subspecies of *C. psychrotolerans*.

3.3.6 A18.2 genome annotation

3.3.6.1 Genome annotaion overview

The A18.2 and the *C. psychrotolerans* (0549^T type strain, CGMCC 1.5382^T) genomes were submitted to PROKKA for annotation. The overview **(Table 12)** provides the number of CDS assigned in each genome.

Table 12. A18.2 and *C. psychrotolerans* type strain 0549^T CGMCC 1.5382 overview. The two genomes are compared in the table below.

	A18.2	***C. psychrotolerans* strain CGMCC 1.5382**
Contigs:	2	45
Bases:	4,119,964	3,247,111
CDS:	7,649	3,015
tRNA:	52	53
rRNA:	9	4

3.3.6.2 A18.2 Gene profile

Both genome annotations were examined for stress genes, cold and heat shock genes and other genes assocatioated with cold-adaptation. Genes common across both geneomes are shown in **Figure 31**. A full table providing frequency of gene type is available in **Appendix, Table 22.** The general stress protein 69 gene (yhdN) is abundant (copy number) in both A18.2 and *C. psychrotolerans* 0549^T, along with gyrA and gyrB (DNA gyrase subunits A and B).

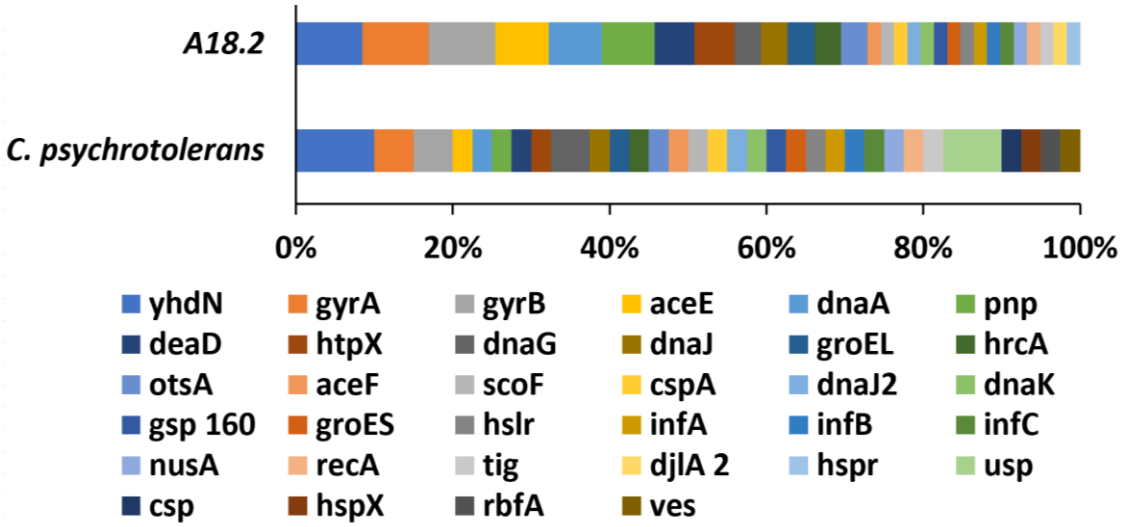

Figure 31. Cold-adaption associated, shock and stress genes in A18.2 and *C. psychrotolerans* 0549^{T}. The genes common in each genome as assigned by PROKKA annotation are shown in the 100% stacked bar chart. General stress protein 69 (yhdN) is most abundant in *C. psychrotolerans* and one of the most abundant in A18.2, alongside gyrA and gyrB (DNA gyrase subunits A and B), which are also predominant in *C. psychrotolerans.* Universal stress protein (usp) is also a dominant gene in *C. psychrotolerans.*

3.3.7 Carotenoid biosynthesis

The ability of A18.2 to biosynthesise carotenoids was supported using several bioinformatic approaches. Firstly, the A18.2 genome was submitted to antiSMASH, which detects secondary metabolite biosynthesis clusters. This web-based tool identified three regions, one of which was a carotenoid cluster. The query sequence when aligned with most similar carotenoid biosynthesis clusters indicated up to 37% of genes showed similarity (**Figure 32**). Additionally, the *C. psychrotolerans* 0549^{T} genome was submitted to antiSMASH. A single cluster, a carotenoid region, was identified. When the query sequence was aligned with most similar carotenoid biosynthetic clusters, up to 37% of genes showed similarity (**Figure 33**). In both A18.2 and *C. psychrotolerans* 0549^{T} alignments, the sequence with the highest percentage of similar genes was the BGC0000637 sequence.

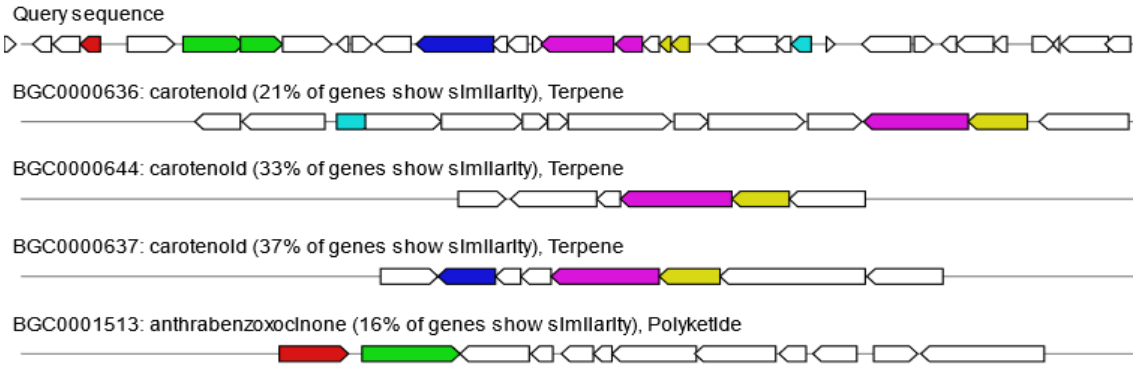

Figure 32. The A18.2 carotenoid biosynthesis cluster in antiSMASH. The query sequence is aligned with the most similar clusters. The query sequence showed 37% gene similarity to the BGC0000637 sequence.

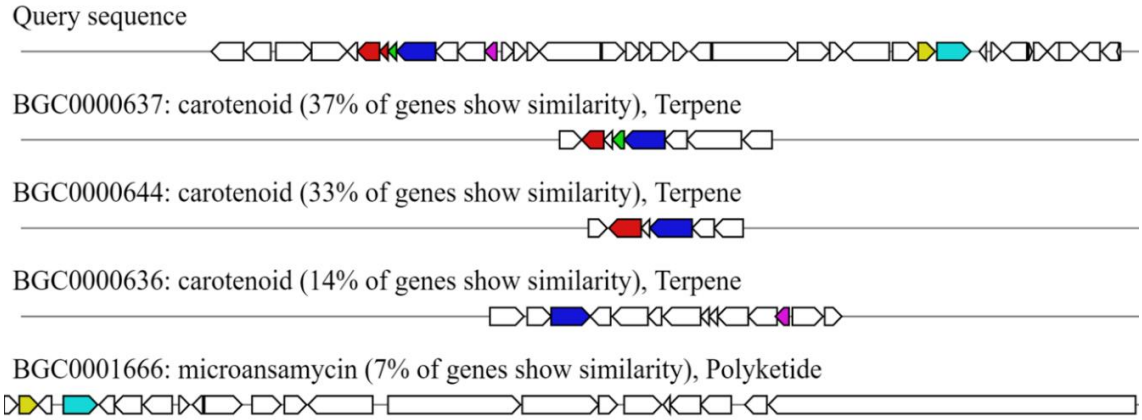

Figure 33. The *C. psychrotolerans* 0549^{T} carotenoid biosynthesis cluster in antiSMASH. The query sequence is aligned with the most similar clusters. The query sequence showed 37% gene similarity to the BGC0000637 sequence.

The presence of carotenoid *crt* genes were also examined in both A18.2 and *C. psychrotolerans* 0549^{T} genomes using PROKKA annotation (**Table 13**). The crtB gene was present in *C. psychrotolerans* alone, the crtN gene in A18.2 alone and both genomes contained the carA2 gene. Additionally, both the genomes had the phytochrome-like protein cph2 gene, (3 copies in A18.2, a single copy in *C. psychrotolerans*) (not shown).

Table 13. Carotenoid biosynthesis genes in A18.2 and *C. psychrotolerans* 0549^T. The genes identified by PROKKA are listed in the table below.

Gene	Description	A18.2	*C. psychrotolerans*
crt	Short-chain-enoyl-CoA hydratase	1	2
crtB	All-trans-phytoene synthase/15-cis-phytoene synthase	0	1
crtN	Dehydrosqualene desaturase	1	0
carA2	Zeta-carotene-forming phytoene desaturase	1	1

Lastly, both genomes were submitted to RAST and the carotenoid and terpenoid metabolic models produced were assessed. The same profile was seen in both A18.2 and *C. psychrotolerans* 0549^T. For terpenoid backbone biosynthesis, the RAST (SEED viewer) recorded 11 ECs (Enzyme Commission numbers, a numerical classification scheme for enzymes) out of 27 (40.7%) (**Figure 34**). For carotenoid biosynthesis, 7 out of 19 ECs (36.8 %) were found.

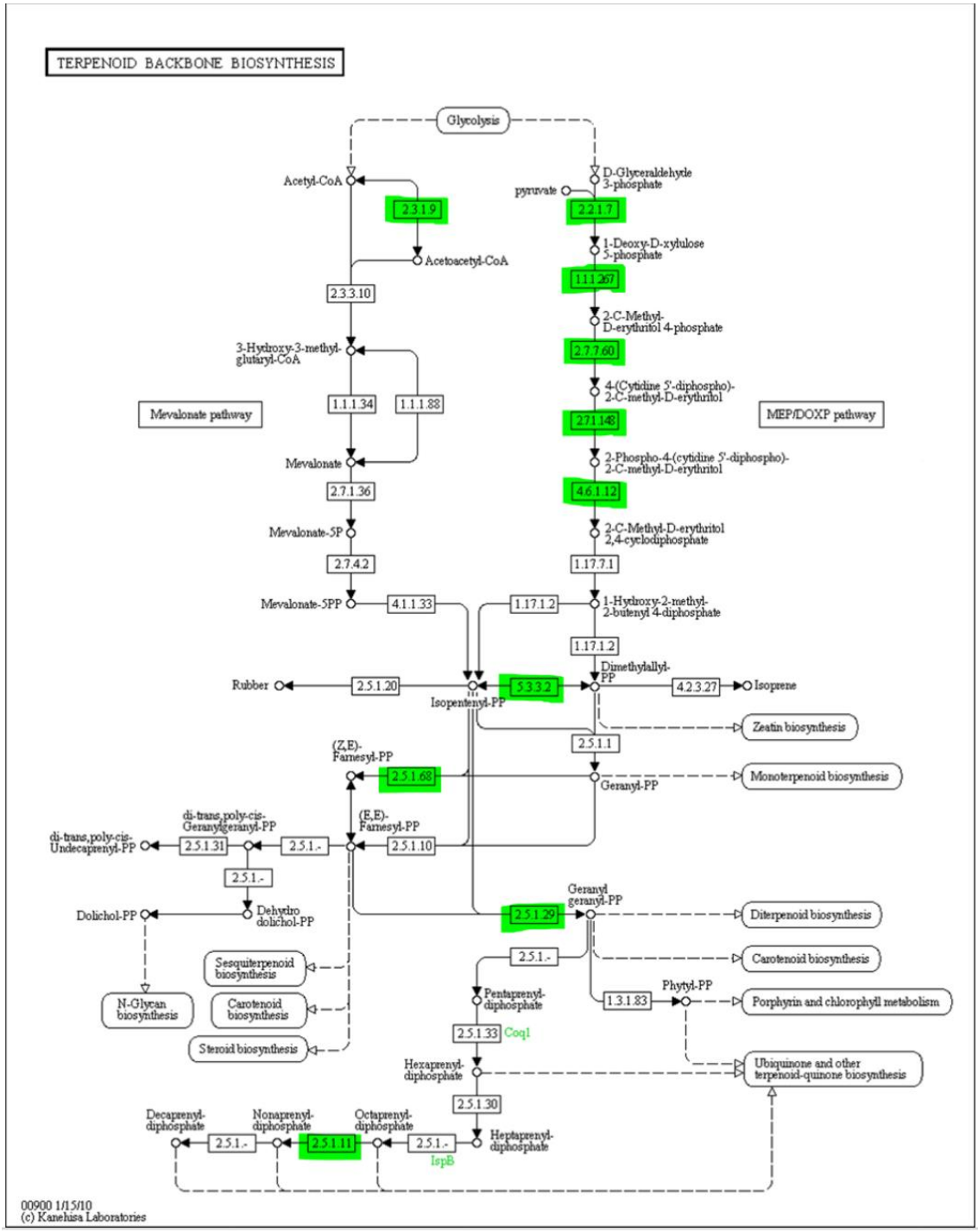

Figure 34. A18.2 KEGG metabolic model for terpenoid backbone biosynthesis. Highlighted in green are the ECs, 11 out of the 27 (40.7%).

3.4 Discussion

A range of responses to the applied cryospheric stresses were observed between individual taxa. Cryoconite isolates responded differently to the sub-zero temperature incubations - responses included an increase, no difference and a decrease in CFU/ml $^{-1}$ value. Pigment production following continual illumination was observed in the A18.2 isolate, however any protective effect against UV irradiation that the pigment may have conferred was non-significant at this stage. Following assembly of the A18.2 genome, the identity of the isolate and the carotenoid biosynthesis ability were assessed. The A18.2 *Cryobacterium sp.*, although very closely related to *C. psychrotolerans* 0549^{T}, could represent a novel species and has the capacity to both detect light and synthesise carotenoids. Furthermore, the genomic mechanisms of individual taxa to produce protective responses to cryospheric stress were compared and common strategies identified.

3.4.1 S11 isolate sub-zero incubations

Although the S11 isolates incubated at -5 °C presented a range of results, almost a third (30.8%) had an increase in CFU/ml $^{-1}$ following incubation (**Table 7**). This appears consistent with the proportions of bacterial isolates observed to be able to grow at −10 °C (20%) and at –2.5 °C (67%) from permafrost (Rivkina *et al.,* 2018). Specifically, four of the isolates, S11D, S11G, S11I and S11L showed statistically significant higher CFU/ml $^{-1}$ post-freeze compared to pre-freeze at each incubation point (four, eight and twelve weeks) (S11D, S11G, S11I $p< 0.001$) (S11L $p<0.05$). Additionally, isolate S11I (99.84% identity to *Variovorax* sp. HW81, see chapter 2) also showed increased attenuance post-freeze compared to pre-freeze. The ubiquitous *Variovorax* genus are known to be successful in a range of habitats, including extreme and cold environments (Satola *et al.,* 2013), indeed, *V. paradoxus* has been isolated from surface snow (Segawa *et al.,* 2005). The S11I isolate, a peach-coloured isolate, along with a few other isolates, appeared to increase in pigment intensity following incubation at -5 °C (**Appendix, Figure 35**) although this was an observation only and not quantified, however, pigment production

is shown to be upregulated under temperature stress in some species (Ram *et al.,* 2020) thought to be for the purpose of cryoprotection or to maintain membrane fluidity at these low temperatures (Collins and Margesin, 2019).

Interestingly, the *Polaromonas* spp. isolates (S11C and S11L, 99.86% and 94.16% identity to *Polaromonas* sp. strain EXB-L-2565 respectively and S11F 100% identity to *P. glacialis* strain HCR18h) displayed the full range of responses; both a decrease (S11F), no difference (S11C) and an increase (S11L) in CFU/ml $^{-1}$ post-freeze compared to pre-freeze (**Table 7**). The metabolically versatile "opportunitrophic" *Polaromonas* genus are one of the predominant bacteria in cold environments (Darcy *et al.,* 2011). The genus is shown to be able to adapt to and utilize a range of energy sources, in part due to the high levels of horizontal gene transfer (HGT) (Darcy *et al.,* 2011), which is predominantly plasmid mediated. Indeed, the plasmids of psychrotolerant *Polaromonas spp.* have been shown to play a role in the ability to adapt to the polar environments they live in (Ciok *et al.,* 2018). It seems possible therefore, that the three *Polaromonas* strains (S11C, S11F and S11L) isolated and tested in this study showed different responses to sub-zero temperatures due to the presence or absence of particular auxiliary genes on their plasmids.

Isolates S11D and S11G are as yet unidentified although it is promising that both produced more CFU/ml $^{-1}$ post-freeze compared to pre-freeze. Isolate S11M (92.06% identity to *Pseudomonas* sp. strain ANT_J9B) had variable responses with no observed trend, with both increases and decreases of CFU/ml $^{-1}$ at different time points in different dilutions. This could be due to human error or a result of the types of cells plated. It is possible that a sub-population of the *Pseudomonas* isolate entered a dormant, or viable but not culturable (VBNC) state when subjected to sub-zero temperatures. Indeed, *P. aeruginosa* has been shown to display a dormancy phenotype, changing morphology from rod to coccid during long-term survival in water (Lewenza *et al.,* 2018). Psychrotolerant species of *Pseudomonas* are documented (Panicker *et al.,* 2002; Hauser *et al.,* 2004) however growth or division at temperatures below 0 °C to my knowledge has not been reported.

A substantial proportion of the S11 isolates produced additional colonies following incubation at -5 °C. There are however a number of ways to optimize, extend and improve the experiment. Firstly, the OD_{600} readings were pooled (n=3) and as such had no error bars. Additional sample volume and time allowances would allow for discrete readings and give more robust data and allow for statistical analyses. Additionally, the method of taking optical density readings, given that samples may sediment or suspend in liquid in a different manner after being frozen, may not have been the best method to monitor increase in cell concentration. The use of flow cytometry would be an alternative measure to confirm the change in cell abundance and viability in a given volume of sample pre- to post- freeze, such as in the study by Bakermans and Skidmore., 2011. The length of isolate incubation time could also be extended to establish if some isolates grow slower than others and needed longer to divide. Lower or higher temperatures, such as -10 °C or -2.5 °C could be used to determine if some isolates can continue to withstand or even grow at lower temperatures and indeed if others can grow at sub-zero but need a higher temperature than -5 °C to manage this (Rivkina *et al.,* 2018). The media type could also be varied to account for the different substrate preferences of isolates , as well as the concentration of glycerol added (3% in this work), which could be altered to establish if this impacts on growth following sub-zero incubation (Panwar *et al.,* 2019). Lastly, colony counts at additional intervals between 5 days and the 3.5-week point would capture more detail and enable the collection of discrete colony count numbers instead of fully confluent growth in some cases.

Clearly, organisms that are found living in the cryoconite community need to withstand sub-zero temperatures, however, identifying whether individual taxa overwinter and enter dormant states or are indeed active during the winter would help establish which members of the community are involved in the rapid response seen in the community microcosm experiment and uncover the physiological ability of individual taxa.

However, the only isolates used in experiments in this work were the Proteobacteria (S11 isolates, *Pseudomonas, Polaromonas, Variovorax*) and the Actinobacteria (A18.2 *Cryobacterium*). Further experimentation with existing isolates of different species, genera, as well as phyla in combination with further isolation (and sequencing) in order to obtain different genera and phyla is necessary to determine the response and

mechanisms that different taxa produce to cryospheric stressors. Additional stressors could be used such as extremes of salinity, pH or nutrient and water availability (Poniecka *et al.,* 2020). Many more isolates from dominant cryoconite phyla such as Bacteroidetes, Acidobacteria and Firmicutes are needed. To generate a range of isolates multiple media types, samples and isolation conditions should be incorporated (Gilichinsky *et al.,* 2008).

3.4.2 S11 isolate representative genome characteristics

Although the S11 representative genomes are only representative, and therefore do not give a fully informative profile of the individual isolates, they are useful as a general indicator of the types of genes present in the genera and where possible, the closest species (phylogenetically) with an available genome. Full genome sequencing of each isolate is however necessary to not only identify species (if known) but to annotate specific genes in order to identify those likely used in the response and adaption to sub-zero temperature stress. Of the three representative genomes, the *Variovorax paradoxus* at 7.3 Mb was the largest (**Table 9**), and although the corresponding isolate (S11I) was the only isolate to show both increased colony count and attenuance post-compared to pre-freeze, the *Pseudomonas psychrotolerans* genome was the only genome with CSPs. However, several types of stress, shock and cold-adaption associated genes were seen in all the representative genomes, and generally, all three genomes had similar such gene types, albeit in different quantities (**Figure 27**). Intriguingly, whilst the S11L isolate also showed an increase in colony count, S11C and S11F (all three are *Polaromonas* spp. and are represented by the *Polaromonas* sp. Pch-p genome) did not show an increase and neither did the S11M isolate (represented by the *Pseudomonas psychrotolerans* genome). As discussed, this could be due to the varied auxiliary genes in plasmids of *Polaromonas* spp. and to potential dormancy phenotypes in *Pseudomonas* spp. The fact that all three representative genomes have very similar stress, shock and cold-adaption gene profiles and contained both light-sensing and carotenoid biosynthesis genes (**Appendix Table 21**) is relatively unsurprising given that all are Proteobacterial, however, the occurrence of these types of gene could be part of the

reason such genera are so successful in cryospheric environments. Full genome sequencing of the individual isolates is crucial if the exact genes present are to be identified, and therefore their suggested role in sub-zero tolerance and growth. However, of note is the general stress protein 69 gene (yhdN) which, of the set of stress, shock and cold-adaption genes surveyed, was the most abundant gene (most copies) within two of the three representative genomes (*Pseudomonas psychrotolerans and Variovorax paradoxus*) and present in the third genome (*Polaromonas* sp. Pch-p). The yhdN gene was also present in both metagenomes. The yhdN protein has an aldo-keto reductase function, converts methylglyoxal (a toxic by-product of glycolysis) to acetol (Chandrangsu *et al.,* 2014) and is involved in stress response (Höper *et al.,* 2005). However, the physiological function of yhdN in stress response remains elusive at this point and to my knowledge, gsp69 has not been connected to cold-adaption, stress or tolerance thus far. I suggest further investigation of the prevalence of the yhdN gene in cryospheric sequence data sets as well as determining the role and function of yhdN in cold tolerance and adaption.

Other genes that predominated the stress and shock profiles of the S11 representative genomes included the heat shock genes htpX and dnaK, which although heat shock genes, are often abundant in cold-adapted genomes/metagenomes (Teoh *et al.,* 2018; Varin *et al.,* 2012; Koo *et al.,* 2018).

The Gammaproteobacterial *Pseudomonas psychrotolerans* genome had additional stress, shock and cold-adaption genes not present in the Betaproteobacterial *(V. paradoxus and Polaromonas* sp. Pch-p) genomes (**Appendix, Table 21**; 5 copies of cspA, 1 copy of cspD, 1 copy of deaD and 1 copy of uspA2). Whether these are present in the S11M *Pseudomonas* spp. isolate however is unknown. As mentioned, full genome sequencing of each isolate is necessary to determine the genomic abilities of individual taxa, however, the presence of so many types of shock, stress and cold-adaption associated genes in all of the representative genomes is indicative of the abilities of these genera to succeed in hostile environments. Furthermore, identifying common genes across the cryoconite heterotrophic community is useful in developing a cold-adaption profile of this population.

3.4.3 A18.2 pigment production and UV tolerance

After three weeks of growth under illumination, the A18.2 isolate had produced a bright lemon-yellow pigment. When grown in the dark, the isolate was cream in colour. Once extracted, the pigment was subjected to a range of wavelengths, between 350 – 525 nm (**Figure 25**). The peak absorbance point was at 450 nm, characteristic of carotenoids (Zaghdoudi *et al.,* 2017; Vila *et al.,* 2019). The mean AU value at 450 nm for the light grown extracts was 0.34, over five times higher than the value for the dark grown extracts (0.06) and is a statistically significant ($p<0.001$) increase, indicating that carotenogenesis in isolate A18.2 is indeed light induced, be it either substantial up-regulation of constitutive production or indeed light induced production of a non-constitutive manner. The production of pigment in response to illumination is an economic strategy - there is a trade-off between the costs of production and the contribution to fitness. This adaptability to changing environmental stimulus and response to light stress was also seen in the cryoconite community as a whole (Chapter 2). In order to characterize the pigment, the chromatographic and spectroscopic characteristics should be assessed by methods such as high-performance liquid chromatography (HPLC) and mass spectrometry (Vila *et al.,* 2019).

The intended characterisation was not possible due to the COVID 19 restrictions put in place; however, I believe it is very likely a carotenoid for a number of reasons. Firstly, the extract showed peak absorbance at 450 nm, which is characteristic of carotenoids (Zaghdoudi *et al.,* 2017; Vila *et al.,* 2019), secondly, carotenoid biosynthesis genes were present in the genome, third, of the pigments produced by bacteria, carotenoids are the most extensively produced (Malik *et al*., 2012; Kirti *et al*., 2014; Sajjad *et al*., 2020), fourth, cold-adapted bacteria are known to produce carotenoids (Dieser *et al.,* 2010) and lastly whilst a number of *Cryobacterium* isolates are documented as being pigmented (Reddy *et al*., 2010; Zhang *et al*., 2007; Dastager *et al*., 2008) and a recently released study confirmed the abundance of pigment producing genes in the *Cryobacterium* genus (Liu *et al*., 2020), to date a single study by Vila *et al*., 2019 has established pigment identity of a *Cryobacterium* isolate that produced a yellow C.p 450 carotenoid.

Additional stressors could be applied to the isolate, such as a range of pH levels or salinity concentrations, to establish if the upregulation or inducement of carotenoid production occurs under differing stresses (Ram., *et al* 2020).

When tested, the protective effect of the pigment produced by A18.2 against UV irradiation was statistically non-significant, however It should be noted though, that the binary statistical test (Fisher exact) counted all growth whether sparse or not, as growth. Indeed, only the light grown, pigmented culture grew at every single UV dosage tested whilst the non-pigmented, dark grown culture failed to grow at higher doses in a number of cases (at the upmost dose of 200,00 µJ, in the dark grown test 4 out of 9 did not grow, a further 2 of those 9 grew sparsely, thus only 3 grew fully, whilst all 9 light grown tests grew fully at that dosage). Whilst it has long been recognised that carotenoids provide a protective UV benefit (Mathews and Krinsky., 1965; Mueller *et al.,* 2005; Dieser *et al.,* 2010; Shen *et al.,* 2018) the UV dosage range did not extend far enough to observe the maximum limits of UV tolerance for either the light or dark grown cultures (**Figure 26**). This could be due to the ability of the isolate to withstand higher UV levels than typical bacteria, which extremophilic bacteria are often able to do (Rasuk *et al.,* 2017), potentially due to UV damage repair mechanisms. Or the high dosage tolerated could be due to the age and therefore power of the UV bulbs in the Stratalinker®, which were over a year old. Higher dosages and new bulbs would ensure the cut-off point for all growth is reached and the protective benefits of the pigment could then be determined with higher certainty.

Additional methods to establish if the pigment offers a protective benefit could include tests similar to those conducted by Mohana *et al*., 2013 who by using carotenoid produced by other species, proved the UV protective properties of the pigments by adding the extracted pigments to a UV susceptible strain (Mohana *et al*., 2013).

3.4.4 A18.2 assembly and identity

The assembly of A18.2 resulted in a 4.1 Mb contig with a 40Kb repeat section. Viewed in BANDAGE, the genome was circularised. The CANU assembler pipeline was an affective assembly tool, however, to improve, further polishing to remove any indels could improve the accuracy of the assembly further (Deschamps *et al.,* 2016). I believe indels, specifically insertions and duplications are present in the A18.2 genome due to the higher number of CDS and gene copies I observed in A18.2 compared to the *C. psychrotolerans* 0549^{T} (type strain) genome and when compared to the values (CDS) in the recent *Cryobacterium* genomic study by Liu *et al.,* 2020. Furthermore, hybrid assembly using traditional sequencing reads combined with Nanopore reads could enhance the accuracy and produce a reference quality genome (De Maio *et al.,* 2019).

The identity of A18.2 was investigated using a number of methods, both 16S rRNA gene BLASTn and maximum likelihood tree-building as well as ANI using the whole genome against *C. psychrotolerans* CGMCC 1.5382^{T} the type strain of *C. psychrotolerans,* which was first described by Zhang *et al.,* in 2007. With a 16S rRNA gene sequence similarity value of 98.5% (<98.7%, the cut-off point regarded to be indicative of a new species) and an ANI value of 80.9% (<95%, the cut-off point regarded to be indicative of a new species) the A18.2 isolate is potentially a new *Cryobacterium* species (Chun *et al.,* 2018) or at the very least a new subspecies of *C. psychrotolerans*. Liu and colleagues (Liu *et al.,* 2019) propose that the diversity of *Cryobacterium* species inhabiting glaciers may be hugely underestimated when using the 16S rRNA gene alone due to the near identical gene sequences observed between species which correspond with very low DNA–DNA hybridization (DDH) values, as such, distinguishing between closely related species is difficult (Liu *et al.,* 2019). Indeed, with ANI values between 76.66% - 83.79% (to closest related species) Liu and colleagues proposed two novel *Cryobacterium* species, thus with an ANI value of 80.9% for A18.2 (to its closest related species), the isolate could indeed represent a new species of *Cryobacterium,* although, the accuracy of the assembly needs to be verified and further polishing to remove indels (using tools such as Medaka distributed under the terms of the Mozilla Public License 2.0 © 2018 Oxford Nanopore Technologies Ltd.) as well as potentially constructing a hybrid assembly (De Maio et al., 2019) using additional reads would ensure this.

3.4.5 A18.2 stress, shock and cold-adaption gene profile

When comparing the A18.2 and *C. psychrotolerans* 0549^T (CGMCC 1.5382) annotations, the stress, shock and cold-adaption profiles are similar (**Figure 31**), with the yhdN gene (general stress protein 69) dominant in both, along with gyrA and gyrB (DNA gyrase subunits A and B). Primarily, the number of genes in the the stress, shock and cold-adaption profiles differed (more copies in A18.2) rather than the types of genes, but in some instances, genes were detected in one genome and not the other, such as the universal stress protein in the *C. psychrotolerans* 0549^T genome, which was a dominant gene, but wasn't detected in the A18.2 genome, as well as single copies of csp, hspX, rbfA and ves whilst the A18.2 genome contained genes not detected in the *C. psychrotolerans* genome (djlA2 and hspR) (**Appendix, Table 22**). In both genomes however, heat shock genes were more abundant than cold shock genes, a finding recently noted in other psychrophilic *Cryobacterium spp.* (Liu *et al.,* 2020).

3.4.6 A18.2 Carotenogenesis

A18.2 demonstrated carotenogenesis upon illumination. As such, light sensing photoreceptors are necessary in order to detect light. The phytochrome-like protein cph2 was detected in both A18.2 (3 copies) and *C. psychrotolerans* 0549^T (1 copy). Carotenoid biosynthesis clusters and genes were also compared. The antiSMASH tool found that both A18.2 and *C. psychrotolerans* had a cluster with 37% gene similarity to the closet match carotenoid biosynthesis cluster. Similarly, the RAST SEED viewer tool, detected 7 out of 19 ECs (36.8%) for carotenoid biosyntheisis in both genomes. Additionally, 11 ECs out of 27 (40.7%) of terepenoid backbone biosytheisis genes were detected in each genome too.

It seems highly likely that the A18.2 phytochrome, a light-regulated two-component histidine kinase, detects light before generating an output signal which regulates the production of carotenoid in this isolate. To confirm this, the knockout of the cph2 gene (all copies) followed by confirmation of the absence of pigment under illumination is necessary. Furthermore, the wavelength of light that triggers the phytochrome could be investigated by using different colour filters (Auldridge and Forest, 2011).

3.4.7 Chapter conclusion

Individual taxa tolerate sub-zero temperature stress to different extents. In this study, the *Variovorax* isolate, one of the *Polaromonas* isolates and two (as yet) unidentified isolates produced significantly more colonies following incubation at -5 °C than at the pre-freeze point. However, another *Polaromonas* isolate showed no difference, whilst a further *Polaromonas* isolate had a decrease in colony count. The varied ability the *Polaromonas* isolates display could be due to the high levels of plasmid mediated HGT the genus undergoes and therefore the presence or absence of auxiliary genes (Darcy *et al.,* 2011). The A18.2 (*Cryobacterium*) isolate when subjected to continual illumination for three weeks produced a bright yellow pigment. The pigment provided some protective benefit against UV irradiation, although it was not statistically significant at this stage, potentially due to the unexpected high dosage tolerated by the isolate. Further work using higher UV dosages is needed to confirm the protective benefit statistically. Undoubtedly the microbial inhabitants of a cryoconite hole experience multiple stressors and must respond and adapt accordingly. Although individual taxa do so in different ways and to different extents, similar strategies and mechanisms to counter stress were identified within the heterotrophic community. Pigmentation is one example of a common tactic cold-adapted, psychrophilic and psychrotolerant species employ. Indeed, all three representative genomes and both the A18.2 and *C. psychrotolerans* 0549^{T} genomes contained carotenoid biosynthesis genes as well as light sensing phytochrome genes. This trait was also found in the community genomic survey in Chapter 2. Genomic assessments also revealed other common traits and strategies. Stress, shock and cold-adaption genes similar in both the S11 isolate representative genomes and the A18.2 and *C. psychrotolerans* were identified. Of interest is the general stress protein 69 gene (yhdN) which as well as being present in both A18.2 and the three S11 representative genomes, was also common in both metagenome surveys of cold-adaption, stress and shock genes (Chapter 2). Other trends noted are the high abundance of specific heat shock and stress response genes. Currently, there are limited cold-adaption, stress or shock gene surveys of cryoconite.

In order to extend the investigation into the ability of individual taxa to respond and counter cryospheric stress, several additional factors could be applied. For example,

adding more stresses, such as pH, salinity or altering the nutrient and water availability to establish the extent of the extremophilic nature and ability of isolates. Also, the stressors already used (low temperature, freeze/thaw, continual light/dark and UV irradiation) should be applied to all current isolates from all samples, taken from separate locations. Furthermore, additional isolation in order to isolate different genera and phyla is necessary to determine the response and mechanisms that different taxa produce to the cryospheric stresses applied. Here, just *Proteobacteria* (S11 isolates) and the *Actinobacteria* (A18.2) were assessed, other isolates from dominant cryoconite phyla such as *Bacteroidetes*, *Acidobacteria* and *Firmicutes* are needed. Full genome sequencing of isolates to complement any wet laboratory work is imperative if we are to reveal and verify the nature of the stress counter mechanisms used by individual taxa in cryospheric environments.

4 – Thesis conclusions

The intention of this thesis was to further the knowledge and understanding of cryospheric microorganisms, specifically by testing the response of cryoconite inhabitants to two of the main types of cryospheric stress, light and temperature. Both 24-hour dark and 24-hour light conditions were applied as well as both positive and negative temperatures of +2 °C and -5 °C to the cryoconite community as a whole and to individual isolates. Additionally, UV exposure as a form of light stress was applied to an individual isolate. Furthermore, sequencing and assembly of metagenomes and genomes followed by taxonomic classification and the annotation and surveying of shock, stress, cold-adaption associated, light-sensing and carotenoid biosynthesis genes was completed. By uncovering both physiological ability and response to light and temperature stress as well as gaining genomic insight, understanding into the cryospheric way of life has been extended.

4.1 Evaluation of thesis aims and objectives

The first aim of this thesis was to determine how temperature stress affects cryoconite microorganisms. The response from individual cryoconite isolates to temperatures above and below 0 °C (+2 °C and -5 °C), specifically by testing their ability to produce colonies following incubation at sub-zero, was assessed. This was accomplished by incubating them at these temperatures and comparing both CFU/ml $^{-1}$ and attenuance of sub-zero incubations to that of pre-freeze. Additionally, the response of the whole community to diurnal (freeze/thaw) transition stresses, by combining both temperature and light stress (24-hour light and 24-hour dark) was assessed. This was achieved by measuring the DO concentration of microcosms. Previously, the majority of cryoconite biological studies examined summer communities or the primary producer Cyanobacteria, specifically the *Phormidesmis* spp. Snapshots of community productivity do not recognize the capacity to recover and adapt rapidly to the transition between the day and night or the seasons. Moreover, few studies examined the stress response and physiological abilities of the heterotrophic taxa from cryoconite. Here, the microcosm community tested demonstrated a rapid recovery following a freeze/thaw cycle. Additionally, isolates incubated at sub-zero temperatures produced more CFU/ml $^{-1}$ than they did pre-freeze, an ability that has not been demonstrated from cryoconite isolates to date.

The second aim of this thesis was to determine how light stress affects cryoconite microorganisms. The response of the community revealed in culture to different light conditions was tested by assessing whether colonies produced conspicuous pigment in response to illumination. Replica plates of cryoconite dilutions were placed under continual dark / light conditions and the proportion of visibly pigmented colonies in each condition was recorded. Additionally, how an individual isolate (A18.2) responded to different light conditions was assessed, also by testing if conspicuous pigment was produced. The pigment produced by A18.2 was extracted, and the peak absorbance established. (Unfortunately, due to COVID-19 the pigment characterisation planned could not proceed). Furthermore, to test whether the pigment produced by A18.2

offered any protection against light stress (UV irradiation), cultures of A18.2 grown under two conditions, both light (which produced visibly pigmented culture) and dark (which produced visibly non-pigmented culture) were subjected to UV irradiation and the resulting growth was compared to growth pre-exposure. Hitherto, whilst pigment production in the cold-adapted algae is documented, the ability of cold-adapted bacteria and fungi to produce pigments is relatively overlooked and as mentioned, few studies examined the stress response and physiological abilities of the individual taxa from cryoconite. Here, a light-induced increase in pigment production was demonstrated in both the community and an individual isolate, which has not been shown in cryoconite biological studies to date.

The third aim of this thesis was to gain genomic insight of cryoconite microorganisms. To establish taxonomic distribution of the samples and to identify shock, stress and cold-adaptation genes as well as stress countering mechanisms, such as pigment production, both genomes and metagenomes were assembled and annotated. Specifically, assembly and annotation were performed on both a Svalbard 2019 (S19) and Greenland 2018 (G18) cryoconite metagenome as well as the A18.2 isolate. Representative genomes for S11 isolates were obtained from National Center for Biotechnology Information (NCBI) and annotated. Whilst taxonomic distribution of the genomes and metagenomes agreed with previous studies of cryoconite, this work supports and adds to such studies. Previously, a limited number of studies examined the cryoconite inhabitant's genomic ability in relation to cold-adaption and none to my knowledge assessed light detection. Here, as well as revealing which cold-adaption and stress genes are core in cryoconite organisms, the yhdN gene (general stress protein 69), identified in every genome and metagenome, may be linked to cold-adaption for the first time. Furthermore, phytochromes and other light sensing protein encoding genes as well as numerous carotenoid biosynthesis genes were identified with the genomic and metagenomic data. The identification of genes involved in cold-adaption, light detection and carotenoid production substantiate the wet laboratory results.

4.2 Future scope

As mentioned throughout, there are a number of ways to extend, improve and advance the experimental work conducted. In particular, I recommend as follows.

For the community recovery microcosm experiment, I only tested a Svalbard sample which was fairly aged (2011 collected, frozen then thawed and used two months later). As such, fresher samples from more locations need to be tested to see if the rapid recovery that was seen (48 hour) is even faster with fresher cryoconite and if recovery differs with different samples and different temperature incubations. To extend the sub-zero incubation experiment as well as trialling longer incubations and different sub-zero temperatures, the use of flow cytometry to establish increases in cell number following the incubations would be a good method to confirm if growth and division of isolates is occurring at sub-zero. Additionally, many more isolates are needed, especially of different taxa to those already isolated, before testing the physiological capabilities of these by applying light and temperature stress as well as more cryospheric stresses, such as pH, salinity and altered nutrient and water availabilities.

In the light-induced pigmentation community experiment, pigment extraction of the whole plate and/or the use of image J to quantify the difference between light and dark conditions would be useful additional quantitative methods to use. The light-induced pigment production exhibited by the *Cryobacterium* isolate (A18.2) could be extended to determine if the phytochromes (cph) present in the genome are detecting light and signalling to initiate the production of pigment, via the knock out of the cph genes. To test whether the pigment produced by A18.2 does provide protective benefits against UV irradiation higher doses of UV exposure are needed and potentially, the extraction of the pigment before addition to a UV susceptible strain with subsequent exposure to UV.

To improve and extend the genomic insights gained, genome assembly could be refined by further polishing and hybrid assembly. Additionally, genome and metagenome comparison to mesophilic microorganisms would support the identification of genes crucial to cold-adaption. The role that the general stress protein 69 (yhdN gene) may play in cold-adaption needs to be assessed, potentially by monitoring gene expression

via the means of inserting a reporter gene or using transcriptomics. Metabolomic and transcriptomic analysis of the cryoconite community under different stressful conditions would be useful to verify whether the core genes identified in cold-adaption do indeed play a role in the adaptive response to cryospheric stresses.

4.3 Concluding remarks

The aim of this thesis was to further the knowledge and understanding of cryospheric microbial inhabitants, specifically cryoconite microorganisms by testing their ability to counter temperature and light stress, as well as investigate their genomic capacity to produce such adaptive responses. Counter tactics, responses and genetic insight to the applied stresses not previously demonstrated have been shown and therefore, extend the knowledge of such microorganisms.

To summarise, there are two main findings.

Firstly, the incredible ability of cryoconite microorganisms to counter sub-zero temperature stress, as demonstrated by both the community and individual taxa in both wet and dry laboratory investigations. The capacity of the community to recover so rapidly to freezing, dark conditions and return to net O_2 productivity within 48 hours is indicative of the adaptive ability the microbial community shows to changing, seasonal cryospheric stresses. Furthermore, the ability of isolates to produce more CFU/ml $^{-1}$ following weeks of incubation at -5 °C compared to pre-freeze is suggestive of the capacity of some members of the community, namely the Proteobacteria phyla, to remain active over winter. The ability to counteract sub-zero temperature stress is substantiated by the presence of a number of core stress, shock and cold-adaption associated genes from the genomic surveys undertaken, including the identification of a gene, yhdN, not previously linked to cold-adaption.

Secondly, the pervasive tactic of light-induced pigment upregulation and / or production to counter light stress, as demonstrated by both the community and individual taxa in both wet and dry laboratory investigations. The significantly higher proportion of conspicuously pigmented colonies produced by the community revealed in culture

under illumination compared to the replica plates under dark conditions revealed how widespread this tactic may be. Additionally, the *Cryobacterium* isolate A18.2 exhibited the same tactic, light-induced pigment upregulation / production as a response to light stress. Light sensing phytochrome and carotenoid biosynthesis genes were present in the A18.2 genome and the multiple phytochrome and carotenoid biosynthesis genes detected within the metagenomes substantiates the response observed, that in response to light, carotenoids are produced as a defensive, protective strategy.

Undoubtedly, the cryosphere is a challenging habitat. Although now, more than ever before, attention is being given to cryospheric microorganisms, there remains a vast underexplored realm to be considered. Faced with numerous harsh conditions and multiple stressors, microorganisms that inhabit such environments need to be well adapted and able to counter these extremes. This thesis uncovers just some of the sophisticated ways cryoconite microbial inhabitants adapt to and counter the cryospheric stresses they experience.

5- Bibliography

Anderson, D., Ferreras, E., Trindade, M. and Cowan, D., 2015. A novel bacterial Water Hypersensitivity-like protein shows in vivo protection against cold and freeze damage. *FEMS Microbiology Letters*, 362(15), p.fnv110.

Anesio, A.M., and Laybourn-Parry, J., 2012. Glaciers and ice sheets as a biome. *Trends in Ecology and Evolution*, 27(4), pp.219-225.

Anesio, A.M., Hodson, A.J., Fritz, A., Psenner, R. and Sattler, B., 2009. High microbial activity on glaciers: importance to the global carbon cycle. *Global Change Biology*, 15(4), pp.955-960.

Anesio, A.M., Lutz, S., Chrismas, N.A. and Benning, L.G., 2017. The microbiome of glaciers and ice sheets. *Nature Partner Journals (npj) Biofilms and Microbiomes,* 3(1), pp.1-11.

Anisimova M., and Gascuel, O., 2006. Approximate likelihood ratio test for branchs: A fast, accurate and powerful alternative. *Systematic Biology*. 55(4):539-52.

Atlung, T. and Hansen, F.G., 1999. Low-Temperature-Induced DnaA Protein Synthesis Does Not Change Initiation Mass in *Escherichia coli* K-12. *Journal of Bacteriology*, 181(18), pp.5557-5562.

Auldridge, M.E. and Forest, K.T., 2011. Bacterial phytochromes: more than meets the light. *Critical Reviews in Biochemistry and Molecular Biology*, *46*(1), pp.67-88.

Bae, W., Xia, B., Inouye, M. and Severinov, K., 2000. *Escherichia coli* CspA-family RNA chaperones are transcription antiterminators. *PNAS,* 97(14), pp.7784-7789.

Bagshaw, E.A., Wadham, J.L., Tranter, M., Perkins, R., Morgan, A., Williamson, C.J., Fountain, A.G., Fitzsimons, S. and Dubnick, A., 2016. Response of Antarctic cryoconite microbial communities to light. *FEMS Microbiology Ecology*, 92(6).

Bakermans, C. and Skidmore, M., 2011. Microbial respiration in ice at subzero temperatures (− 4 C to− 33 C). *Environmental Microbiology Reports*, *3*(6), pp.774-782.

Beran, R.K. and Simons, R.W., 2001. Cold-temperature induction of *Escherichia coli* polynucleotide phosphorylase occurs by reversal of its autoregulation. *Molecular Microbiology*, 39(1), pp.112-125.

Białkowska, A., Majewska, E., Olczak, A. and Twarda-Clapa, A., 2020. Ice Binding Proteins: Diverse Biological Roles and Applications in Different Types of Industry. *Biomolecules*, *10*(2), p.274.

Blin, K., Medema, M.H., Kazempour, D., Fischbach, M.A., Breitling, R., Takano, E. and Weber, T., 2013. antiSMASH 2.0—a versatile platform for genome mining of secondary metabolite producers. *Nucleic Acids Research,* 41(W1), pp.W204-W212.

Blin, K., Shaw, S., Steinke, K., Villebro, R., Ziemert, N., Lee, S.Y., Medema, M.H. and Weber, T., 2019. antiSMASH 5.0: updates to the secondary metabolite genome mining pipeline. *Nucleic Acids Research,* 47(W1), pp.W81-W87.

Blin, K., Wolf, T., Chevrette, M.G., Lu, X., Schwalen, C.J., Kautsar, S.A., Suarez Duran, H.G., de Los Santos, E.L., Kim, H.U., Nave, M. and Dickschat, J.S., 2017. antiSMASH 4.0—improvements in chemistry prediction and gene cluster boundary identification. *Nucleic Acids Research,* 45(W1), pp.W36-W41.

Boetius, A., Anesio, A., Deming, J., Mikucki, J. and Rapp, J., 2015. Microbial ecology of the cryosphere: sea ice and glacial habitats. *Nature Reviews Microbiology*, 13(11), pp.677-690

Brankatschk, R., Töwe, S., Kleineidam, K., Schloter, M. and Zeyer, J., 2011. Abundances and potential activities of nitrogen cycling microbial communities along a chronosequence of a glacier forefield. *The ISME journal*, *5*(6), pp.1025-1037.

Caldas, T., Laalami, S. and Richarme, G., 2000. Chaperone properties of bacterial elongation factor EF-G and initiation factor IF2. *Journal of Biological Chemistry*, 275(2), pp.855-860.

Castresana, J., 2000. Selection of conserved blocks from multiple alignments for their use in phylogenetic analysis. *Molecular Biology and Evolution*, 17(4), pp.540-552.

Cavicchioli, R., 2016. On the concept of a psychrophile. *The ISME journal*, *10*(4), p.793.

Chandler, D.M., Alcock, J.D., Wadham, J.L., Mackie, S.L. and Telling, J., 2014. Seasonal changes of ice surface characteristics and productivity in the ablation zone of the Greenland Ice Sheet. *Cryosphere Discuss*, *8*, pp.1337-1382.

Chandrangsu, P., Dusi, R., Hamilton, C.J. and Helmann, J.D., 2014. Methylglyoxal resistance in *Bacillus subtilis*: contributions of bacillithiol-dependent and independent pathways. *Molecular microbiology*, *91*(4), pp.706-715.

Chevenet, F., Brun, C., Bañuls, A.L., Jacq, B. and Christen, R., 2006. TreeDyn: towards dynamic graphics and annotations for analyses of trees. *BMC bioinformatics*, 7(1), p.439.

Chrismas, N.A., Barker, G., Anesio, A.M. and Sánchez-Baracaldo, P., 2016. Genomic mechanisms for cold tolerance and production of exopolysaccharides in the Arctic cyanobacterium *Phormidesmis priestleyi* BC1401. *BMC genomics,* 17(1), p.533.

Chun, J., Oren, A., Ventosa, A., Christensen, H., Arahal, D.R., da Costa, M.S., Rooney, A.P., Yi, H., Xu, X.W., De Meyer, S. and Trujillo, M.E., 2018. Proposed minimal standards for the use of genome data for the taxonomy of prokaryotes. *International Journal of Systematic and Evolutionary Microbiology*, *68*(1), pp.461-466.

Ciok, A., Budzik, K., Zdanowski, M.K., Gawor, J., Grzesiak, J., Decewicz, P., Gromadka, R., Bartosik, D. and Dziewit, L., 2018. Plasmids of psychrotolerant *Polaromonas* spp. isolated from arctic and antarctic glaciers–diversity and role in adaptation to polar environments. *Frontiers in Microbiology*, *9*, p.1285.

Cockell, C.S. and Jones, H.L., 2009. Advancing the case for microbial conservation. *Oryx*, *43*(4), pp.520-526.

Collins, T., and Margesin, R. 2019. Psychrophilic lifestyles: mechanisms of adaptation and biotechnological tools. *Applied Microbiology Biotechnology.* 103, 2857–2871.

Cook, J., Edwards, A., Takeuchi, N. and Irvine-Fynn, T., 2016a. Cryoconite: the dark biological secret of the cryosphere. *Progress in Physical Geography*, 40(1), pp.66-111.

Cook, J., Hodson, A., Telling, J., Anesio, A., Irvine-Fynn, T. and Bellas, C., 2010. The mass–area relationship within cryoconite holes and its implications for primary production. *Annals of Glaciology*, 51(56), pp.106-110.

Cook, J.M., Edwards, A., Bulling, M., Mur, L.A., Cook, S., Gokul, J.K., Cameron, K.A., Sweet, M. and Irvine-Fynn, T.D., 2016b. Metabolome-mediated biocryomorphic evolution promotes carbon fixation in Greenlandic cryoconite holes. *Environmental Microbiology,* 18(12), pp.4674-4686.

Cook, J.M., Sweet, M., Cavalli, O., Taggart, A. and Edwards, A., 2018. Topographic shading influences cryoconite morphodynamics and carbon exchange. *Arctic, Antarctic, and Alpine Research,* 50(1), p.S100014.

D'Amico, S., Collins, T., Marx, J.C., Feller, G., and Gerday, C., 2006. Psychrophilic microorganisms: challenges for life. *EMBO Reports* 7(4):385–389.

Darcy, J.L., Lynch, R.C., King, A.J., Robeson, M.S. and Schmidt, S.K., 2011. Global distribution of *Polaromonas* phylotypes-evidence for a highly successful dispersal capacity. *PLoS One, 6*(8), p.e23742.

Dastager, S.G., Lee, J.C., Ju, Y.J., Park, D.J. and Kim, C.J., 2008. *Cryobacterium mesophilum* sp. nov., a novel mesophilic bacterium. *International Journal of Systematic and Evolutionary Microbiology*, *58*(5), pp.1241-1244.

De Coster, W., D'Hert, S., Schultz, D.T., Cruts, M. and Van Broeckhoven, C., 2018. NanoPack: visualizing and processing long-read sequencing data. *Bioinformatics*, *34*(15), pp.2666-2669.

De Maio, N., Shaw, L.P., Hubbard, A., George, S., Sanderson, N.D., Swann, J., Wick, R., AbuOun, M., Stubberfield, E., Hoosdally, S.J. and Crook, D.W., 2019. Comparison of long-read sequencing technologies in the hybrid assembly of complex bacterial genomes. *Microbial Genomics*, *5*(9).

Dereeper, A., Audic, S., Claverie, J.M. and Blanc, G., 2010. BLAST-EXPLORER helps you building datasets for phylogenetic analysis. *BMC Evolutionary Biology,* 10(1), pp.1-6.

Dereeper, A., Guignon, V., Blanc, G., Audic, S., Buffet, S., Chevenet, F., Dufayard, J.F., Guindon, S., Lefort, V., Lescot, M. and Claverie, J.M., 2008. Phylogeny. fr: robust phylogenetic analysis for the non-specialist. *Nucleic Acids Research,* 36(2), pp.W465-W469.

Deschamps, S., Mudge, J., Cameron, C., Ramaraj, T., Anand, A., Fengler, K., Hayes, K., Llaca, V., Jones, T.J. and May, G., 2016. Characterization, correction and de novo assembly of an Oxford Nanopore genomic dataset from *Agrobacterium tumefaciens*. *Scientific Reports*, 6, p.28625.

Dieser, M., Greenwood, M. and Foreman, C.M., 2010. Carotenoid pigmentation in Antarctic heterotrophic bacteria as a strategy to withstand environmental stresses. *Arctic, Antarctic, and Alpine Research,* 42(4), pp.396-405.

Edgar, R.C., 2004. MUSCLE: multiple sequence alignment with high accuracy and high throughput. *Nucleic acids research*, 32(5), pp.1792-1797.

Edwards, A., Anesio, A.M., Rassner, S.M., Sattler, B., Hubbard, B., Perkins, W.T., Young, M. and Griffith, G.W., 2011. Possible interactions between bacterial diversity, microbial activity and supraglacial hydrology of cryoconite holes in Svalbard. *The ISME journal*, 5(1), pp.150-160.

Edwards, A., Cameron, K.A., Cook, J.M., Debbonaire, A.R., Furness, E., Hay, M.C. and Rassner, S.M., 2020. Microbial genomics amidst the Arctic crisis. *Microbial Genomics*, p.mgen000375.

Edwards, A., Debbonaire, A.R., Nicholls, S.M., Rassner, S.M., Sattler, B., Cook, J.M., Davy, T., Soares, A., Mur, L.A. and Hodson, A.J., 2019. In-field metagenome and 16S rRNA gene amplicon nanopore sequencing robustly characterize glacier microbiota. *BioRxiv*, p.073965.

Edwards, A., Debbonaire, A.R., Sattler, B., Mur, L.A. and Hodson, A.J., 2016. Extreme metagenomics using nanopore DNA sequencing: a field report from Svalbard, 78 N. *BioRxiv*, p.073965.

Edwards, A., Mur, L.A., Girdwood, S.E., Anesio, A.M., Stibal, M., Rassner, S.M., Hell, K., Pachebat, J.A., Post, B., Bussell, J.S. and Cameron, S.J., 2014. Coupled cryoconite ecosystem structure–function relationships are revealed by comparing bacterial communities in alpine and Arctic glaciers. *FEMS Microbiology Ecology* 89(2), pp.222-237.

Edwards, A., Pachebat, J.A., Swain, M., Hegarty, M., Hodson, A.J., Irvine-Fynn, T.D., Rassner, S.M. and Sattler, B., 2013. A metagenomic snapshot of taxonomic and functional diversity in an alpine glacier cryoconite ecosystem. *Environmental Research Letters*, *8*(3), p.035003.

Eggleston, S. and Galbraith, E. D., 2018. The devil's in the disequilibrium: multi-component analysis of dissolved carbon and oxygen changes under a broad range of forcings in a general circulation model, *Biogeosciences,* 15, 3761–3777.

Elasri, M.O. and Miller, R.V., 1999. Study of the response of a biofilm bacterial community to UV radiation. *Applied and Environmental Microbiology*, *65*(5), pp.2025-2031.

Foreman, C.M., Dieser, M., Greenwood, M., Cory, R.M., Laybourn-Parry, J., Lisle, J.T., Jaros, C., Miller, P.L., Chin, Y.P. and McKnight, D.M., 2011. When a habitat freezes solid: micro-organisms over-winter within the ice column of a coastal Antarctic lake. *FEMS Microbiology Ecology,* 76(3), pp.401-412.

Fountain, A.G., and Walder, J.S., 1998. Water flow through temperate glaciers. *Reviews of Geophysics*, 36(3), pp.299-328.

Fountain, A.G., Nylen, T.H., Tranter, M. and Bagshaw, E., 2008. Temporal variations in physical and chemical features of cryoconite holes on Canada Glacier, McMurdo Dry Valleys, Antarctica. *Journal of Geophysical Research: Biogeosciences*, 113(G1).

Fountain, A.G., Tranter, M., Nylen, T.H., Lewis, K.J. and Mueller, D.R., 2004. Evolution of cryoconite holes and their contribution to meltwater runoff from glaciers in the McMurdo Dry Valleys, Antarctica. *Journal of Glaciology*, 50(168), pp.35-45.

Franzetti, A., Navarra, F., Tagliaferri, I., Gandolfi, I., Bestetti, G., Minora, U., Azzoni, R.S., Diolaiuti, G., Smiraglia, C. and Ambrosini, R., 2017. Potential sources of bacteria colonizing the cryoconite of an Alpine glacier. *PLoS One*, *12*(3).

Franzetti, A., Tagliaferri, I., Gandolfi, I., Bestetti, G., Minora, U., Mayer, C., Azzoni, R.S., Diolaiuti, G., Smiraglia, C. and Ambrosini, R., 2016. Light-dependent microbial metabolisms drive carbon fluxes on glacier surfaces. *The ISME journal*, *10*(12), pp.2984-2988.

Gilichinsky, D., Vishnivetskaya, T., Petrova, M., Spirina, E., Mamykin, V. and Rivkina, E., 2008. Bacteria in permafrost. In *Psychrophiles: from biodiversity to biotechnology* (pp. 83-102). Springer, Berlin, Heidelberg.

Giuliodori, A.M., Brandi, A., Giangrossi, M., Gualerzi, C.O. and Pon, C.L., 2007. Cold-stress-induced de novo expression of infC and role of IF3 in cold-shock translational bias. *Rna*, 13(8), pp.1355-1365.

Gokul, J.K., 2017. Supraglacial systems biology of dynamic Arctic microbial ecosystems. PhD thesis from Aberystwyth University. http://hdl.handle.net/2160/46221

Gokul, J.K., Hodson, A.J., Saetnan, E.R., Irvine-Fynn, T.D., Westall, P.J., Detheridge, A.P., Takeuchi, N., Bussell, J., Mur, L.A. and Edwards, A., 2016. Taxon interactions control the distributions of cryoconite bacteria colonizing a High Arctic ice cap. *Molecular Ecology,* 25(15), pp.3752-3767.

Gomelsky, M. and Hoff, W.D., 2011. Light helps bacteria make important lifestyle decisions. *Trends in Microbiology*, *19*(9), pp.441-448.

Gragerov, A., Nudler, E., Komissarova, N., Gaitanaris, G.A., Gottesman, M.E. and Nikiforov, V., 1992. Cooperation of GroEL/GroES and DnaK/DnaJ heat shock proteins in preventing protein misfolding in *Escherichia coli*. *PNAS*, 89(21), pp.10341-10344.

Grau, R., Gardiol, D., Glikin, G.C. and de Mendoza, D., 1994. DNA supercoiling and thermal regulation of unsaturated fatty acid synthesis in *Bacillus subtilis*. *Molecular Microbiology*, 11(5), pp.933-941.

Griffith, G.W., 2012. Do we need a global strategy for microbial conservation? *Trends in Ecology and Evolution*, *27*(1), pp.1-2.

Grogan, D.W., 1989. Phenotypic characterization of the archaebacterial genus *Sulfolobus*: comparison of five wild-type strains. *Journal of Bacteriology.* 171:6710–6719

Gualerzi, C.O., Giuliodori, A.M. and Pon, C.L., 2003. Transcriptional and post-transcriptional control of cold-shock genes. *Journal of Molecular Biology*, 331(3), pp.527-539.

Guindon, S. and Gascuel, O., 2003. A simple, fast, and accurate algorithm to estimate large phylogenies by maximum likelihood. *Systematic Biology*. 52(5):696-704.

Hall, T.A., 1999. BioEdit: a user-friendly biological sequence alignment editor and analysis program for Windows 95/98/NT. *Nucleic Acids Symposium* 41(41) pp. 95-98.

Han, Y., Zhou, D., Pang, X., Zhang, L., Song, Y., Tong, Z., Bao, J., Dai, E., Wang, J., Guo, Z. and Zhai, J., 2005. DNA microarray analysis of the heat-and cold-shock stimulons in *Yersinia pestis*. *Microbes and Infection*, 7(3), pp.335-348.

Hauser, E., Kämpfer, P. and Busse, H.J., 2004. *Pseudomonas psychrotolerans* sp. nov. *International Journal of Systematic and Evolutionary Microbiology*, *54*(5), pp.1633-1637.

Herigstad, B., Hamilton, M. and Heersink, J., 2001. How to optimize the drop plate method for enumerating bacteria. *Journal of Microbiological Methods*, *44*(2), pp.121-129.

Hodgson, D.A. and Murillo, F.J., 1993. Genetics of regulation and pathway of synthesis of carotenoids. Myxobacteria II. *American Society for Microbiology*, Washington, DC, pp.157-181.

Hodson, A., Anesio, A.M., Ng, F., Watson, R., Quirk, J., Irvine-Fynn, T., Dye, A., Clark, C., McCloy, P., Kohler, J. and Sattler, B., 2007. A glacier respires: quantifying the distribution and respiration CO2 flux of cryoconite across an entire Arctic supraglacial ecosystem. *Journal of Geophysical Research: Biogeosciences,* 112(G4).

Hodson, A., Anesio, A.M., Tranter, M., Fountain, A., Osborn, M., Priscu, J., Laybourn-Parry, J. and Sattler, B., 2008. Glacial ecosystems. *Ecological Monographs,* 78(1), pp.41-67.

Hodson, A., Brock, B., Pearce, D., Laybourn-Parry, J. and Tranter, M., 2015. Cryospheric ecosystems: a synthesis of snowpack and glacial research. *Environmental Research Letters,* 10(11), p.110201.

Hodson, A., Cameron, K., Bøggild, C., Irvine-Fynn, T., Langford, H., Pearce, D. and Banwart, S., 2010. The structure, biological activity and biogeochemistry of cryoconite

aggregates upon an Arctic valley glacier: Longyearbreen, Svalbard. *Journal of Glaciology*, 56(196), pp.349-362.

Höper, D., Völker, U. and Hecker, M., 2005. Comprehensive characterization of the contribution of individual SigB-dependent general stress genes to stress resistance of *Bacillus subtilis. Journal of Bacteriology*, *187*(8), pp.2810-2826.

Jansson, P., Hock, R. and Schneider, T., 2003. The concept of glacier storage: a review. *Journal of Hydrology,* 282(1-4), pp.116-129.

Jones, P.G. and Inouye, M., 1994. The cold-shock response—a hot topic. *Molecular Microbiology,* 11(5), pp.811-818.

Jones, P.G., Krah, R.E.G.I.S., Tafuri, S.R. and Wolffe, A.P., 1992. DNA gyrase, CS7. 4, and the cold shock response in *Escherichia coli. Journal of Bacteriology*, 174(18), pp.5798-5802.

Jones, P.G., VanBogelen, R.A. and Neidhardt, F.C., 1987. Induction of proteins in response to low temperature in *Escherichia coli. Journal of Bacteriology*, 169(5), pp.2092-2095.

Kaštovská, K., Elster, J., Stibal, M. and Šantrůčková, H., 2005. Microbial assemblages in soil microbial succession after glacial retreat in Svalbard (High Arctic). *Microbial Ecology*, *50*(3), p.396.

Kirti, K., Amita, S., Priti, S., Mukesh Kumar, A. and Jyoti, S., 2014. Colorful world of microbes: carotenoids and their applications. *Advances in Biology*, *2014*.

Koo, H., Hakim, J.A., Fisher, P.R., Grueneberg, A., Andersen, D.T. and Bej, A.K., 2016. Distribution of cold adaptation proteins in microbial mats in Lake Joyce, Antarctica: Analysis of metagenomic data by using two bioinformatics tools. *Journal of Microbiological Methods*, *120*, pp.23-28.

Koo, H., Hakim, J.A., Morrow, C.D., Crowley, M.R., Andersen, D.T. and Bej, A.K., 2018. Metagenomic analysis of microbial community compositions and cold-responsive stress genes in selected Antarctic lacustrine and soil ecosystems. *Life*, *8*(3), p.29.

Koren, S., Rhie, A., Walenz, B.P., Dilthey, A.T., Bickhart, D.M., Kingan, S.B., Hiendleder, S., Williams, J.L., Smith, T.P. and Phillippy, A.M., 2018. De novo assembly of haplotype-resolved genomes with trio binning. *Nature Biotechnology*, 36(12), pp.1174-1182.

Koren, S., Walenz, B.P., Berlin, K., Miller, J.R., Bergman, N.H. and Phillippy, A.M., 2017. Canu: scalable and accurate long-read assembly via adaptive k-mer weighting and repeat separation. *Genome Research,* 27(5), pp.722-736.

Lamers, P.P., van de Laak, C.C., Kaasenbrood, P.S., Lorier, J., Janssen, M., De Vos, R.C., Bino, R.J. and Wijffels, R.H., 2010. Carotenoid and fatty acid metabolism in light-stressed *Dunaliella salina. Biotechnology and Bioengineering*, *106*(4), pp.638-648.

Langford, H., Hodson, A., Banwart, S. and Bøggild, C., 2010. The microstructure and biogeochemistry of Arctic cryoconite granules. *Annals of Glaciology*, 51(56), pp.87-94.

Lederberg, J. and Lederberg, E.M., 1952. Replica plating and indirect selection of bacterial mutants. *Journal of Bacteriology*, *63*(3), p.399.

Lee, Y.M., Kim, S.Y., Jung, J., Kim, E.H., Cho, K.H., Schinner, F., Margesin, R., Hong, S.G. and Lee, H.K., 2011. Cultured bacterial diversity and human impact on alpine glacier cryoconite. *The Journal of Microbiology*, *49*(3), pp.355-362.

Lewenza, S., Abboud, J., Poon, K., Kobryn, M., Humplik, I., Bell, J.R., Mardan, L. and Reckseidler-Zenteno, S., 2018. *Pseudomonas aeruginosa* displays a dormancy phenotype during long-term survival in water. *PLoS One*, *13*(9), p.e0198384.

Liu, Q., Liu, H.C., Zhou, Y.G. and Xin, Y.H., 2019. Genetic diversity of glacier-inhabiting *Cryobacterium* bacteria in China and description of *Cryobacterium zongtaii* sp. nov. and *Arthrobacter glacialis* sp. nov. *Systematic and Applied Microbiology*, *42*(2), pp.168-177.

Liu, Y., Shen, L., Zeng, Y., Xing, T., Xu, B. and Wang, N., 2020. Genomic insights of *Cryobacterium* isolated from ice core reveal genome dynamics for adaptation in glacier. *Frontiers in Microbiology*, 11, p.1530.

López-García, P. and Forterre, P., 1999. Control of DNA topology during thermal stress in hyperthermophilic archaea: DNA topoisomerase levels, activities and induced

thermotolerance during heat and cold shock in *Sulfolobus. Molecular Microbiology*, 33(4), pp.766-777.

Lutz, S., Anesio, A., Edwards, A. and Benning, L., 2015. Microbial diversity on Icelandic glaciers and ice caps. *Frontiers in Microbiology,* 6. p.307

Lutz, S., Ziolkowski, L. A., and Benning, L. G. (2019). The biodiversity and geochemistry of cryoconite holes in queen maud land, East Antarctica. *Microorganisms* 7:160.

Maccario, L., Sanguino, L., Vogel, T.M. and Larose, C., 2015. Snow and ice ecosystems: not so extreme. *Research in Microbiology*, *166*(10), pp.782-795.

Mackelprang, R., Burkert, A., Haw, M., Mahendrarajah, T., Conaway, C.H., Douglas, T.A. and Waldrop, M.P., 2017. Microbial survival strategies in ancient permafrost: insights from metagenomics. *The ISME Journal*, *11*(10), pp.2305-2318.

Makhalanyane, T.P., Van Goethem, M.W. and Cowan, D.A., 2016. Microbial diversity and functional capacity in polar soils. *Current Opinion in Biotechnology*, *38*, pp.159-166.

Malik, K., Tokkas, J. and Goyal, S., 2012. Microbial pigments: a review. *International Journal of Microbial Resource Technology, 1*(4), pp.361-365.

Marchi, P., Longhi, V., Zangrossi, S., Gaetani, E., Briani, F. and Dehò, G., 2007. Autogenous regulation of *Escherichia coli* polynucleotide phosphorylase during cold acclimation by transcription termination and antitermination. *Molecular Genetics and Genomics,* 278(1), pp.75-84.

Margesin, R. and Collins, T., 2019. Microbial ecology of the cryosphere (glacial and permafrost habitats): current knowledge. *Applied Microbiology and Biotechnology*, *103*(6), pp.2537-2549.

Margesin, R. and Fell, J.W., 2008. *Mrakiella cryoconiti* gen. nov., sp. nov., a psychrophilic, anamorphic, basidiomycetous yeast from alpine and arctic habitats. *International Journal of Systematic and Evolutionary Microbiology*, *58*(12), pp.2977-2982.

Margesin, R., Zacke, G. and Schinner, F., 2002. Characterization of heterotrophic microorganisms in alpine glacier cryoconite. *Arctic, Antarctic, and Alpine Research*, 34(1), pp.88-93.

Martins, Z., Cottin, H., Kotler, J.M., Carrasco, N., Cockell, C.S., de la Torre Noetzel, R., Demets, R., De Vera, J.P., d'Hendecourt, L., Ehrenfreund, P. and Elsaesser, A., 2017. Earth as a tool for astrobiology—a European perspective. *Space Science Reviews*, *209*(1-4), pp.43-81.

Mathews, M.M. and Krinsky, N.I., 1965. The relationship between carotenoid pigments and resistance to radiation in non-photosynthetic bacteria. *Photochemistry and Photobiology*, *4*(4), pp.813-817.

Medema, M.H., Blin, K., Cimermancic, P., de Jager, V., Zakrzewski, P., Fischbach, M.A., Weber, T., Takano, E. and Breitling, R., 2011. antiSMASH: rapid identification, annotation and analysis of secondary metabolite biosynthesis gene clusters in bacterial and fungal genome sequences. *Nucleic Acids Research*, 39(suppl_2), pp.W339-W346.

Menzel, P., Ng, K.L. and Krogh, A., 2016. Fast and sensitive taxonomic classification for metagenomics with Kaiju. *Nature Communications*, *7*(1), pp.1-9.

Methé, B.A., Nelson, K.E., Deming, J.W., Momen, B., Melamud, E., Zhang, X., Moult, J., Madupu, R., Nelson, W.C., Dodson, R.J. and Brinkac, L.M., 2005. The psychrophilic lifestyle as revealed by the genome sequence of *Colwellia psychrerythraea* 34H through genomic and proteomic analyses. *PNAS, 102*(31), pp.10913-10918.

Meyer, F., Paarmann, D., D'Souza, M., Olson, R., Glass, E.M., Kubal, M., Paczian, T., Rodriguez, A., Stevens, R., Wilke, A. and Wilkening, J., 2008. The metagenomics RAST server–a public resource for the automatic phylogenetic and functional analysis of metagenomes. *BMC Bioinformatics*, *9*(1), p.386.

Mihoub, F., Mistou, M.Y., Guillot, A., Leveau, J.Y., Boubetra, A. and Billaux, F., 2003. Cold adaptation of *Escherichia coli*: microbiological and proteomic approaches. *International Journal of Food Microbiology,* 89(2-3), pp.171-184.

Moeller, R., Horneck, G., Facius, R. and Stackebrandt, E., 2005. Role of pigmentation in protecting *Bacillus* sp. endospores against environmental UV radiation. *FEMS Microbiology Ecology*, *51*(2), pp.231-236.

Mohana, D., Thippeswamy, S. and Abhishe, R., 2013. Antioxidant, antibacterial, and ultraviolet-protective properties of carotenoids isolated from *Micrococcus* spp. *Radiation Protection and Environment*, *36*(4), pp.168-174.

Morgulis, A., Coulouris, G., Raytselis, Y., Madden, T.L., Agarwala, R. and Schäffer, A.A., 2008. Database indexing for production MegaBLAST searches. *Bioinformatics,* 24(16), pp.1757-1764.

Mueller, D.R. and Pollard, W.H., 2004. Gradient analysis of cryoconite ecosystems from two polar glaciers. *Polar Biology,* 27(2), pp.66-74.

Mueller, D.R., Vincent, W.F., Bonilla, S. and Laurion, I., 2005. Extremotrophs, extremophiles and broadband pigmentation strategies in a high arctic ice shelf ecosystem. *FEMS Microbiology Ecology*, 53(1), pp.73-87.

Mueller, D.R., Vincent, W.F., Pollard, W.H. and Fritsen, C.H., 2001. Glacial cryoconite ecosystems: a bipolar comparison of algal communities and habitats. *Nova Hedwigia Beiheft,* 123, pp.173-198.

Mulders, K.J., Lamers, P.P., Martens, D.E. and Wijffels, R.H., 2014. Phototrophic pigment production with microalgae: biological constraints and opportunities. *Journal of Phycology*, *50*(2), pp.229-242.

Mykytczuk, N.C., Foote, S.J., Omelon, C.R., Southam, G., Greer, C.W. and Whyte, L.G., 2013. Bacterial growth at− 15 C; molecular insights from the permafrost bacterium *Planococcus halocryophilus* Or1. *The ISME journal,* 7(6), pp.1211-1226.

Nurk, S., Walenz, B.P., Rhie, A., Vollger, M.R., Logsdon, G.A., Grothe, R., Miga, K.H., Eichler, E.E., Phillippy, A.M. and Koren, S., 2020. HiCanu: accurate assembly of segmental duplications, satellites, and allelic variants from high-fidelity long reads. *BioRxiv.*

Oechel, W.C., Vourlitis, G. and Hastings, S.J., 1997. Cold season CO2 emission from arctic soils. *Global Biogeochemical Cycles*, 11(2), pp.163-172.

Overbeek, R., Olson, R., Pusch, G.D., Olsen, G.J., Davis, J.J., Disz, T., Edwards, R.A., Gerdes, S., Parrello, B., Shukla, M. and Vonstein, V., 2014. The SEED and the Rapid

Annotation of microbial genomes using Subsystems Technology (RAST). *Nucleic Acids Research,* 42(D1), pp.D206-D214.

Panicker, G., Aislabie, J., Saul, D. and Bej, A.K., 2002. Cold tolerance of *Pseudomonas* sp. 30-3 isolated from oil-contaminated soil, Antarctica. *Polar Biology*, *25*(1), pp.5-11.

Panwar, A.S., Molpa, D. and Joshi, G.K., 2019. Biotechnological potential of some cold-adapted bacteria isolated from North-Western Himalaya. *Microbiology*, *88*(3), pp.343-352.

Parks, D.H., Rinke, C., Chuvochina, M., Chaumeil, P.A., Woodcroft, B.J., Evans, P.N., Hugenholtz, P. and Tyson, G.W., 2017. Recovery of nearly 8,000 metagenome-assembled genomes substantially expands the tree of life. *Nature Microbiology*, *2*(11), pp.1533-1542.

Pautler, B.G., Dubnick, A., Sharp, M.J., Simpson, A.J. and Simpson, M.J., 2013. Comparison of cryoconite organic matter composition from Arctic and Antarctic glaciers at the molecular-level. *Geochimica et Cosmochimica Acta,* 104, pp.1-18.

Peccia, J. and Hernandez, M., 2002. Rapid immunoassays for detection of UV-induced cyclobutane pyrimidine dimers in whole bacterial cells. *Applied and Environmental Microbiology*, *68*(5), pp.2542-2549.

Perkins, R.G., Bagshaw, E., Mol, L., Williamson, C.J., Fagan, D., Gamble, M. and Yallop, M.L., 2017. Photoacclimation by Arctic cryoconite phototrophs. *FEMS Microbiology ecology,* 93(5), p.fix018.

Pittino, F., Maglio, M., Gandolfi, I., Azzoni, R.S., Diolaiuti, G., Ambrosini, R. and Franzetti, A., 2018. Bacterial communities of cryoconite holes of a temperate alpine glacier show both seasonal trends and year-to-year variability. *Annals of Glaciology,* 59(77),

Poniecka, E.A., Bagshaw, E.A., Sass, H., Segar, A., Webster, G., Williamson, C., Anesio, A.M. and Tranter, M., 2020. Physiological capabilities of cryoconite hole microorganisms. *Frontiers in Microbiology*, *11*, p.1783.

Ram, S., Mitra, M., Shah, F., Tirkey, S.R. and Mishra, S., 2020. Bacteria as an alternate biofactory for carotenoid production: A review of its applications, opportunities and challenges. *Journal of Functional Foods*, *67*, p.103867.

Rasuk, M.C., Ferrer, G.M., Kurth, D., Portero, L.R., Farías, M.E. and Albarracín, V.H., 2017. UV-Resistant Actinobacteria from High-Altitude Andean Lakes: Isolation, Characterization and Antagonistic Activities. *Photochemistry and Photobiology*, *93*(3), pp.865-880.

Reasoner, D.J. and Geldreich, E.E., 1985. A new medium for the enumeration and subculture of bacteria from potable water. *Applied Environmental Microbiology*, *49*(1), pp.1-7.

Reddy, G.S.N., Pradhan, S., Manorama, R. and Shivaji, S., 2010. *Cryobacterium roopkundense* sp. nov., a psychrophilic bacterium isolated from glacial soil. *International Journal of Systematic and Evolutionary Microbiology*, *60*(4), pp.866-870.

Remias, D., Lütz-Meindl, U. and Lütz, C., 2005. Photosynthesis, pigments and ultrastructure of the alpine snow alga *Chlamydomonas nivalis. European Journal of Phycology*, *40*(3), pp.259-268.

Rilling, H.C., 1962. Photoinduction of carotenoid synthesis of a *Mycobacterium* sp. *Biochimica et biophysica acta,* 60(3), pp.548-556.

Rivkina, E., Abramov, A., Spirina, E., Petrovskaya, L., Shatilovich, A., Shmakova, L., Scherbakova, V. and Vishnivetskaya, T., 2018. Earth's perennially frozen environments as a model of cryogenic planet ecosystems. *Permafrost and Periglacial Processes*, *29*(4), pp.246-256.

Rivkina, E., E. Friedmann, C. McKay, and D. Gilichinsky . 2000. Metabolic activity of permafrost bacteria below the freezing point. *Applied and Environmental Microbiology* 66: 3230– 3233.

Rodriguez, L.M. and Konstantinidis KT., 2016. The enveomics collection: a toolbox for specialized analyses of microbial genomes and metagenomes. *PeerJ Preprints* 4:e1900v1.

Ruan, J. and Li, H., 2020. Fast and accurate long-read assembly with wtdbg2. *Nature Methods,* 17(2), pp.155-158.

Ryan, J.C., Hubbard, A., Box, J.E., Brough, S., Cameron, K., Cook, J.M., Cooper, M., Doyle, S.H., Edwards, A., Holt, T. and Irvine-Fynn, T., 2017. Derivation of high spatial resolution albedo from UAV digital imagery: application over the Greenland Ice Sheet. *Frontiers in Earth Science,* 5, p.40.

Sajjad, W., Din, G., Rafiq, M., Iqbal, A., Khan, S., Zada, S., Ali, B. and Kang, S., 2020. Pigment production by cold-adapted bacteria and fungi: colorful tale of cryosphere with wide range applications. *Extremophiles*, p.1.

Santos, A.L., Oliveira, V., Baptista, I., Henriques, I., Gomes, N.C., Almeida, A., Correia, A. and Cunha, Â., 2013. Wavelength dependence of biological damage induced by UV radiation on bacteria. *Archives of Microbiology*, *195*(1), pp.63-74.

Satola, B., Wübbeler, J.H. and Steinbüchel, A., 2013. Metabolic characteristics of the species *Variovorax paradoxus. Applied Microbiology and Biotechnology*, *97*(2), pp.541-560.

Säwström, C., Mumford, P., Marshall, W., Hodson, A. and Laybourn-Parry, J., 2002. The microbial communities and primary productivity of cryoconite holes in an Arctic glacier (Svalbard 79 N). *Polar Biology,* 25(8), pp.591-596.

Schumann, P., Zhang, D.C., Redzic, M. and Margesin, R., 2012. *Alpinimonas psychrophila* gen. nov., sp. nov., an actinobacterium of the family Microbacteriaceae isolated from alpine glacier cryoconite. *International Journal of Systematic and Evolutionary Microbiology*, 62(11), pp.2724-2730.

Sebastião, F.A., Furlan, L.R., Hashimoto, D.T. and Pilarski, F., 2015. Identification of bacterial fish pathogens in Brazil by direct colony PCR and 16S rRNA gene sequencing. *Advances in Microbiology*, *5*(06), p.409.

Seemann, T., 2014. Prokka: rapid prokaryotic genome annotation. *Bioinformatics*, *30*(14), pp.2068-2069.

Segawa, T., Miyamoto, K., Ushida, K., Agata, K., Okada, N. and Kohshima, S., 2005. Seasonal change in bacterial flora and biomass in mountain snow from the Tateyama Mountains, Japan, analyzed by 16S rRNA gene sequencing and real-time PCR. *Applied and Environmental Microbiology,* 71(1), pp.123-130.

Segawa, T., Yonezawa, T., Edwards, A., Akiyoshi, A., Tanaka, S., Uetake, J., Irvine-Fynn, T., Fukui, K., Li, Z. and Takeuchi, N., 2017. Biogeography of cryoconite forming cyanobacteria on polar and Asian glaciers. *Journal of Biogeography,* 44(12), pp.2849-2861.

Seviour, R.J. and Codner, R.C., 1973. Effect of light on carotenoid and riboflavin production by the fungus *Cephalosporium diospyri. Microbiology*, *77*(2), pp.403-415.

Sharrock, R.A., 2008. The phytochrome red/far-red photoreceptor superfamily. *Genome Biology*, *9*(8), p.230.

Shen, L., Liu, Y., Wang, N., Jiao, N., Xu, B. and Liu, X., 2018. Variation with depth of the abundance, diversity and pigmentation of culturable bacteria in a deep ice core from the Yuzhufeng Glacier, Tibetan Plateau. *Extremophiles*, *22*(1), pp.29-38.

Singh, P., Hanada, Y., Singh, S.M. and Tsuda, S., 2014a. Antifreeze protein activity in Arctic cryoconite bacteria. *FEMS Microbiology Letters*, 351(1), pp.14-22.

Singh, P., Kapse, N., Arora, P., Singh, S.M. and Dhakephalkar, P.K., 2015. Draft genome of *Cryobacterium* sp. MLB-32, an obligate psychrophile from glacier cryoconite holes of high Arctic. *Marine Genomics*, *21*, pp.25-26.

Singh, P., Singh, S.M. and Dhakephalkar, P., 2014b. Diversity, cold active enzymes and adaptation strategies of bacteria inhabiting glacier cryoconite holes of High Arctic. *Extremophiles*, *18*(2), pp.229-242.

Sommers, P., Porazinska, D.L., Darcy, J.L., Zamora, F., Fountain, A.G. and Schmidt, S.K., 2019. Experimental cryoconite holes as mesocosms for studying community ecology. *Polar Biology*, *42*(11), pp.1973-1984.

Stibal, M. and Tranter, M., 2007. Laboratory investigation of inorganic carbon uptake by cryoconite debris from Werenskioldbreen, Svalbard. *Journal of Geophysical Research: Biogeosciences*, *112*(G4).

Takano, H., Asker, D., Beppu, T. and Ueda, K., 2006. Genetic control for light-induced carotenoid production in non-phototrophic bacteria. *Journal of Industrial Microbiology and Biotechnology*, *33*(2), pp.88-93.

Takano, H., Obitsu, S., Beppu, T. and Ueda, K., 2005. Light-induced carotenogenesis in *Streptomyces coelicolor* A3 (2): identification of an extracytoplasmic function sigma factor that directs photodependent transcription of the carotenoid biosynthesis gene cluster. *Journal of Bacteriology*, 187(5), pp.1825-1832.

Takeuchi, N., 2002. Optical characteristics of cryoconite (surface dust) on glaciers: the relationship between light absorbency and the property of organic matter contained in the cryoconite. *Annals of Glaciology*, *34*, pp.409-414.

Takeuchi, N., S. Kohshima, and K. Fujita . 1998. Snow algae community on a Himalayan glacier, Glacier AX010 East Nepal: relationship with summer mass balance. *Bulletin of Glacier Research,* 16: 43– 50.

Takeuchi, N., S. Kohshima, and K. Seko . 2001. Structure, formation and darkening process of albedo-reducing material (cryoconite) on a Himalayan glacier: a granular algal mat growing on the glacier. *Arctic, Antarctic, and Alpine Research* 33: 115– 122.

Telling, J., Anesio, A.M., Hawkings, J., Tranter, M., Wadham, J.L., Hodson, A.J., Irvine-Fynn, T. and Yallop, M.L., 2010. Measuring rates of gross photosynthesis and net community production in cryoconite holes: a comparison of field methods. *Annals of Glaciology,* 51(56), pp.153-162.

Teoh, C.P., Wong, C.M.V.L., Lee, D.J.H., González, M.A., Najimudin, N., Lee, P.C. and Cheah, Y.K., 2018. Genome sequences of two cold-adapted *Cryobacterium* spp. SO1 and SO2 from Fildes Peninsula, Antarctica. *Current Science*, *115*(9), p.1706.

Thomas-Hall, S.R., Turchetti, B., Buzzini, P., Branda, E., Boekhout, T., Theelen, B. and Watson, K., 2010. Cold-adapted yeasts from Antarctica and the Italian Alps—description

of three novel species: *Mrakia robertii* sp. nov., *Mrakia blollopis* sp. nov. and *Mrakiella niccombsii* sp. nov. *Extremophiles*, *14*(1), pp.47-59.

Ting, L., Williams, T.J., Cowley, M.J., Lauro, F.M., Guilhaus, M., Raftery, M.J. and Cavicchioli, R., 2010. Cold adaptation in the marine bacterium, *Sphingopyxis alaskensis,* assessed using quantitative proteomics. *Environmental microbiology,* 12(10), pp.2658-2676.

Tribelli, P.M. and López, N.I., 2018. Reporting key features in cold-adapted bacteria. Life, 8(1), p.8.

Tsuji, M., Tanabe, Y., Vincent, W.F. and Uchida, M., 2018. *Mrakia arctica* sp. nov., a new psychrophilic yeast isolated from an ice island in the Canadian High Arctic. *Mycoscience*, *59*(1), pp.54-58.

Varin, T., Lovejoy, C., Jungblut, A.D., Vincent, W.F. and Corbeil, J., 2012. Metagenomic analysis of stress genes in microbial mat communities from Antarctica and the High Arctic. *Applied and Environmental Microbiology,* 78(2), pp.549-559.

Vila, E., Hornero-Méndez, D., Azziz, G., Lareo, C. and Saravia, V., 2019. Carotenoids from heterotrophic bacteria isolated from Fildes Peninsula, King George Island, Antarctica. *Biotechnology Reports*, *21*, p.e00306.

Vincent, W.F., Callaghan, T.V., Dahl-Jensen, D., Johansson, M., Kovacs, K.M., Michel, C., Prowse, T., Reist, J.D. and Sharp, M., 2011. Ecological implications of changes in the Arctic cryosphere. *Ambio,* 40(1), pp.87-99.

Weber, T., Blin, K., Duddela, S., Krug, D., Kim, H.U., Bruccoleri, R., Lee, S.Y., Fischbach, M.A., Müller, R., Wohlleben, W. and Breitling, R., 2015. antiSMASH 3.0—a comprehensive resource for the genome mining of biosynthetic gene clusters. *Nucleic acids research,* 43(W1), pp.W237-W243.

Weeks, O.B. and Garner, R.J., 1967. Biosynthesis of carotenoids in *Flavobacterium dehydrogenans* Arnaudi. *Archives of Biochemistry and Biophysics*, 121(1), pp.35-49.

Whitworth, D.E. and Hodgson, D.A., 2001. Light-induced carotenogenesis in *Myxococcus xanthus*: evidence that CarS acts as an anti-repressor of CarA. *Molecular Microbiology*, 42:809–819

Wick, R.R., Schultz, M.B., Zobel, J. and Holt, K.E., 2015. Bandage: interactive visualization of de novo genome assemblies. *Bioinformatics*, 31(20), pp.3350-3352.

Williamson, C.J., Anesio, A.M., Cook, J., Tedstone, A., Poniecka, E., Holland, A., Fagan, D., Tranter, M. and Yallop, M.L., 2018. Ice algal bloom development on the surface of the Greenland Ice Sheet. *FEMS Microbiology Ecology*, 94(3), p.fiy025.

Williamson, C.J., Cameron, K.A., Cook, J.M., Zarsky, J.D., Stibal, M. and Edwards, A., 2019. Glacier algae: A dark past and a darker future. *Frontiers in Microbiology*, *10*, p.524.

Williamson, C.J., Cook, J., Tedstone, A., Yallop, M., McCutcheon, J., Poniecka, E., Campbell, D., Irvine-Fynn, T., McQuaid, J., Tranter, M. and Perkins, R., 2020. Algal photo-physiology drives darkening and melt of the Greenland Ice Sheet. *PNAS* 117(11), pp.5694-5705.

Wu, V.C.H., 2008. A review of microbial injury and recovery methods in food. *Food Microbiology*, *25*(6), pp.735-744.

Zaghdoudi, K., Ngomo, O., Vanderesse, R., Arnoux, P., Myrzakhmetov, B., Frochot, C. and Guiavarc'h, Y., 2017. Extraction, identification and photo-physical characterization of Persimmon (Diospyros kaki L.) carotenoids. *Foods*, *6*(1), p.4.

Zarsky, J.D., Stibal, M., Hodson, A., Sattler, B., Schostag, M., Hansen, L.H., Jacobsen, C.S. and Psenner, R., 2013. Large cryoconite aggregates on a Svalbard glacier support a diverse microbial community including ammonia-oxidizing archaea. *Environmental Research Letters,* 8(3), p.035044.

Zawierucha, K., Buda, J. and Nawrot, A., 2019. Extreme weather event results in the removal of invertebrates from cryoconite holes on an Arctic valley glacier (Longyearbreen, Svalbard). *Ecological Research,* 34(3), pp.370-379.

Zhang, C., 2018. Biosynthesis of carotenoids and apocarotenoids by microorganisms and their industrial potential*. Progress in Carotenoid Research*, pp.85-105.

Zhang, D.C., Busse, H.J., Liu, H.C., Zhou, Y.G., Schinner, F. and Margesin, R., 2011. *Sphingomonas glacialis* sp. nov., a psychrophilic bacterium isolated from alpine glacier cryoconite. *International Journal of Systematic and Evolutionary Microbiology*, *61*(3), pp.587-591.

Zhang, D.C., Wang, H.X., Cui, H.L., Yang, Y., Liu, H.C., Dong, X.Z. and Zhou, P.J., 2007. *Cryobacterium psychrotolerans* sp. nov., a novel psychrotolerant bacterium isolated from the China No. 1 glacier. *International Journal of Systematic and Evolutionary Microbiology*, *57*(4), pp.866-869.

Zhang, Z., Schwartz, S., Wagner, L. and Miller, W., 2000. A greedy algorithm for aligning DNA sequences. *Journal of Computational biology*, 7(1-2), pp.203-214.

Zhou, Q., Zhang, P. and Zhang, G., 2014. Biomass and carotenoid production in photosynthetic bacteria wastewater treatment: effects of light intensity. *Bioresource Technology*, *171*, pp.330-335.

Zion, M., Guy, D., Yarom, R. and Slesak, M., 2006. UV radiation damage and bacterial DNA repair systems. *Journal of Biological Education*, *41*(1), pp.30-33.

6 - Appendix

Table 14. General stress genes within the metagenomes. Total gene numbers and abundance (%) of all (Coding Sequences) CDS from PROKKA (*Prokka: rapid prokaryotic genome annotation)* annotated Svalbard and Greenland metagenomes are given in the table below. In total PROKKA assigned Svalbard 182,719 CDS and Greenland 74,805 CDS.

Gene	Protein	Svalbard	Greenland
		Total genes (% of all)	Total genes (% of all)
gspA	General stress protein A	1 (0.001)	0 (0)
mrgA	Metalloregulation DNA-binding stress protein	4 (0.002)	0 (0)
n/a	Universal stress protein	3 (0.002)	0 (0)
srkA	Stress response kinase A	1 (0.001)	0 (0)
teaD	TRAP-T-associated universal stress protein	1 (0.001)	0 (0)
yceD	General stress protein 16U	3 (0.002)	0 (0)
ydaD	General stress protein 39	7 (0.004)	0 (0)
yhdN	General stress protein 69	23 (0.012)	10 (0.013)
yugI	General stress protein 13	1 (0.001)	0 (0)

Table 15. Genes associated with cold-adaption within the metagenomes.

Total gene numbers and abundance (%) of all (Coding Sequences) CDS from PROKKA (*Prokka: rapid prokaryotic genome annotation)* annotated Svalbard and Greenland metagenomes are given in the table below. In total PROKKA assigned Svalbard 182,719 CDS and Greenland 74,805 CDS.

Gene	Protein	Svalbard	Greenland
		Total genes (% of all)	Total genes (% of all)
aceE	Pyruvate dehydrogenase E1 component	29 (0.016)	3 (0.004)
aceF	Dihydrolipoyllysine-residue acetyltransferase component of pyruvate dehydrogenase complex	11 (0.006)	0 (0)
csp	Cold shock protein	2 (0.001)	0 (0)
cspA	Cold shock protein A	6 (0.003)	0 (0)
cspB	Cold shock protein B	0 (0)	0 (0)
cspC	Cold shock protein C	0 (0)	0 (0)
cspD	Cold shock-like protein D	2 (0.001)	0 (0)
cspE	Cold shock protein E	0 (0)	0 (0)
cspF	Cold shock protein F	0 (0)	0 (0)
cspG	Cold shock-like protein G	4 (0.002)	0 (0)
deaD	ATP-dependent RNA helicase	13 (0.007)	0 (0)
DnaA	Chromosomal replication initiator protein	27 (0.015)	6 (0.008)
DnaG	DNA primase	25 (0.014)	3 (0.004)
DnaJ	Chaperone protein	52 (0.028)	3 (0.004)
DnaJ1	Chaperone protein	2 (0.001)	0 (0)
DnaJ2	Chaperone protein	2 (0.001)	0 (0)
DnaK	Chaperone protein	71 (0.039)	10 (0.013)
DnaK2	Chaperone protein	26 (0.014)	1 (0.001)
groEL	GroEL / grol 60 kDa chaperonin	72 (0.04)	7 (0.009)
groES	GroES / gros 10 kDa chaperonin	11 (0.006)	3 (0.004)
gyrA	DNA gyrase subunit A	68 (0.037)	12 (0.016)
gyrB	DNA gyrase subunit B	59 (0.032)	6 (0.008)
gyrBR	DNA gyrase subunit B, novobiocin-resistant	4 (0.002)	0 (0)
hscA	dnaK chaperone protein	7 (0.004)	0 (0)
infA	Translation initiation factor IF-1	6 (0.003)	0 (0)
infB	Translation initiation factor IF-2	47 (0.026)	6 (0.008)
infC	Translation initiation factor IF-3	22 (0.012)	3 (0.004)
nusA	Transcription termination/antitermination protei	18 (0.01)	2 (0.003)
otsA	Trehalose-6-phosphate synthase	11 (0.006)	0 (0)
otsB	Trehalose-6-phosphate phosphatase	2 (0.001)	0 (0)
pnp	Polyribonucleotide nucleotidyltransferase	54 (0.03)	5 (0.007)
rbfA	Ribosome-binding factor A	4 (0.002)	0 (0)
recA	Protein RecA	41 (0.022)	4 (0.005)
rnr	Ribonuclease R	34 (0.019)	1 (0.001)
tig	Trigger factor	20 (0.011)	0 (0)
yhdn	General stress protein 69	23 (0.012)	10 (0.013)

Table 16. Cold and heat shock genes within the metagenomes. MG RAST assigned cold and heat shock genes within the metagenomes.

		Svalbard	Greenland
Cold Shock			
cspA	Cold shock protein CspA	11	1
cspC	Cold shock protein CspC	2	0
cspE	Cold shock protein CspE	0	1
cspG	Cold shock protein CspG	6	1
Heat Shock			
dnaJ	Chaperone protein DnaJ	16	0
dnaK	Chaperone protein DnaK	41	15
grpE	Heat shock protein GrpE	2	0
hrcA	Heat-inducible transcription repressor HrcA	11	3
hspR	HspR, transcriptional repressor of DnaK operon	3	0
lepA	Translation elongation factor LepA	8	4
prmA	Ribosomal protein L11 methyltransferase (EC 2.1.1.-)	11	0
rph	Ribonuclease PH (EC 2.7.7.56)	9	1
rpoH	RNA polymerase sigma factor RpoH	6	0
smpB	tmRNA-binding protein SmpB	4	2
ysnA	Xanthosine/inosine triphosphate pyrophosphatase	4	2

Table 17. Crt and carotenoid genes within the metagenomes. Total gene numbers and abundance (%) of all (Coding Sequences) CDS from PROKKA (*Prokka: rapid prokaryotic genome annotation)* annotated Svalbard and Greenland metagenomes are given in the table below. In total PROKKA assigned Svalbard 182,719 CDS and Greenland 74,805 CDS.

Gene	Protein	Svalbard	Greenland
		Total genes (% of all)	Total genes (% of all)
carA2	zeta-carotene-forming phytoene desaturase	2 (0.001)	0 (0)
carC	All-trans-zeta-carotene desaturase 1.3.99.26	1 (0.001)	0 (0)
crt	Short-chain-enoyl-CoA hydratase	4 (0.002)	2 (0.003)
crtB	All-trans-phytoene synthase	15 (0.008)	3 (0.004)
crtC	Acyclic carotenoid 1,2-hydratase	3 (0.002)	0 (0)
crtD	Hydroxyneurosporene desaturase	3 (0.002)	1 (0.001)
crtF	Demethylspheroidene O-methyltransferase	2 (0.001)	0 (0)
crtI	Phytoene desaturase (lycopene-forming)	11 (0.006)	3 (0.004)
crtI	Phytoene desaturase (neurosporene-forming)	8 (0.004)	0 (0)
crtL	Lycopene beta cyclase	1 (0.001)	0 (0)
crtN	Dehydrosqualene desaturase	3 (0.002)	0 (0)
crtP	Diapolycopene oxygenase	1 (0.001)	0 (0)
crtQ	4,4'-diaponeurosporenoate glycosyltransferase	1 (0.001)	0 (0)
crtX	Zeaxanthin glucosyltransferase	4 (0.002)	0 (0)
pds (crtP)	15-cis-phytoene desaturase	13 (0.007)	2 (0.003)
sll1541	Apocarotenoid-15,15'-oxygenase	12 (0.007)	0 (0)
slr1963	Orange carotenoid-binding protein	13 (0.007)	0 (0)

Table 18. Light sensitive genes in the metagenomes. Total gene numbers and abundance (%) of all (Coding Sequences) CDS from PROKKA (*Prokka: rapid prokaryotic genome annotation)* annotated Svalbard and Greenland metagenomes are given in the table below. In total PROKKA assigned Svalbard 182,719 CDS and Greenland 74,805 CDS.

Gene	Protein	Svalbard	Greenland
		Total genes (% of all)	Total genes (% of all)
bluF	Blue light- and temperature-regulated antirepressor BluF	4 (0.002)	0 (0)
bphP	Bacteriophytochrome	7 (0.004)	0 (0)
cph1	Phytochrome-like protein cph1	42 (0.023)	1 (0.001)
cph2	Phytochrome-like protein cph2	76 (0.042)	5 (0.007)
cry2	Cryptochrome-like protein cry2	5 (0.0027)	2 (0.0027)
CRYD	Cryptochrome DASH	10 (0.005)	1 (0.001)
ELI_04755	Light-activated DNA-binding protein EL222	1 (0.001)	0 (0)
lov	Blue-light-activated histidine kinase	8 (0.004)	0 (0)
n/a	Blue-light absorbing proteorhodopsin	1 (0.001)	0 (0)
n/a	Green-light absorbing proteorhodopsin	6 (0.003)	0 (0)
n/a	Light-harvesting protein B-880 alpha chain	0 (0)	1 (0.001)
n/a	Light-harvesting protein B-880 beta chain	1 (0.001)	0 (0)
pfyP	Blue-light photoreceptor	2 (0.001)	0 (0)
PSPTO_2896	Blue-light-activated protein	10 (0.005)	3 (0.004)
puf2A	Light-harvesting protein B-808/866 alpha chain	1 (0.001)	0 (0)
pufA	Light-harvesting protein B-870 alpha chain	4 (0.002)	0 (0)
pyp	Photoactive yellow protein	1 (0.001)	0 (0)

Table 19. S11 isolate descriptors. Colony morphology and characteristics of S11 isolates.

Isolate ID	Description	Absorbance at OD_{600} (pre-freeze)
S11A	Grown on solid and liquid R2A at +2 °C in light and dark conditions. Originally purple pigmented, lost the colour after subculture. Thick, sticky, and difficult to handle. Form -irregular, elevation – convex, margin – undulate, opaque, glistening. 3-8mm sized colonies. Lumpy in suspension, cloudy, opaque broth.	0.16
S11B	Grown on solid and liquid R2A at +2 °C in light and dark conditions. Yellow pigmented. Opaque in centre, with translucent halo. Smells. Form – irregular, elevation – flat, margin – undulate. 3mm sized colonies. Fairly even in suspension, opaque broth.	0.59
S11C	Grown on solid and liquid R2A at +2 °C in light conditions. Originally red pigmented, lost the colour entirely after subculture, white coloured. Opaque in centre, with translucent halo. Irregular, raised, undulate. 2-4mm sized colonies. Even suspension with a sediment.	0.94
S11D	Grown on solid and liquid R2A at +2 °C in light and dark conditions. Opaque. Peachy/pink coloured, slight colour variance in dark/light. Irregular, raised, entire. 1-3mm sized colonies. Even suspension with small amount of sediment.	0.48
S11E	Grown on solid and liquid R2A at +2 °C and at room temperature, in light and dark conditions. Circular, flat, entire, punctiform. Cream coloured, opaque in dark and more translucent in light. Even, opaque suspension.	0.7

Table 19. cont.…

Isolate ID	Description	Absorbance at OD_{600} (pre-freeze)
S11F	Grown on solid and liquid R2A at +2 °C in light conditions. Varied opacity. Cream. Irregular, raised, undulate, punctiform. Fairly even suspension, cloudy.	0.42
S11G	Grown on solid and liquid R2A at +2 °C in light and dark conditions. Opaque. Peachy yellow. Very tough to loop and spread. Irregular, convex, undulate, 3-8mm sized colonies. Lumpy in suspension, uneven.	0.4
S11H	Grown on solid and liquid R2A at +2 °C in light and dark conditions. Yellow and cream. Possible 2 isolates together, symbiosis. Or unusual morphology. Smells. Very tough to loop and spread. Irregular, convex, undulate, 2-8mm sized colonies. Cloudy, uneven suspension. Sediment.	0.75
S11I	Grown on solid and liquid R2A at +2 °C in light conditions. Originally cream, has become pink/peach with time. Opaque in centre, translucent edges. Irregular, convex, undulate. 2-6mm sized colonies. Mucoid texture and thick to spread. Even suspension.	1.24
S11J	Grown on solid and liquid R2A at +2 °C in light conditions. Pale pink coloured. Circular, flat, undulate, 1-6mm sized colonies. Mixed opacity. Even suspension.	0.4
S11K	Grown on solid and liquid R2A at +2 °C in light conditions. Pale pink on solid media, has become different shade – orange – in liquid media. Varied opacity. Irregular, flat, entire, 1-5 mm sized colonies. Even suspension, with thick sediment.	0.19

Table 19. cont.…

Isolate ID	Description	Absorbance at OD_{600} (pre-freeze)
S11L	Grown on solid and liquid R2A at +2 °C in light conditions. Varied opacity. Orange/cream. Circular, flat, undulate, 2-4mm sized colonies. Even suspension.	0.52
S11M	Grown on solid and liquid R2A at +2 °C in light conditions. Varied opacity. Bright orange. Irregular, flat, undulate, 1-6mm sized colonies. Even suspension, with thick sediment.	0.57

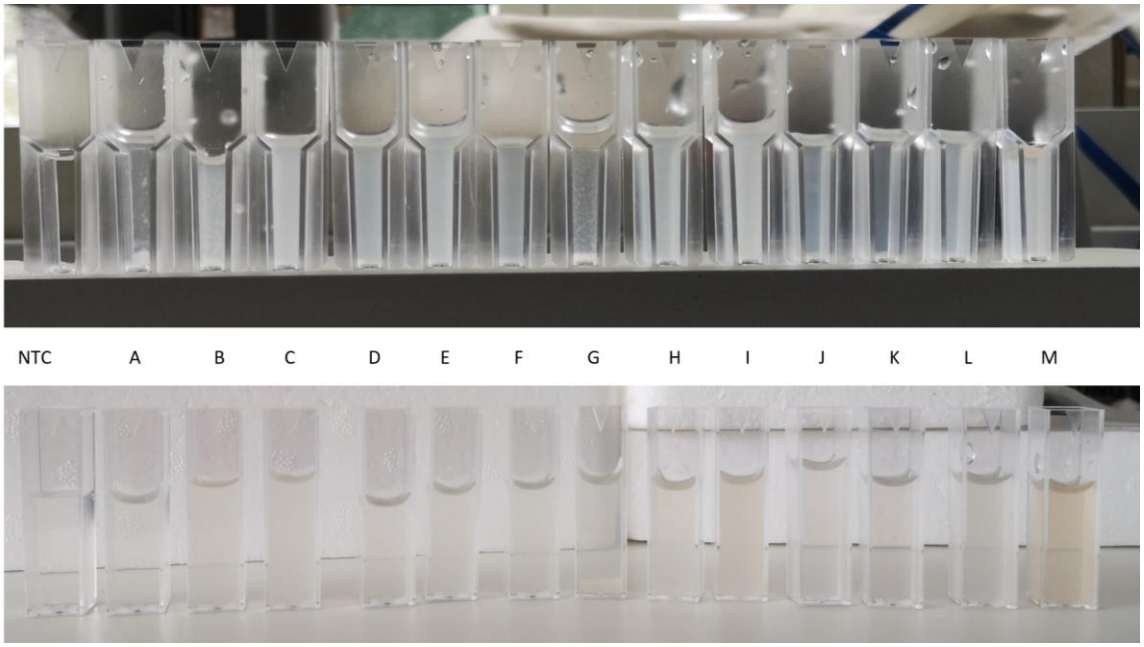

Figure 35. Sub-zero incubation culture. S11 culture in cuvettes at the pre-freeze (top row) and 8-week incubation (bottom row) point. The pigment seemed to intensify in many cases, especially so in S11I and S11M.

Table 20. Raw absorbance values. Data and mean AU values for pigment production at different wavelengths. D > L denotes Dark grown inoculum placed into Light conditions, L > L denotes Light grown inoculum placed into Light conditions and so forth.

Wavelength (nm)		350	375	400	425	450	475	500	525
D > L	1	0.02	0.06	0.145	0.275	0.39	0.311	0.123	0.017
	2	0.018	0.055	0.123	0.235	0.305	0.25	0.101	0.016
	3	0.023	0.065	0.136	0.25	0.345	0.285	0.108	0.018
	4	0.019	0.07	0.121	0.223	0.294	0.265	0.103	0.021
	mean	**0.02**	**0.0625**	**0.13125**	**0.24575**	**0.3335**	**0.27775**	**0.10875**	**0.018**
L > L	1	0.009	0.045	0.09	0.134	0.197	0.141	0.068	0.017
	2	0.013	0.05	0.089	0.126	0.191	0.135	0.067	0.018
	mean	**0.011**	**0.0475**	**0.0895**	**0.13**	**0.194**	**0.138**	**0.0675**	**0.0175**
L > D	1	0.008	0.022	0.034	0.042	0.06	0.036	0.022	0.011
	2	0.006	0.025	0.037	0.028	0.057	0.043	0.023	0.013
	3	0.017	0.048	0.06	0.072	0.089	0.068	0.042	0.02
	4	0.011	0.058	0.056	0.067	0.074	0.055	0.033	0.02
	mean	**0.0105**	**0.03825**	**0.04675**	**0.05225**	**0.07**	**0.0505**	**0.03**	**0.016**
D > D	1	0.006	0.02	0.022	0.034	0.043	0.027	0.017	0.008
	2	0.009	0.026	0.034	0.039	0.072	0.044	0.023	0.013
	3	0.012	0.027	0.04	0.027	0.075	0.032	0.027	0.012
	4	0.011	0.03	0.036	0.039	0.069	0.025	0.029	0.014
	mean	**0.0095**	**0.02575**	**0.033**	**0.03475**	**0.06475**	**0.032**	**0.024**	**0.01175**

Table 21. Full stress, shock, cold-adaption associated, carotenoid biosynthesis and light-sensing gene table. S11 representative genomes from NCBI annotated using PROKKA.

Gene	Protein	*Variovorax paradoxus*	*Polaromonas* sp. Pch-P	*Pseudomonas psychrotolerans*
-	Putative universal stress protein	1	4	0
aceE	Pyruvate dehydrogenase E1 component	1	2	1
aceF	Dihydrolipoyllysine-residue acetyltransferase component of pyruvate dehydrogenase complex	1	1	0
bluF	Blue light- and temperature-regulated antirepressor	3	3	2
bphP	Bacteriophytochrome	0	0	1
cph1	phytochrome	0	2	2
cph2	phytochrome	1	0	7
crt	Short-chain-enoyl-CoA hydratase	4	2	0
crtB	All-trans-phytoene synthase/15-cis-phytoene synthase	2	2	1
crtE	Geranylgeranyl diphosphate synthase	0	0	1
crtI	Phytoene desaturase (lycopene-forming)	0	0	1
crtL	Lycopene beta cyclase	0	0	1
crtN	Dehydrosqualene desaturase	0	0	0
crtX	Zeaxanthin glucosyltransferase	0	0	1
csp	Cold shock protein	0	0	0
cspA	Cold shock protein A	0	0	5
cspB	Cold shock protein B	0	0	0
cspC	Cold shock protein C	0	0	0
cspD	Cold shock-like protein D	0	0	1
cspE	Cold shock protein E	0	0	0
cspF	Cold shock protein F	0	0	0
cspG	Cold shock-like protein G	0	0	0
deaD	ATP-dependent RNA helicase	0	0	1
djlA_2	DnaJ-like protein DjlA	0	0	1
DnaA	Chromosomal replication initiator protein	1	1	1
DnaG	DNA primase	2	1	1
DnaJ	Chaperone protein	2	2	1
DnaJ1	Chaperone protein	0	0	0
DnaJ2	Chaperone protein	0	0	0
DnaK	Chaperone protein	2	2	2
DnaK2	Chaperone protein	0	0	0
GroEL	GroEL / grol 60 kDa chaperonin	*1*	1	1
GroES	GroES	1	1	1
gsp 160	yocK	0	0	0
gsp18	yfkm	1	0	0
gsp39	ydad	2	0	2
gsp69	yhdN	4	1	6
gyrA	DNA gyrase subunit A	1	2	1
gyrB	DNA gyrase subunit B	1	1	1
gyrBR	DNA gyrase subunit B, novobiocin-resistant	0	0	0

Table 21. cont…

Gene	Protein	*Variovorax paradoxus*	*Polaromonas* sp. Pch-P	*Pseudomonas psychrotolerans*
hns	Nucleoid protein, transcriptional repressor and DNA supercoiling	0	0	0
hrcA	hrcA	1	1	0
hscA	dnaK chaperone protein	1	1	1
hscB	Co-chaperone protein	1	1	1
hslr	Heat shock protein 15	1	1	1
hspr	Putative heat shock protein HspR	0	0	0
hspX	Alpha-crystallin	0	0	0
htpX	Protease HtpX	1	4	1
hupB	Nucleoid protein and DNA supercoiling	2	1	1
ibaG	Acid stress protein IbaG	1	1	1
infA	Translation initiation factor IF-1	1	2	1
infB	Translation initiation factor IF-2	1	1	1
infC	Translation initiation factor IF-3	1	1	1
lpxP	Lipid A biosynthesis palmitoleoyltransferase	1	1	1
NhaX	Stress response protein NhaX	0	2	0
nusA	Transcription termination/antitermination protein	1	1	1
otsA	Trehalose-6-phosphate synthase	1	1	1
otsB	Trehalose-6-phosphate phosphatase	1	1	1
pasI	Persistence and stress-resistance antitoxin PasI	1	1	1
pds	(crtP) 15-cis-phytoene desaturase	1	1	0
pnp	Polyribonucleotide nucleotidyltransferase	1	1	1
PSPTO_2896	Blue-light-activated protein	0	0	11
rbfA	Ribosome-binding factor A	1	1	1
recA	Protein RecA	2	1	1
rnr	Ribonuclease R	1	1	1
scoF	Cold shock protein ScoF	0	0	0
srkA	stress response kinase A	2	0	1
teaD	TRAP-T-associated universal stress protein TeaD	2	3	1
tig	Trigger factor	1	1	1
usp	Universal stress protein	0	0	0
uspA2	Universal stress protein A	0	0	1
ves	Unknown function, cold- and stress-inducible.	1	1	1
yfia	Protein Y, associated with 30S ribosomal subunit, inhibits translation (A-site).	0	0	0

Table 22. Full stress, shock and cold-adaption associated gene table of A18.2 and *Cryobacterium psychrotolerans.* Genomes annotated using PROKKA.

Gene	Protein	*C. psychrotolerans*	A18.2
-	Putative universal stress protein	0	0
NhaX	Stress response protein NhaX	0	0
pasI	Persistence and stress-resistance antitoxin PasI	0	0
aceE	Pyruvate dehydrogenase E1 component	1	4
aceF	Dihydrolipoyllysine-residue acetyltransferase component of pyruvate dehydrogenase complex	1	1
csp	Cold shock protein	1	0
cspA	Cold shock protein A	1	1
cspB	Cold shock protein B	0	0
cspC	Cold shock protein C	0	0
cspD	Cold shock-like protein D	0	0
cspE	Cold shock protein E	0	0
cspF	Cold shock protein F	0	0
cspG	Cold shock-like protein G	0	0
deaD	ATP-dependent RNA helicase	1	3
djlA_2	DnaJ-like protein DjlA	0	1
DnaA	Chromosomal replication initiator protein	1	4
DnaG	DNA primase	2	2
DnaJ	Chaperone protein	1	2
DnaJ1	Chaperone protein	0	0
DnaJ2	Chaperone protein	1	1
DnaK	Chaperone protein	1	1
DnaK2	Chaperone protein	0	0
GroEL	GroEL / grol 60 kDa chaperonin	1	2
GroES	GroES	1	1
gsp 160	yocK	1	1
gsp18	yfkm	0	0
gsp39	ydad	0	0
gsp69	yhdN	4	5
gyrA	DNA gyrase subunit A	2	5
gyrB	DNA gyrase subunit B	2	5
gyrBR	DNA gyrase subunit B, novobiocin-resistant	0	0
hns	Nucleoid protein, transcriptional repressor and DNA supercoiling	0	0

Table 22. cont.…

Gene	Protein	*C. psychrotolerans*	A18.2
hrcA	hrcA	1	2
hscA	dnaK chaperone protein	0	0
hscB	Co-chaperone protein	0	0
hslr	Heat shock protein 15	1	1
hspr	Putative heat shock protein HspR	0	1
hspX	Alpha-crystallin	1	0
htpX	Protease HtpX	1	3
hupB	Nucleoid protein and DNA supercoiling	0	0
ibaG	Acid stress protein IbaG	0	0
infA	Translation initiation factor IF-1	1	1
infB	Translation initiation factor IF-2	1	1
infC	Translation initiation factor IF-3	1	1
lpxP	Lipid A biosynthesis palmitoleoyltransferase	0	0
nusA	Transcription termination/antitermination protein	1	1
otsA	Trehalose-6-phosphate synthase	1	2
otsB	Trehalose-6-phosphate phosphatase	0	0
pnp	Polyribonucleotide nucleotidyltransferase	1	4
rbfA	Ribosome-binding factor A	1	0
recA	Protein RecA	1	1
rnr	Ribonuclease R	0	0
SC7.0	Cold shock-like protein 7.0	0	0
scoF	Cold shock protein ScoF	1	1
srkA	stress response kinase A	0	0
teaD	TRAP-T-associated universal stress protein	0	0
tig	Trigger factor	1	1
usp	Universal stress protein	3	0
uspA2	Universal stress protein A	0	0
ves	Unknown function, cold- and stress-inducible	1	0
yfia	Protein Y, associated with 30S ribosomal subunit, inhibits translation (A-site).	0	0